U.PORTO
FEUP FACULDADE DE ENGENHARIA
UNIVERSIDADE DO PORTO

U.PORTO
INSTITUTO DE CIÊNCIAS
BIOMÉDICAS ABEL SALAZAR
UNIVERSIDADE DO PORTO

Development of a bi-functional 3D scaffold composed by glucomannan and biphasic calcium phosphates for bone tissue engineering applications.

Inês Maria Rodrigues Pintão

Dissertation for the Degree of Master of Science in Bioengineering at Faculdade de Engenharia da Universidade do Porto and Instituto de Ciências Biomédicas Abel Salazar da Universidade do Porto

Integrated Master in Bioengineering

Page intentionally left in blank

Development of a bi-functional 3D scaffold composed by glucomannan and biphasic calcium phosphates for bone tissue engineering applications.

Inês Maria Rodrigues Pintão

Dissertation for the Degree of Master of Science in Bioengineering at Faculdade de Engenharia da Universidade do Porto and Instituto de Ciências Biomédicas Abel Salazar da Universidade do Porto

Integrated Master in Bioengineering

Supervisor: Aureliana Sousa, PhD
Co-supervisors: Susana Olhero, PhD and Manuel Barros, MSc

October 2020

“Science have no idea how much it owes to the imagination” - Ralph Emerson

Page intentionally left in blank

Acknowledgments

First, I want to thank to the person who taught me almost everything I learnt in the last few months. Filipa thought me not only what it takes to be a scientist but also how to take advantage from all that was happening, including when things did not work as planned. Even when I was more discouraged, Filipa always knew what to say and supported me in everything I needed, always bearing great ideas to surpass all the hardship. A big thank you for never stopping to believe in my capabilities and for your kind compliments, always welcome with great affection.

Second, I would like to thank to Manel, who accompanied me since the beginning and who thaught me the basis of working on a lab, always with a smile on his face. Thank you for being this fantastic and supportive person who I had the pleasure to work with. An acknowledgment also to Rafaela who was always available to help me whenever necessary.

To Marta, for her everyday companionship and support. It was a great pleasure to have the opportunity to get to know her a little bit more. Thank you for your joyful spirit and for being someone with whom I could share the good and the bad moments. Also, I would like to thank to the people who shared the lab with me and were always available to help me, especially Marco that helped me in develop my work. It would not have been so complete without your help.

An acknowledgment to Susana Olhero for providing the robocasting and to Ana Filipa Rodrigues who gave me a huge help on the robocasting and made me feel welcome every time I went to Aveiro.

I have to acknowledge the support of Maria Lazaro from the Bioimaging i3S Scientific Platform, member of the national infrastructure PPBI - Portuguese Platform of Bioimaging (PPBI-POCI-01-0145- FEDER-022122), José da Neves and Ana Baião from the Nanomedicines and Translational drug delivery group and Frederico Silva from the Biochemical and Biophysical Technologies Scientific Platform.

Finally, I want to thank to the persons I love the most in this world. My parents and my sister who were the most supportive they could be, always cheering me up and motivating me to do my best every day. To Tiago that never stopped believing in me and for understanding the long hours of working, especially in those final moments.

The research described in this thesis was financially supported in the framework of FCT-Fundac¸ão para a Ciência e Tecnologia *project 2BBone - Sintering-free Bifunctional CaP-based Biomaterials for Bone Cancer Treatment and Regeneration (*PTDC/CTM-CER/29940/2017)

Page intentionally left in blank

Abstract

Due to the accelerated growth of human population and the consecutive increase of life expectancy, several problems related to aging have started to arise in the last decades. Therefore, there is a demand for strategies capable to address problems like osteoporosis, bone cancer and bone infections. One of those strategies is based on the use of materials that are similar to the real bone so, the first step to succeed in finding a good bone substitute is to choose the best suitable material. Since the natural bone is composed by an organic and an inorganic part, the use of a hybrid polymeric-ceramic material sounds promising. The polymeric part gives the material its biocompatibility and biodegradability, besides acting as a supportive matrix, and the ceramic part confers the properties that mimic the mineral phase of bone. In this work, Konjac Glucomannan (KGM) and powders of Hydroxyapatite (HA) and ß-Tricalcium Phosphate (ß-TCP) were used to develop 3D scaffolds via an additive manufacturing technique (robocasting) because its ability to produce scaffolds with predefined morphology and structure, such as 3D porous scaffolds that are ideal for bone ingrowth. The goal is that these scaffolds can promote bone regeneration and at same time treat bone infections or kill cancer cells.

In the first part of this work the hybrid polymeric-ceramic 3D scaffolds were submitted to *in vitro* tests, to evaluate their capacity to promote the adherence and proliferation of human Mesenchymal stem cells (hMSCs). The results obtained confirmed this hypothesis, but further tests would have been necessary to evaluate if the cells were able to differentiate into the osteogenic lineage.

After, nanoparticles incorporated with a drug, levofloxacin, were developed to be incorporated on the scaffolds in order to grant them anti-microbial properties. Polydopamine particles were also included in the scaffolds' materials as a strategy to provide a multi-functional material with hyperthermic properties for cancer treatment applications. However, it was not possible to see the incorporation of the drug into the nanoparticles, which lead us to a new strategy to develop a bi-functional scaffold for bone tissue engineering applications.

This strategy consisted on the incorporation of polydopamine (PDA) particles into the scaffolds since their proven potential in the field of photothermal therapy to treat cancer cells. The *in vitro* tests revealed improved adherence and proliferation of hMSCs throughout the entire time of culture. In addition, an U20S osteosarcoma cell line was also used on the in *vitro tests* of these scaffolds and the results demonstrate that these cells had a better adhesion on the scaffolds that did not include the PDA in their constitution. However further assays need to be performed, to evaluate the ability of these scaffolds increase their temperature under laser irradiation. A simulated body fluid (SBF) assay revealed that the developed material could form a carbonated apatite-like layer at their surface, showing promising properties for future in vivo applications.

Taking together all the results obtained during this work and the previously demonstrated features of the PDA particles, we can conclude that the hybrid organic-inorganic 3D scaffolds

developed are promising candidates to be used in bone tissue engineering approaches and, in particular, may act as a bi-functional material.

List of Contents

Abbreviation list

ACN - acetonitrile

ALG – alginate

AM - Addictive manufacturing

α-MEM - α-Minimum Essential Medium

AMP's - antimicrobial peptides

BCPs - Biphasic Calcium Phosphates

BGS - bone graft substitutes

BLC - Bone lining cell

BM – basal medium

BMPs - bone morphogenetic proteins

BSP - Bone sialoprotein

CAD - computer-aided design

CaP - Calcium Phosphate

CF - continuous flow

CS – chitosan

DAPI - 4',6-diamidine-2′-phenylindole dihydrochloride

DDM - direct digital manufacturing

dH_2O - deionized water

DIW - Direct Ink Writing

DM - dialysis membrane

DWA - Direct-Write Assembly

ECM - extracellular matrix

EM - Expansion Medium

FBS - Fetal Bovine Serum

FDM - Fused deposition modelling

FGFs - fibroblast growth factors

FTIR - Fourier-transform infrared spectroscopy

GDF-5 - growth differentiation factor 5

hMSCs - Human mesenchymal stromal cells

HPLC - High performance liquid chromatography

HPLC–DAD - high-performance liquid chromatography–diode array detection

IAFF - infection after fracture fixation

IGFI – insulin growth factor-I

IL-6 - Interleukin-6

ISOs - International standards organizations

KGM - Konjac glucomannan

LFX – levofloxacin

LIPUS - low-intensity pulsed ultrasound

M-CSF - monocyte/macrophage colony stimulating factor
microCT - X-ray computed microtomography
NIR – Near infrared
NPs – Nanoparticles
OCN – Osteocalcin
OM – Osteogenic médium
ON - overnight
OS – Osteosarcoma
PCL – Polycaprolactone
PDA - polydopamine
PdI - polydispersity index
PEMF - pulsed electromagnetic fields
PFA - paraformaldehyde
PGA – poly (glycolic acid)
PJ - prosthetic joint
PLA – Poly (lactic acid)
PPF – Poly (propylene fumarate)
P/S - Penicillin/Streptomycin
PTH - parathyroid hormone
PU - Polyurethane
PVA – Poly (vinyl alcohol)
RM - rapid manufacturing
RP - rapid prototyping
RT – room temperature
SBF - simulated body fluid
SEM - Scanning electron microscope
SF - silk fibroin
SFF - solid freeform fabrication
SLA - Stereolithography
SLS - Selective laser sintering
SS - sample and separate
TCP - tricalcium phosphate
3D – three-dimensional
3DP - 3D printing
TGF ß - transforming growth factor ß
TH - parathyroid hormone
TNF-α - tumour necrosis factor-α
UV-Vis - Ultraviolet–visible
VEGF - vascular endothelial growth factor

List of figures

List of tables

Introduction

1. Bone tissue

Bone are living, active tissues that are constantly being remodelled. Specifically, bone is a type of connective tissue that provides important functions in the body such as locomotion, support and protection of internal organs and soft tissues. Moreover, bones function as a storage for minerals (e.g. calcium and phosphate), as well as harbouring site for the bone marrow [1].

With the advance of the knowledge in the health area and the technological developments, life expectancy is increasing thus leading to a rise of the amount of individuals that suffer of age-related tissue loss or impairment. These events give rise to a reduced quality of life since it can lead to a reduction of their capacity to perform basic tasks, such as walking, or even cause social and psychological problems. In this way, it is urgent to find new and better approaches to overcome this problem [2]. Bone graft is the second most commonly transplanted tissue [3], approximately 2.2 million bone grafting procedures are performed annually worldwide [4] .

Given the importance of this tissue, there is a need to know the structural, molecular and functional biology of bone to better understand this tissue as a multicellular unit and with dynamic structure [1].

1.1. Bone tissue – composition

1.1.1. Cellular composition

Bone is composed of 4 types of cells: osteoblasts, osteocytes, bone lining cells, and osteoclasts. The origin of these cells is different as well as their location and functions (Figure 1) [5].

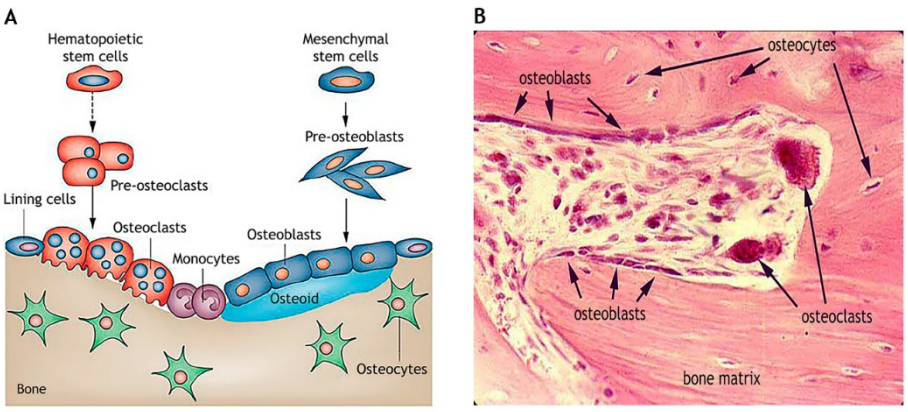

Figure 1 - Bone cells. Different origins and locations: (A) A schematic representation of the bone cells and its different origins: Osteoblasts are originated from mesenchymal stem cells, which can originate subsequently osteocytes and bone lining cells. Osteoclasts derive from hemopoietic stem cells. (B) histological representation of the bone cells, showing its different localizations: Osteoblasts and osteoclasts are found on the bone's surface, whereas osteocytes are located in the interior. Adapted from [6,7].

Osteoblasts are cuboidal cells (Figure 1) representing 4-6% of total resident cells in the bone and are known for their capacity of bone building. They derive from mesenchymal stem cells (Figure 1. A) and can further differentiate into osteocytes or become bone lining cells [8]. Their morphologic characteristics include an abundant rough endoplasmatic reticulum and prominent Golgi apparatus, as well as various secretory vesicles [1]. Since they can be classified as polarized cells, osteoblasts are responsible to secret osteoid (unmineralized organic bone matrix), that is formed before the maturation of the bone tissue. This matrix, which contains a high amount of collagen (94%) and several proteins, growth factors and cytokines, allows the mineralization of the tissue [9].

Osteocytes represent 95% of the total amount of bone cells and are the cells with the higher life span (up to 25 years) [10]. They are spider-shaped cells that are embedded in the mineralized bone matrix (Figure 1) and are formed when a number of osteoblasts become completely surrounded by the matrix (at the end of a bone formation cycle) since, once encapsulated in the bone, the cell is called osteocyte [11]. These cells are tightly connected to each other through gap junctions, forming a three-dimensional net buried in the bone matrix. These features allow them to have sensing and signal transport functions and they can act as mechanosensors, since their interconnected network has the capacity to detect mechanical pressures and loads, helping the adaptation of bone to daily mechanical forces [12]. Moreover, osteocyte apoptosis plays a key role in the bone resorption, acting as a chemotactic signal (during bone resorption, apoptotic osteocytes are engulfed by osteoclasts). In this way, osteocytes act as orchestrators of bone remodelling, through regulation of osteoblast and osteoclast activities [1].

Bone lining cells (BLC's) are thin, elongated cells that cover inactive (nonremodeling) bone surfaces in the mature/adult skeleton and are linked to each other or to osteocytes through cytoplasmic extensions or gap junctions [5]. Regarding their origin, it is though that they derive from previously active osteoblasts that have entered a quiescent phase [13], so they can be referred as "resting osteoblasts" or "surface osteocytes" [5]. In fact, BLC's can differentiate into osteoblasts able of producing osteoid and the matrix vesicles responsible for the mineralization process, in the bone formation cycle [13]. Though not completely understood, it is thought that these cells hamper the direct interaction between osteoclasts and bone matrix when bone resorption is not supposed to happen, and participate in osteoclast differentiation [1].

Osteoclasts are multinucleated cells (Figure 1) that are responsible for the bone resorption during the bone remodelling process. They derive from Hematopoietic Stem cells (Figure 1. A), in particular from the monocyte-macrophage lineage [14], and they become differentiated when stimulated by two essential factors: the monocyte/macrophage colony stimulating factor (M-CSF) and receptor activation of NF-κB ligand (RANKL) [15]. The correct balance between bone formation and destruction is essential to form an adequate bone mass so it is important to maintain the correct balance between the activity of osteoblasts and osteoclasts. This is achieved not only by systemic factors but also by keeping a cross-talk between osteoblasts and

osteoclasts. In this way, osteoclasts can produce factors that stimulate osteoblast differentiation and function [8,15].

1.1.2. Extracellular matrix

The extracellular matrix (ECM) of each tissue is formed by the secreted product of resident cells of that tissue and organ, being composed by a mixture of structural and functional proteins arranged in a three-dimensional ultra-structure. The ECM is able not only to bind the cells together, but also, to influence their survival, development, shape and migratory behaviour [16].

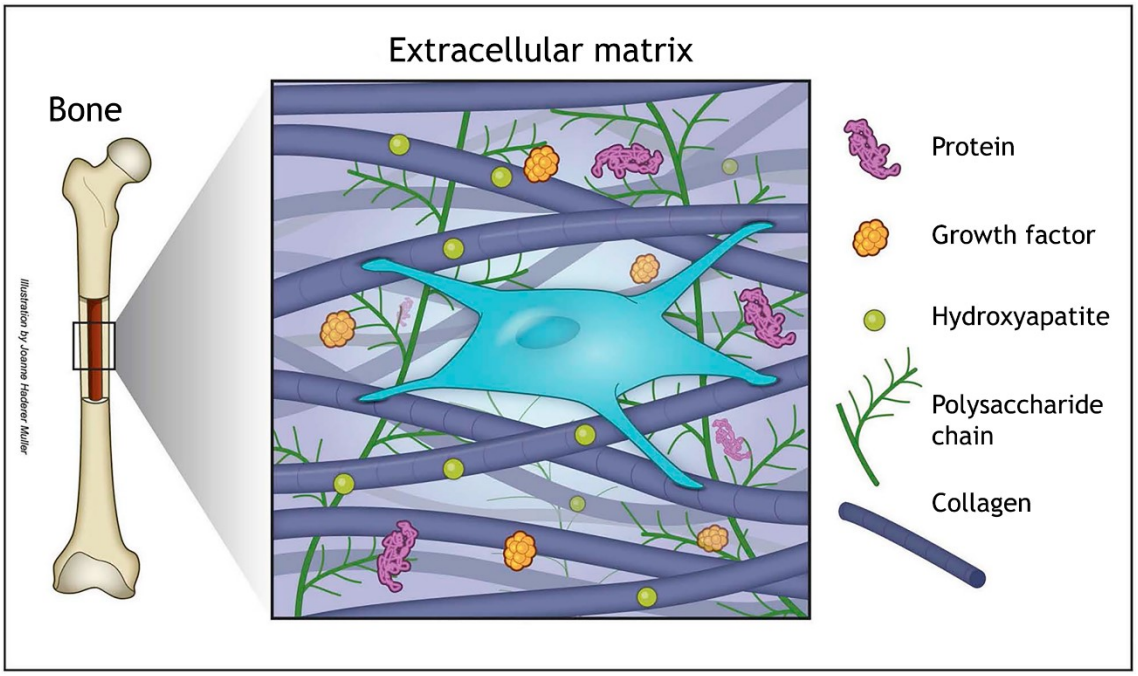

Figure 2 - Principal components of the bone ECM. Bones consist of living cells embedded in a matrix that has both organic and non-organic components: The organic constituents are both collagenous and noncollagenous proteins, whereas the inorganic part is composed essentially of hydroxyapatite. The bone ECM has also important biomolecules, such as growth factors and polysaccharides. Adapted from [17].

Bone ECM is composed of both an organic component (approximately 35% of the total weight of bone tissue) and an inorganic component (65%) (figure 2) [5]. The organic matrix contains collagenous proteins (90%), that are predominantly type I collagen, and noncollagenous proteins including osteocalcin, osteonectin, osteopontin, fibronectin and bone sialoprotein II, bone morphogenetic proteins (BMPs), growth factors and polysaccharides. In addition, it is also composed by small leucine-rich proteoglycans including decorin, biglycan, lumican, osteoaderin, and seric proteins [1,17]. The inorganic matrix is composed by mineral salts, containing predominantly calcium and phosphate ions, that are responsible to form the hydroxyapatite crystals, but phosphorus, sodium, magnesium, bicarbonate, potassium, citrate, carbonate, fluorite, zinc barium, and strontium are also present. These two types of matrix, are responsible for the characteristic stiffness and resistance of bone tissue, since the collagen

and the noncollagenous matrix proteins form a scaffold for hydroxyapatite deposition (figure 3), which hardens this connective tissue [1,5].

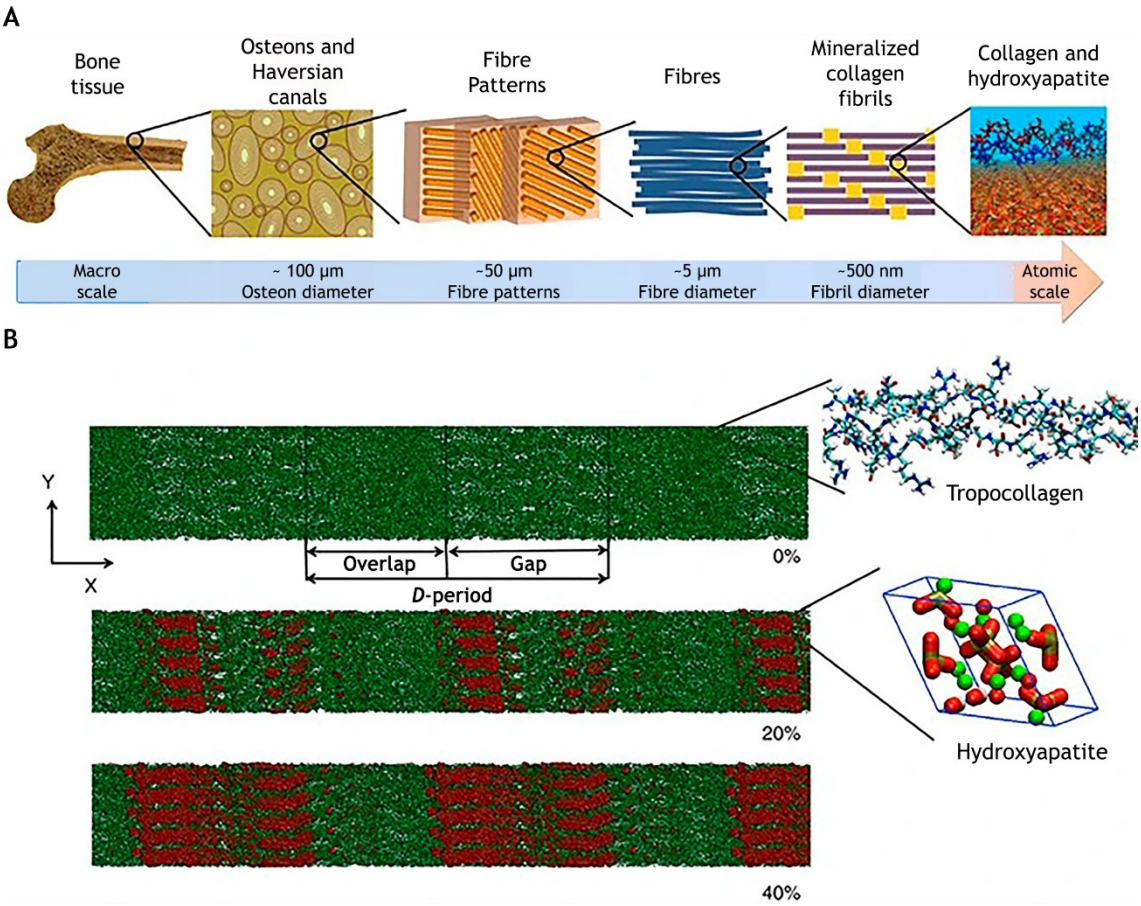

Figure 3 - The collagenous and noncollagenous proteins of bone ECM (organic matrix) form a scaffold for the deposition of hydroxyapatite (inorganic matrix). (A) Hierarchical structure of the bone - collagenous molecules assemble into fibrils that are mineralized via the formation of apatite crystals, such as hydroxyapatite (B) Collagen microfibril model representing 0% mineralization (it is only present the basic structural unit of collagen, Tropocollagen), 20% mineral content (inset shows a hydroxyapatite unit cell) and 40% mineral content - Hydroxyapatite deposits into the gap region of the collagen microfibrils. Adapted from [18].

1.2. Bone Tissue - structure

The adult skeleton is composed by 80% of cortical (compact) bone and 20% of trabecular (cancellous) bone. These two forms of bone tissue have the same composition and structure, but differ in terms of density, porosity and location in the skeleton [19]. The cortical bone comprises the outer tubular shell of the long bones (figure 4) and the outer surface of the small and the flat bones, whereas the trabecular bone occurs near the ends of long bones (figure 4), in the interior of small bones and between the surface of flat bones [20]. In addition, the cortical bone is harder, denser and has less porosity (approximately 10%) than the cancellous bone and it surrounds the bone marrow and the cancellous bone plates [19]. Its fundamental functional units are the osteons, also called Haversian systems, from which blood vessels run, allowing nutrient diffusion within the bone [21]. They have a cylindrical shape, forming a network with several branches (figure 4) [22]. Regarding the trabecular bone, it is characterized

by an interconnected network of small bone trabeculae, that are aligned in the direction of the loading stress (figure 4). This form of bone has a porosity of 50-90%, where these pores are filled with bone marrow and cells. Due to this high porosity, the trabecular bone provides less mechanical support when compared with cortical bone [21,23]. Given the structure of the trabecular bone with larger surface area exposed to the bone marrow (when compared with the cortical bone) and since bone resorption and formation occurs on the bones surface, it is possible to assume that the trabecular bone displays higher metabolically activity than the cortical bone. In this way, it is possible to conclude that the cortical bone provides the mechanical and protective functions of the bone, whereas the cancellous bone provides its metabolic function (it serves, for example, to maintain serum mineral homeostasis) and it is crucial for transmitting loads from the joint surface to the cortex [13].

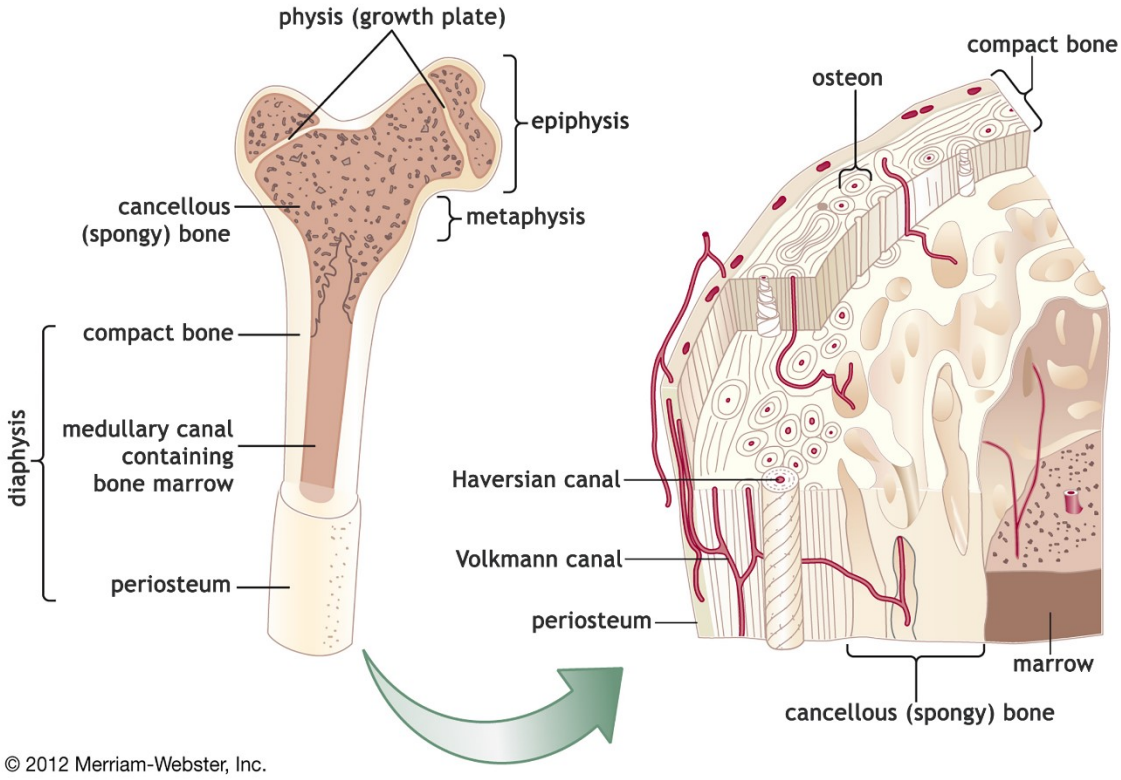

Figure 4 - Bone structure. Bone is composed by cortical (compact) bone, which has cylindrical shaped osteons that have in their centre Harvesian canals to allow the passage of blood vessels. It is also composed by trabecular (cancellous) bone, that is an interconnected network of small bone trusses (trabeculae) aligned in the direction of loading stress. Adapted from [24].

1.3. Bone Remodelling and Regeneration

Bone is a dynamic tissue that is continuously renewed through an active and dynamic process called bone remodelling. This process is based on the correct balance between bone resorption by osteoclasts and bone deposition by osteoblasts, since this feature is mandatory to maintain a constant bone mass [25]. In fact, this is a highly complex cycle that is achieved

through the combined action of osteoblasts, osteocytes, osteoclasts and bone lining cells. The activity of these cells, including its formation, proliferation and differentiation is regulated by local and systemic factors. Local factors include growth factors, cytokines, prostaglandins produced by the bone cells and bone matrix factors released during bone resorption and the systemic factors include the parathyroid hormone (PTH), calcitonin, 1,25-dihydroxyvitaminD3 (calcitriol), glucocorticoids, androgens, and estrogens [1]. For example, osteoclasts can produce clastokines that control osteoblast activity during the bone remodelling process so both clastokines and factors embedded in the matrix play complementary roles in the recruitment of osteoblasts [1,26].

In this way, the following phases need to be accomplished to achieve a correct bone remodelling (figure 5) [25].

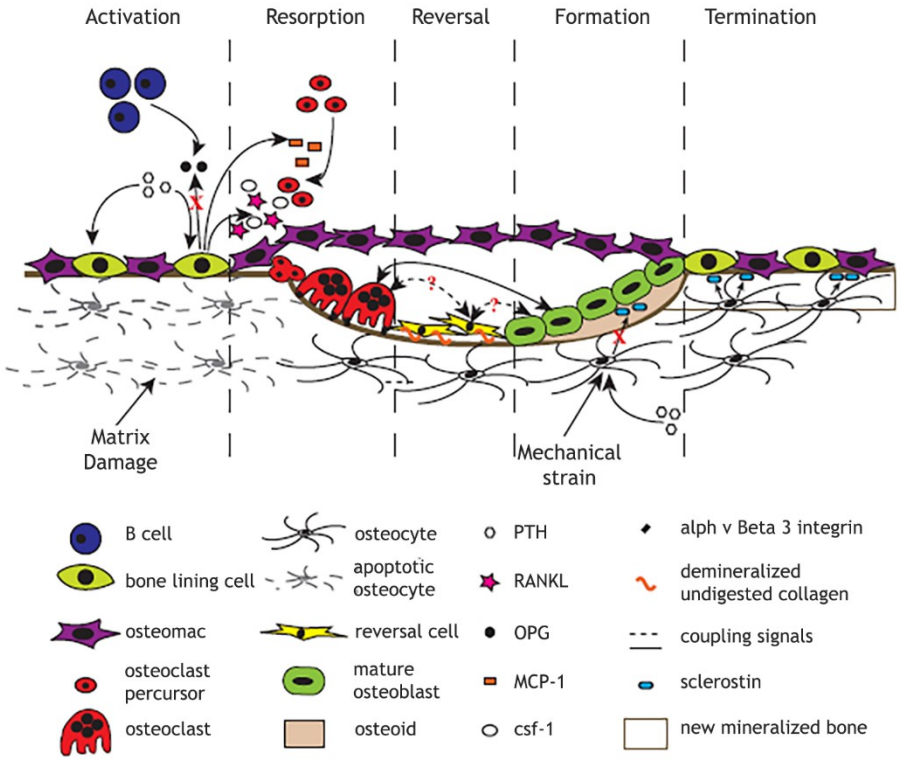

Figure 5 - The process of bone remodelling is composed by five phases. Activation, driven by the detection of an initiating remodelling signal by the osteocytes; Resorption, conducted by the osteoclasts; Reversal, performed by the reverse cells; Formation, where the osteoblasts start to produce new bone matrix and Termination, due to the conclusion of the bone remodelling cycle, that allows the bone surface to return to a resting state. Adapted from [27].

During Activation phase, osteocytes detect different inputs (such as micro-fractures or an alteration of the mechanical loading), or some factors are released in the bone microenvironment (such as insulin growth factor-I (IGFI), tumour necrosis factor-α (TNF-α), parathyroid hormone (PTH) and interleukin-6 (IL-6)), which can lead to the activation of the lining cells (figure 5) and, when they interact with pre-osteoclasts, they fuse and there is a differentiation toward multinucleated osteoclasts [25].

Afterwards, on Resorption phase, osteoblasts recruit osteoclast precursors to the remodelling site, in response to signals generated by osteocytes or by direct endocrine

activation signals, such as PTH [27]. After being differentiated, osteoclasts adhere to the bone surface and start to dissolve bone (figure 5). After performing their function, osteoclasts undergo apoptosis, in order to avoid an excessive bone resorption [25].

The Reversal phase is performed by the reversal cells (figure 5). They are macrophage-like cells that remove the debris produced during the degradation of the matrix, such as undigested demineralized collagen matrix. Afterwards, these reversal cells prepare the bone surface for the upcoming bone formation, which is mediated by osteoblasts [25,27].

On the Formation phase, during the bone matrix resorption, there is a release of several growth factors (BMPs, fibroblast growth factors (FGFs) and transforming growth factor ß (TGF ß)), that are responsible for the recruitment of the osteoblasts in the reabsorbed area (figure 5) [25]. After their recruitment, they secret collagen proteins (mainly type I collagen), noncollagen proteins (Osteocalcin (OCN), osteonectin, Bone sialoprotein (BSP) II and osteopontin) and proteoglycans (such as decorin and biglycan), producing a newly formed bone matrix. This matrix, called osteoid is not calcified at the initial stages but later the osteoblasts are able to promote its mineralization through the synthesis of hydroxyapatite crystals, which completes the bone remodelling process [8].

Finally, the Termination phase takes place when the amount of resorbed bone has been replaced, which indicates the ceasing of bone formation. After the mineralization, mature osteoblasts undergo apoptosis, revert to a phenotype of bone lining cells or become embedded in the mineralized matrix, being differentiated into osteocytes (figure 5). This indicates that the bone surface has returned to a resting stage, that will be maintained until the next cycle of remodelling is initiated [27].

Another important feature of bone is its intrinsic capacity for regeneration. This is a complex physiological process that consists of a well-orchestrated sequence of bone induction and conduction, and involves several cell types and intracellular and extracellular molecular signalling pathways, that have a definable temporal and spatial sequence, with the aim of optimizing the skeletal repair and restore the skeletal function [28]. This process is involved in fracture healing, defects created by trauma, infection, tumor resection, congenital abnormalities and impaired or insufficient regeneration [29]. When it comes to the clinal area, fracture healing is the most common form of bone regeneration and bone healing can be divided into primary and secondary types of healing. The first happens when there is a small fracture gap and no movement at the fracture site and the process of healing is the same as the normal bone remodelling. The second, which is the most frequent type of healing, occurs in the absence of rigid fixation and consists of an organized pattern of interlinked events that aim to activate a number of different cells types, in order to prepare the fracture site for its consolidation, to restore the vascularity and to produce a stable mechanical environment that leads to the ossification of the area [30]. This type of healing occurs in several phases that are described in figure 6.

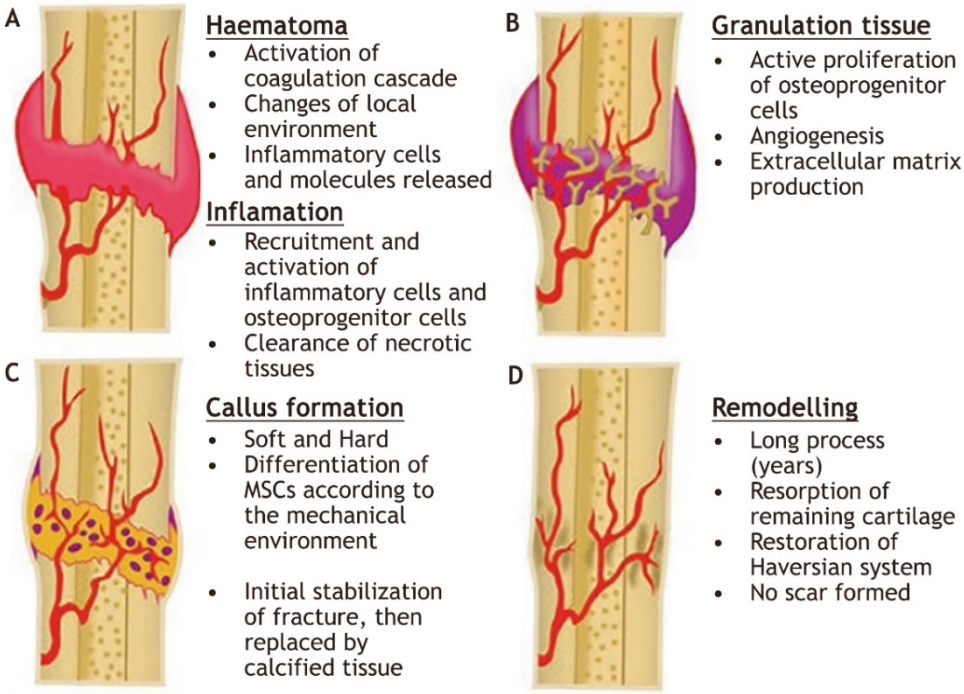

Figure 6 - The stages of secondary bone healing. (A) The healing starts at the time of the injury, with the formation of a fracture hematoma and is followed by the inflammatory stage. (B) The next step is the formation of granulation tissue then, (C) the formation of the soft callus occurs that eventually calcifies and (D) remodels. Adapted from [30].

Unlike what happens in other tissues, the majority of bone fractures can heal without the formation of scar tissue, where the newly formed bone is regenerated with the bone pre-existing properties and it is indistinguishable from the surrounding uninjured bone [28].

Despite having a considerable capacity in repairing, when it comes to regenerating a normal fracture and remaining an active organ over continuous remodelling throughout adult life, sometimes bone regeneration seems necessary in large quantity and might even need clinical interventions, due to the severity of some defects or fractures [31]. In fact, there are several bone regeneration and repair strategies to enhance surgical reconstructive procedures, including the use of alloplastic and allogenic materials, distraction osteogenesis, osteoconductive scaffolds, and bone morphogenetic proteins, being the autologous bone grafting the gold standard, that is used widely for healing critical-size bone defects [29].

2. Bone diseases and current approaches

2.1. Bone fractures and therapeutic approaches

A broken bone or a bone fracture occurs when a force exerted against a bone is stronger than the bone can bear. There are different types of bone fractures (that depend on the strength and direction of the force, what bone is particularly involved, the age of the patient

and its general health) that can result from different causes, such as traumatic incidents like sports injuries, vehicle accidents and falls, and conditions such as osteoporosis and some types of cancer that cause bones to fracture easily [32].

Osteoporosis is acknowledged as the most prevalent bone disorder in the world. It Is a disorder characterized by a reduced bone strength and density, as well an altered microgeometry and microscopic architecture (figure 7), leading to an increase risk of bone fracture [33,34] (figure 7). In fact it is estimated that osteoporosis causes more than 8.9 million fractures annually (1 osteoporotic fracture every 3 seconds), being these fractures a major cause of morbidity and disability in older people and can even lead to a premature death in these individuals, in the case of hip fractures. Another important consequence of these fractures is the considerable economic burden imposed on health services all over the world [35,36]. Despite being more common in women (61% of osteoporotic fractures occur in women, affecting 200 million women worldwide) [36], the risk of fracture increases dramatically with age in both sexes because bones become more fragile and the risk of falling increases [37]. Due to the inevitable aging of the world population, the prevalence of osteoporosis and low mass bone is expected to increase: by 2050, the worldwide incidence of hip fracture in women is projected to increase by 240 % and 310% in men [36].

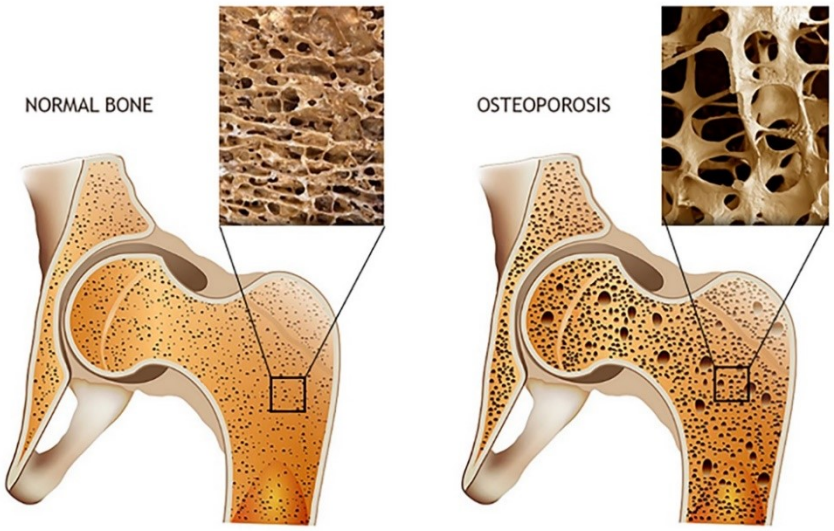

Figure 7 - The differences between a normal and an osteoporotic bone. A normal bone is a honeycomb-like structure, having small and densely packed spaces inside it. This feature allows bones to be strong enough to provide the body structure, as well as being light enough to provide its movement. An osteoporotic bone is characterised by the loss of the honeycomb structure, where the spaces become larger and the bone density is lost, which reflects the decreased bone strength and its increased fragility. Adapted from [38,39].

The repair of bone fractures is a regenerative process that recapitulates many of the biological events of embryonic skeletal development. The events that lead to the healing of a bone fracture are the ones described in section 1.3. This process frequently leads to the successful healing and recovery of the damaged bone but about 5-10% of fractures can lead to a delayed healing or non-union [40].

Current clinical approaches include distraction osteogenesis and bone transport, and the use of different bone-grafting methods, like autologous bone grafts (autografts), allografts, and bone-graft substitutes or growth factors. Also, there is an alternative method, known as the Masquelet technique that is based on a "biological" membrane that is induced after the application of a cement spacer at the first stage and acts as a chamber to the insertion of a non-vascularized autograft at the second stage. Moreover, there are also non-invasive methods of biophysical stimulation (such as low-intensity pulsed ultrasound (LIPUS) and pulsed electromagnetic fields (PEMF)), that can be used as adjuncts to enhance bone regeneration. The "gold-standard" treatment is the autologous bone grafting, where several bone sites can be used for bone-graft harvesting. The anterior and posterior iliac crests of the pelvis are the most commonly used donor sites, since they present all the required elements for bone healing: osteoinduction (BMPs and other growth factors), osteogenesis (osteoprogenitor cells) and osteoconduction (scaffold) (figure 8) [28].

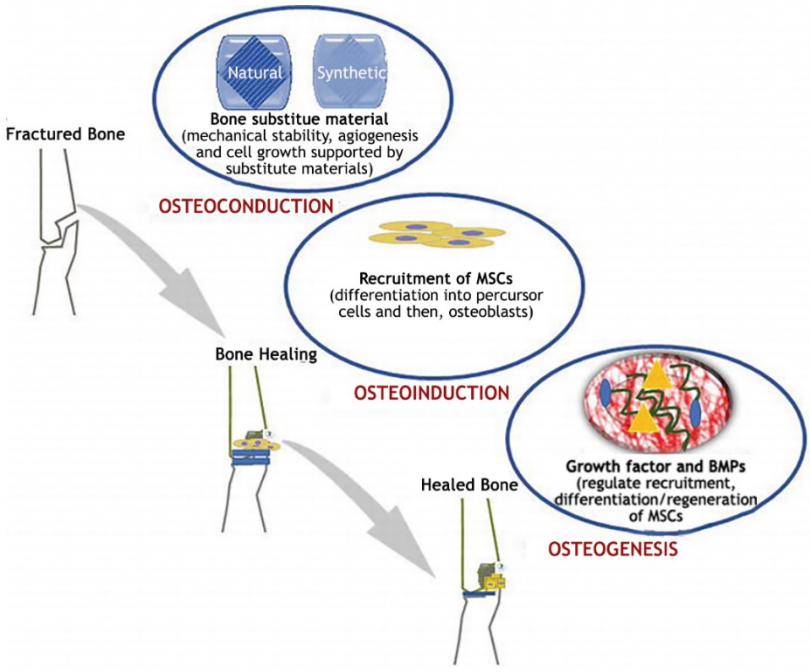

Figure 8 - Schematic representation of the healing process of a damaged bone using bone graft substitutes. Osteoconduction: a degradable support or scaffold material which provides the surface for the new bone production; osteoinduction: a matrix serves as a scaffold to support progenitor cells and osteoblasts, and it also provides a porous structure; osteogenesis: formation of the bone (bone remodelling). Adapted from [4].

Despite all the advances achieved on the last decades, there are still many drawbacks when using bone grafts. The use of autografts can be limited by the volume of bone that is possible to harvest. Furthermore, the transplanted autograft may lead to complications due to defect size. Other drawbacks include the morbidity at the harvest site, local hematoma and remodelling issues of the implanted bone [41]. Regarding allografts (grafts that have been harvested from other individual of the same species), their application can be hampered by bone tissue integration from the host and vascularization tissues. When it comes to the

distraction osteogenesis, where bone is regenerated as a result of gradually separating two viable osteotomized bone edges, it can be painful processes. The distraction phase, which requires overcoming the resistance of a soft tissue (such as skin), implies the use of a pain-inducing force. Pain can also occur as a result of premature consolidation of the bone.

In addition, this technique is also associated with poor healing and re-fracture. Consequently, there is still a need of developing novel treatments as alternatives or adjuvant methods and therapies to the standard methods currently used for bone regeneration [40] since a more sustainable, long term treatment strategy is required. To that end, bone graft substitutes (BGS) may be the answer to help impaired fracture healing.

2.2. Bone cancers and therapeutic approaches

The three most common forms of primary bone cancers are osteosarcoma (OS), Ewing sarcoma family of tumors, and chondrosarcoma, being the osteosarcoma the most common among them. Osteosarcoma as a worldwide incidence of 3.4 per million people per year and it is the third most common cancer in adolescence, affecting more frequently individuals between the ages of 10 and 25 [42,43]. It is characterized by the production of osteoid by the malignant cells and can arise in any bone, however it occurs more often in the juxta-epiphyseal regions of rapidly growing long bones, such as the distal femur, the proximal tibia, and the proximal humerus, with more than half being originated around the knee. Besides these common primary sites, this tumor tends to produce early systemic metastases. The structure is disorganized and can appear as a fine lacey trabecular pattern or as irregular clumps of osteoid (figure 9). This cancer begins as a process of medullary bone that progresses in order to destroy the cortical bone, associated with a large soft tissue component [43,44].

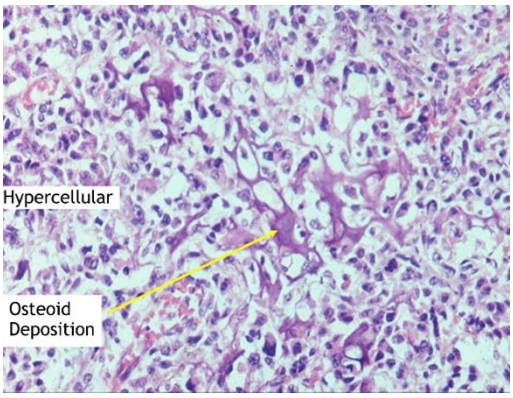

Figure 9 - Microscopic Pathology of a conventional osteosarcoma. This is a hypercellular, spindle cell tumor where cells have different sizes and shapes. It is characterized by the production of osteoid, that is often laid down in a lace-like pattern between the malignant cells. With haematoxylin and eosin stain, osteoid stains pink to red. Adapted from [45].

In terms of clinical approaches, the treatment currently used for this type of cancer includes preoperative (neoadjuvant) chemotherapy followed by surgical removal of all detectable disease (including metastases) and postoperative (adjuvant) chemotherapy. Radiation therapy

is another treatment option as a local treatment of unresectable tumors, despite OS being considered to be resistant to the application of radiation doses [44].

Ewing sarcoma is a small, round, blue cell malignancy that is the second most common primary bone malignancy in children and adolescent individuals, affecting them in the first three decades of life. The most common sites for this cancer are the long tubular bones, being the femur the bone where incidence is higher (25%) [43]. Ewing sarcoma treatment includes as a first approach, six cycles of neoadjuvant chemotherapy followed by three stages of treatment: it starts with an initial cytoreduction, to eradicate micrometastatic disease and facilitate effective local control measures, then it is performed a definitive radiation or surgical therapy to eradicate all known disease. Finally, a consolidation therapy to reduce the likelihood of tumor recurrence is used such as adjuvant chemotherapy [46].

Chondrosarcoma is a malignant mesenchymal tumor described by several differentiated cells that produce chondroid matrix. It occurs mostly in adults with most cases occurring in people over the age of 40 [43]. Regarding the treatment, the surgical resection is the primary and preferred type of treatment for patients with localized disease, whereas radiation therapy is mostly used for treating surgically hard-to-access sites and in the palliation of local symptoms, requiring relatively high doses for cure. Chemotherapy has been considered ineffective in treating this cancer however, it might be considered in certain subtypes of chondrosarcoma, such as the dedifferentiated and mesenchymal subtypes [47].

Taking all this into consideration, it is possible to conclude that surgery, chemotherapy and radiation therapy are the main approaches for treating bone cancers. These therapies present some drawbacks that need to be taken in consideration: the short and long term collateral toxic effects of using chemotherapy and even, in the case of osteoblastomas, there is a possibility of inducing chemotherapeutic agents' resistance [44]. In the case of radiation therapy, for example in treating Ewing's sarcomas (that are quite radiosensitive), this modality is less frequently used given the potential morbidities of this approach, like secondary malignancies and adverse effects on bone growth [46]. For these reasons is urgent to find novel therapeutic modalities and more target-selective treatments for bone cancers.

2.3. Bone infections and therapeutic approaches

Bone defects may occur due to several congenital or acquired conditions. Congenital bone anomalies usually arise due to the bones' absence or maldevelopment, whereas acquired bone defects often appear because of a trauma, infection, cancer, or surgical resection. Some osteodegenerative conditions, such as osteoarthritis, can be also responsible for bone loss over time, causing another type of bone defect [48]. The reconstruction of bone defects is a still a considerable clinical challenge, especially in the case of infection. It is often associated with abnormal bone remodelling due to a massive bone destruction and repair process at the site of infection, in response to bacteria and bacterial toxins [49]. Unfortunately, this phenomenon is not unusually since the region of the defective bone and most of the synthetic bone substitutes

are prone to bacterial adherence and subsequence biofilm formation, which in turn fosters the infection progression [50]. 9-36% of the patients that undergo orthopaedic surgeries suffer from postoperative deep infections after bone tumor surgeries and additional surgery is usually required. Furthermore, the use of antibiotics for extended time periods and delays in the scheduled treatments (such as chemotherapy) can lead to infection [51]. Trauma surgeries can also cause an infection after fracture fixation (IAFF) that is one of the most challenging complications when it comes to trauma surgeries. It can lead to non-union, delayed healing, permanent functional loss, and even amputation of the affected limb. This kind of infection can happen, with less extension in closed fractures (1-2%) and with greater extension in open fractures (reaching up to 30%), resulting in a remarkably prolonged hospitalization and increased economic burden for patients [52]. This infection can be caused by several agents and can be classified according to three stages, that are described in figure 10.

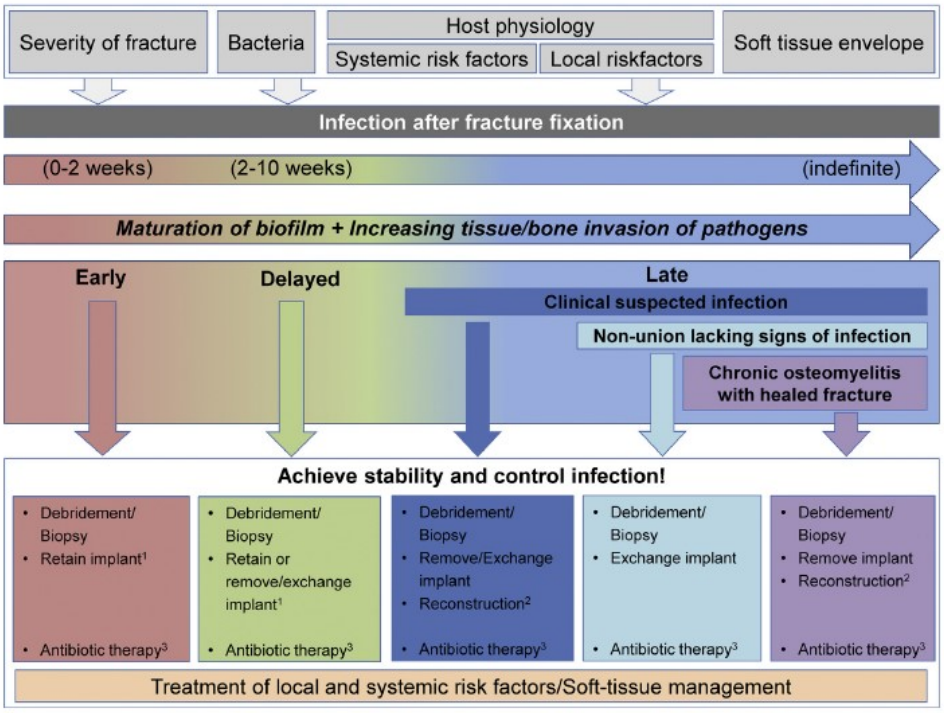

Figure 10 - Pathophysiology, classification and treatment of IAFF according to the infection stage. This classification is a continuum, meaning that there is not a line separating late and delayed infection. However, after 10 weeks, inflammation, fibrous encapsulation and osteolysis are more prone to happen which can potentially result in a delayed or non-union. Adapted from [53].

Regarding the treatment used for IAFF, most of the concepts applied have emerged from the prosthetic joint (PJ) infection treatment algorithms. Despite having similar clinical properties, there are differences regarding the elective arthroplasty patients and the trauma patients, in terms of risk of infection at the primary surgery and in treatment options. The principal difference between IAFF and PJ infection is the fact that, the first is characterized by the presence of a fracture, so there is a need for biomechanical stability for it to heal. In fact, construct stability is important not only for prevention, but also for treating IAFF [53].

The main goals of treating IAFF are the fracture consolidation; the infection eradication or, in certain cases, the infection suppression until fracture consolidation is achieved; the healing of the soft tissue envelop; the prevention of chronic osteomyelitis and the restoration of the bone functionality. It is important to consider that treating the infection is not always the priority, since the internal fixation device can be removed after consolidation is obtained (as a result, it is possible to remove the biofilm, which results in a high chance of clearance of the infection), so the bone healing is usually the primary objective. In some cases, a suppressive therapy can be established with antibiotics and the material must be retrieved after this treatment in order to avoid risk of recrudescence of infection or chronic osteomyelitis [52,53]. This is a progressive infection that results in an inflammatory destruction, necrosis and bone neoformation, that can progress to a chronic and persistent stage, with the possibility of being a lifetime chronic disease. Although there are surgical techniques to be applied to treat this condition (such as muscle grafts and antibiotic bone cements), bone infections are still a challenge. In this way, there is a need to have improvements in both prevention and treatment, so that is possible to achieve a better patient care. Such improvements may be an increased bioavailability of antimicrobial functionalized medical devices (antibacterial functionalized implants) or implant functionalization with antimicrobial peptides (AMP's), since they do not induce resistance within pathogens after exposure, as the antibiotics do [53,54].

3. New solutions – Development of bone substitutes

Bone injuries are very common and cause serious changes in the quality of life of patients. They can limit the ability to accomplish basic tasks, such as walking, and may also cause social and psychological problems. As explain in the latest section, the currently solutions available for these problems are essentially the use of bone graft transplants (autologous, allogenic and xenogenic), bone transport methods and implants based on different types of materials. These types of interventions are needed in order to ensure the regeneration of the bone and restoration of its function. When bone is not capable to regenerate itself, bone tissue engineering shows a great therapeutic potential, since the challenge associated to the current orthopaedic solutions can be solved by the development of suitable osteobiologic materials. They should replace the conventional allografts, autografts and xenografts, serving as implantable materials for bone substitutes for bone repair or remodelling [2,55]. The materials used can be classified into different types, based on substitutes like ceramic-based, metal-based and polymer-based bone graft substitutes, either with or without using various cell types. Some materials can even contain several bioactive molecules, including growth factors, such as BMP-2, TGF ß, growth differentiation factor 5 (GDF-5) and vascular endothelial growth factor (VEGF) or a mixture, expressed during bone regeneration (Table 1) [55].

Table 1 - Examples of different bone graft substitutes and its properties. Adapted from [55].

Type of bone graft	Examples
Autograft-based (Osteoconductive, osteoinductive, osteogenic)	Cancellous autologous graft - [56]
	Cortical autologous graft - [57]
Allograft-based (Osteoconductive, osteoinductive, osteogenic)	Fresh-frozen - [57]
	Freeze-dried allograft- [58]
Growth factor-based (Osteoconductive, osteoconductive and osteoinductive with carrier materials)	BMP and other growth factors - [59]
	Platelet-rich plasma or autologous platelet concentrate - [60]
Cell-based (Osteogenic, osteoconductive and osteoinductive with carrier materials)	Stem cells - [59]
	Collagen - [61]
	Gene - [62]
Ceramic-based (Osteoconductive, limited osteoconductive when mixed with bone marrow)	Hydroxyapatite (HA) - [62]
	Tricalcium Phosphate (TCP) - [63]
	Bioactive Glass - [64]
	Calcium Sulfate - [66]
Polymer-based (Osteoconductive, bioresorbable in degradable polymer)	Natural or synthetic polymers - [65]
	Degradable or non-degradable polymers - [68]
Miscellaneous (Osteoconductive, bioresorbable)	Coral HA granules - [66]

-

Taking all of this into consideration, finding an implanted biomaterial that combines both functions of therapy and regeneration should hold a great promise for diseased and damaged bone.

3.1. Important features of the new bone substitutes

A good bone graft substitute should have high biocompatibility, low immunogenicity and it should be capable to mould itself according to the injured tissue needs. In the field of bone tissue engineering, scaffolds are very important since they are biocompatible 3D structures that help the migration, proliferation and differentiation of osteogenic cells, promoting new bone formation and regeneration. In other words, they mimic the bone properties in terms of mechanical support, cellular activity and protein production through mechanical and biomechanical interactions. They should be stable, biodegradable, biocompatible, have pores and be permeable for cell seeding, nutrient transport, tissue ingrowth, and vascularization [4,67]. Biocompatibility is an important requirement, since this feature allows the material to be benign with the surrounding biological systems and eliciting minimal to mild tissue responses. Regarding biodegradability, this is a vital attribute for bone substitute scaffolds, since they can act as supportive and temporary template for cell attachment and subsequent tissue development. In this way, cells have time to produce their extracellular matrix and eventually replace the scaffold [68]. In addition, they can also be osteoconductive,

osteoinductive, and osseo-integrative in nature, in order to heal a possible damaged bone (figure 8) [4,67].

For bone tissue engineering, a large range of synthetic and natural scaffolds has been used, where they can be divided into composites, ceramics and polymers, each of them having specific properties and limitations, as previously seen in table 1 [4].

Another important feature for the development of new bone substitutes, is their capability of preventing bacterial infection, due to the current challenges associated with bone infection treatments. As such, it is urgent to find substitutes with both osteoinductive and antibacterial ability [69], which will be addressed during this work.

3.2. Ceramic-based scaffolds

Ceramic based scaffolds are inorganic preparations that are ionically bonded, being described as a family of materials with a wide variety of porosity, composition, structure and obtained by various manufacturing techniques/procedures [4]. They have high stiffness and bioactivity, allowing them to act as a temporary framework to provide a suitable environment for cell adhesion, growth and to help bone tissue regeneration. Within this class of materials, there is also the group of bioceramics. They have specific biological or physiological function and can be used directly in the human body, or in applications related to it. Regarding their bioactivity, they can be divided into bioinert or bioactive ceramics, where the difference relies on the fact a bioinert implant do not interact chemically with the living tissue after implantation, meaning that it will not cause a reaction with the host. The bioinert ceramics have a high mechanical strength, excellent biocompatibility and chemical stability, while bioactive ceramics are biodegradable and osteoconductive. In this way, both types of materials can be used as two integral parts of bone tissue engineering [67]. Different types of ceramic-based materials can be used to produce scaffolds. The commonly used bioactive ceramic are tricalcium phosphate (TCP), that has two structures with different atomic arrangements - α-TCP and ß-TCP (ß-TCP has been more commonly studied for bone applications, since the pure α-TCP has a quick resorption rate that is faster than the formation of bone, limiting its use in biomedical applications [70]); Calcium Sulfate ($CaSO_4$); Hydroxyapatite (HA); Akermanite, containing calcium (Ca), silicon (Si) and magnesium (Mg); Diopside (MgCaSi2O6) and Bioglass (BGs), composed by Na_2O, CaO, SiO_2 and P_2O_5. Regarding the bioinert ceramics, the most used materials are Aluminia and Zirconia [71].

Table 2 shows a summary of several studies performed using different bioactive ceramics for bone applications. The examples given are related to experiments performed only with scaffolds that contain the respective ceramic, but some of them have additional components, such as dopant oxides or polymeric binders to help the printing process. Additionally, only studies that had, at least, one *in vitro* test (with cells) or one *in vivo* test were considered for this table and for the ones that follow (table 2-6).

Table 2 – Ceramic scaffolds for bone tissue engineering applications.

Ceramic type	Summary	Scaffold Fabrication method	*In vitro*	*In vivo*	Ref.
B-TCP	Repair of goat tibial defects.	Polymeric sponge method	Goat bone marrow stromal cells	Skeletally mature goats	[72]
	Adequate engineered substitutes for repairing large bone defects.	Stereolithography	Human fetal bone cells	-	[73]
	Rapid bone regeneration and accelerated healing (potentiality in clinical settings).	3D printing	-	Skeletally mature New Zealand white male rabbits	[74]
	Use of these scaffolds for a variety of hard tissue repair and replacement.	3D printing	Human fetal osteoblast cell	Sprague-Dawley rats	[75]
HA	Extremely useful tissue engineering material in bone reconstruction surgery.	Foam-gel method	Rat marrow mesenchymal cells	Syngeneic 7-week-old male Fischer 344 rats	[76]
	Support the attachment, growth and ALP production of human osteoblast type SaOS2 cells.	Polymer sponge replication method	Human osteoblast like SaOS2 cells	-	[77]
	Rapid in growth of new trabecular bone across substantial distances followed by subsequent scaffold infilling.	Direct write assembly	-	Skeletally mature New Zealand White rabbits	[78]
Akermanite	Bone regeneration and bone tissue engineering applications.	Polymer sponge method	Human bone marrow-derived mesenchymal stromal cells	Male New Zealand rabbits	[79]
	New bone implants applied in load-bearing bone defect conditions.	Ceramic ink writing	-	New Zealand male rabbit	[80]
	Excellent candidates for	Selective laser sintering	MG-63 osteoblast-like cells	-	[81]

	bone tissue applications.				
Diopside	Bioactive material to bone tissue engineering.	Polymer sponge template method	Human osteoblastic-like cells	-	[82]
Bioglass	Use of these scaffolds in bone repair and regeneration.	foam replication method and unidirectional freezing of suspensions	Rat bone marrow-derived mesenchymal stem cells	Fisher 344 rats	[83]
	The scaffolds may be an excellent candidate for bone regeneration.	3D printing	Human bone marrow stromal cells	-	[84]
	Biological scaffolds for osseous repair and regeneration.	Polymer foam replication method	MC3T3-E1 preosteoblastic cells	-	[85]
Calcium Sulfate	Give a better insight into the complex nature of the process of fabrication of synthetic bone grafts and scaffolds.	3D printing	MG63 - human osteoblast-like osteosarcoma cells	-	[86]

3.2.1. Calcium Phosphate-based scaffolds

Among the class of ceramic materials for biomedical applications and, in particular, bone scaffolds, Calcium Phosphate (CaP) ceramics are the most widely used. They are available in a variety of products, due to the possibility of changing its chemical composition (Ca/P-ratios) and forms [87]. CaPs are minerals composed of calcium cations and phosphate anions that are known to be the major inorganic material in all native human bones (approximately 60%). Besides that, they are known to be biocompatible, osteoinductive and osteoconductive, which makes them an important asset for bone regeneration [88]. Furthermore, they have a high affinity for adhesion proteins and growth factors, such as Bone morphogenetic protein 2 (BMP-2), which stimulates the proliferation and differentiation of osteoprogenitor cells. In this way, CaPs can play an important role as carries for growth factors and stem cells, without the modification of its chemical surface [89]. However, the use of additives or surface coatings in CaP scaffolds can change their properties in order to enhance angiogenesis and osteogenesis [71]. Bone cements, scaffolds, implants and coating techniques are some of the bone applications that use CaP ceramics, and some of them have been even commercialized [90–92].

Since the osteoconductivity and osteoinductivity of CaP depends on its physical/chemical characteristics (for example the chemistry of the surface and its charge affects protein adsorption; the surface roughness affects the protein adhesion on the calcium phosphate surface, and the porosity of the CaP can have an effect on the bioactivity), it is important to choose the type of calcium phosphate that best suits the desired application [88]. In this way,

based on the composition, some of the most used CaPs are Hydroxyapatite, Tricalcium phosphate and Biphasic Calcium Phosphates (BCPs) (a combination of different concentrations of HA and β-TCP) [88,93], being the BCPs considered nowadays as the gold standard of bone substitutes in reconstructive surgeries [93], as suggested among several clinical studies available in the literature [94–97].

Despite the numerous advantages of CaP scaffolds, there are several circumstances where the use of a single material is not the best option to mimic the composition of natural bone. In this way, researchers started to develop composite materials [98]. In fact, composites have demonstrated to be more effective in enhancing both mechanical properties and bioactivity, compared to single ceramics and polymers [99]. Table 3 shows an overview of the literature available to date about the use of CaP-based scaffolds (composites) for bone applications. In respect to the referenced studies, only the ones that contained CaP as the main component of the scaffold were considered, whereas the polymeric or metal materials that appear associated to them are present in lower amounts or are coated into the scaffolds. In addition, some bioactive molecules may have been loaded onto the scaffolds and there is also an example of a scaffold that was further modified and biofunctionalized with additional materials (not mentioned in the table).

Table 3 – Examples of different CaP-based scaffolds for bone applications.

Scaffolds material	**Summary**	**Scaffold Fabrication method**	***In vitro***	***In vivo***	**Ref.**
β-TCP/HA/ alginate	Bone regeneration using a cost-effective and reproducible technique.	Foam replication method	Human osteoblasts (CRL-11372)	-	[100]
β-TCP/Alginate	Provide a bone tissue engineering construct for improved cell seeding, controlled growth factor release and ability to induce bone formation.	Gel-sponge method	MG-63 osteoblast-like cells	Female Sprague-Dawley rats	[101]
HA/silk fibroin	Biocomposites that can be used in bone repair and as scaffolds in tissue engineering.	Freeze-drying	Human osteosarcoma cell line MG-63	-	[102]
HA/PDLLA	Bone substitutes implanted in cancellous bone in nonweight-bearing lesions.	Composite fibre precipitation method	-	Mature male Japanese White rabbits	[103]

CaP/collagen	Fabricate calcium phosphate scaffolds for applications in preclinical small animal models of bone regeneration.	Low temperature 3D printing	C3H/10T1/2 cells	Female BALB/cJ mice	[104]
HA/TCP	Serve as precise scaffolds for intramuscular bone induction in a rat model.	3D printing	-	Lewis rats	[105]
BCP/Li	Scaffolds can be a potential candidate for bone repair applications.	3D plotting	Mouse bone mesenchymal stem cells	-	[106]
BCP/PCL	Potential tool for bone regeneration in the field of tissue engineering.	Sponge replica method	MC3T3-E1 cells	Sprague-Dawley male rats	[107]
BCP	Generation of custom-made bioartificial bone implants.	Indirect 3D printing	Primary rat osteoblasts	Syngeneic male Lewis rats	[108]
BCP/HA/PLLA	Substitute for damaged or defect bone in bone tissue engineering.	Foam replication method	Immortalized rat osteoblastic ROS 17/2.8 cell line	Sprague-Dawley (SD) rats	[99]
BCP/Chitosan/ calcium alginate	Healing of large segmental bone defects.	Sponge replica method	MC3T3-E1 mouse pre-osteoblast cells	New Zealand white rabbits	[109]
BCP/ Hyaluronic Acid/Gelatin	Scaffold for bone remodelling.	Sponge replica method	Rabbit bone marrow mesenchymal stem cells	New Zealand white rabbits	[110]

The goal of these synthetic scaffolds is not to permanently replace the bone tissue. Instead, they should stimulate bone growth and engage newly formed bone tissue, before being remodelled. Therefore, regardless of the method of scaffold production, they should present a biomimetic surface, have an open porous microstructure for bone ingrowth (figure 11) and should be biodegradable, having suitable degradation kinetics. In addition, the capacity to promote changes in the biological microenvironment to support cellular bone healing would be beneficial [87].

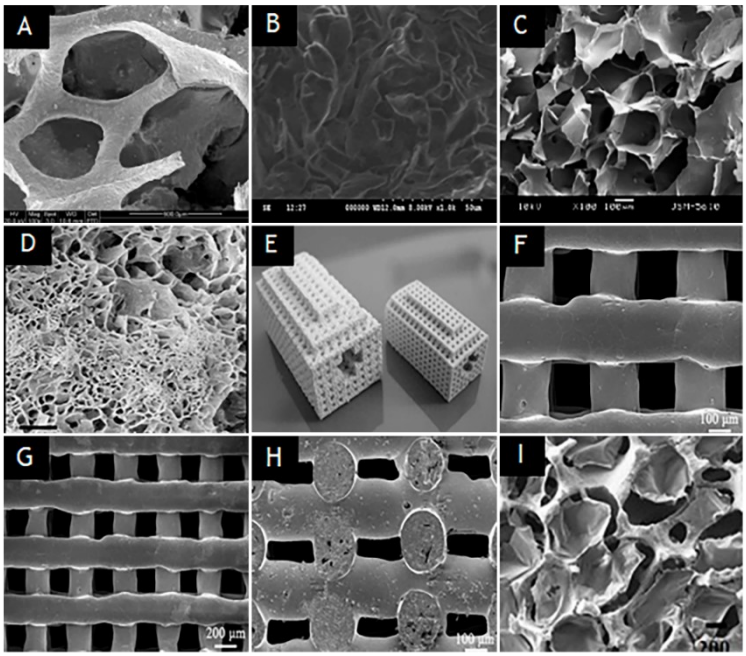

Figure 11 - Different types of CaP-based scaffolds used for bone applications. Representative structures of porous scaffolds: (A) BCP/HA/PLLA scaffold via foam replication method, (B) β-TCP/chitosan scaffold via indirect 3D printing, (C) HA/silk scaffold via freeze-drying, (D) HA/α-TCP/collagen scaffold via 3D printing, (E) HA/TCP scaffold via 3D printing, (F-H) BCP/Li scaffolds via 3D plotting and (I) BCP/Chitosan/calcium alginate scaffold via sponge replica method. Adapted from [99,102,104–106,109,111].

3.3. Polymer-based scaffolds

Polymer-based scaffolds can be distinguished as synthetic or natural, and both have been widely used as biodegradable scaffolds in bone tissue engineering. These polymers and their composites are seen as the most promising candidates for bone regeneration, due to their biocompatibility and biodegradability. Beyond that, they are very versatile, which allow them to be easily tailored to accomplish specific and desired requirements, by manipulating them in terms of chemical composition and structures [112].

Both natural and synthetic polymers have advantages and disadvantages. The former are bioactive, have biomimetic surfaces that contain particular properties that facilitate cell adhesion and cell differentiation, and they can trigger degradation and natural remodelling. However, their limitations include inappropriate immunogenic responses, microbial contamination, weak mechanical strength and they can undergo an uncontrollable degradation [68]. On the other hand, synthetic polymers can be synthesized under more controlled conditions. Giving that, it is possible to have more predictable and reproducible scaffolds, since their physicochemical and biodegradable properties (such as mechanical strength, degradation rate and microstructure) can be adapted to the desired applications. In addition, they feature more reproducibility and long shelf life, when comparing with natural polymers [112]. However, some of these polymers, in particular the ones belonging to the polyester family (which includes

polyglycolides and polylactides) have drawbacks, such as their poor biocompatibility, the release of acidic degradation products, the poor processability and the possibility of losing mechanical properties very early during degradation [113].

The most commonly used natural polymers for bone tissue engineering are collagen, gelatin, silk fibroin (SF), chitosan, alginate and hyaluronic acid. Regarding the synthetic polymers, the most used are Poly(lactic acid) (PLA), poly(glycolic acid) (PGA), the copolymer PLGA (PLA+PGA), Polycaprolactone (PCL), Poly(vinyl alcohol) (PVA), Poly(propylene fumarate) (PPF) and Polyurethane (PU) [112]. In terms of bone applications, some of these polymers can be used alone as is the case of the studies present on table 4.

Table 4 - Natural and synthetic polymers used (alone) as scaffolds for bone applications.

Polymer type	Summary	Scaffold Fabrication method	In vitro	In vivo	Ref.
Collagen	Repair and regenerate bone defects and injuries.	Electrospinning	Human fetal osteoblasts		[114]
Collagen	Promising strategy for osteochondral repair.	Temperature gradient-guided thermal-induced phase-separation technique	Rabbit bone marrow mesenchymal stem cells	Adult male New Zealand white rabbits	[115]
Silk fibroin	Scaffolds suitable for applications involving bone tissue engineering.	Electrospinning	Human mesenchymal stem cells (hMSCs)	Male athymic nude rats	[116]
Silk fibroin	The scaffolds are promising candidates for bone regeneration.	Microparticle aggregation	Osteosarcoma cell line MG63	New Zealand white rabbits	[117]
hyaluronic acid	Cell and growth factor carriers for tissue regeneration.	Michael-type addition reaction	Human mesenchymal stem cells (hMSCs)	Male Sprague Dawley albino rats	[118]
Gelatin	Bone tissue engineering strategies.	Crosslinking and freeze-drying	-	Mature male Wistar rats	[119]
PCL	Great potential for replacement of skeletal tissues.	Selective laser sintering	Primary human gingival fibroblasts	Immunocompromised mice	[120]
	Results need to be translated into more clinically relevant studies before clinical application can be considered.	Fused deposition modelling	Immortalized human mesenchymal stem cells	Female Danish Landrace pigs	[121]
PLGA	Reconstruction of rat calvarial defects	Porogen-leaching technique	Human mesenchymal stem cells	Male non-immunosuppressed	[122]

				Sprague-Dawley rats	
	Scaffolds for new bone growth when implanted in orthotopic sites where transplanted cells and secreted bone growth factors may further induce bone ingrowth from adjacent bone.	Solvent-casting particulate-leaching technique	Rat marrow stromal cells	Fisher 344 rats	[123]
	This work demonstrates the synergy between designing electrospun tissue scaffolds and providing comprehensive evaluation through high resolution imaging of resultant 3-dimensional cell growth within the scaffold.	Electrospinning	Rat osteoblast cell line UMR106 and mouse cell line MC3T3-E1	-	[124]
PLA	Biological bone graft extender for future use in the field of impaction bone grafting.	High pressure carbon dioxide mixing technology	Human bone marrow stromal cells	Male MF-1 nu/nu immunodeficient mice	[125]
	Scaffolds with precise dimensions that can be later assembled in a larger tissue engineered construct for bone repair.	Fused deposition modelling	Human bone marrow stromal cells		[126]
PPF	Scaffolds may be an attractive platform for bone tissue engineering.	Photocrosslinking	-	Male New Zealand White rabbits	[127]

Alternatively, several polymers can be used in combination with other polymers, such as the ones described in the studies reported on table 5. Due to the hight number of polymers available, wither they are natural or synthetic, by combining them, a variety of applications may be addressed, especially in the tissue engineering area.

Table 5 - Natural and synthetic polymers used (in combination with each other) as scaffolds for bone applications.

polymer type	Aim of the paper	Scaffold Fabrication method	In vitro	In vivo	Ref.
Chitosan/ Alginate	Repair of bone defects and functional bone tissue engineering applications, especially with pediatric patients.	Freeze-drying	Rat mesenchymal stem cells and MG-63 Osteoblast like cells	Female Sprague –Dawley rats	[128]
Collagen/ Glycosaminoglycan	Biomaterials that can promote effective healing of a critical-sized rat cranial defect.	Freeze-drying	Rat mesenchymal stem cells	Young-adult male Wistar rats	[129]
Chitosan/ Collagen	Differentiation platform for hMSC for regeneration of bone tissue implant.	Phase separation followed by lyophilization	Human mesenchymal stem cells	-	[130]
SF/ collagen	Scaffolds have the potential to be applied in orthopaedic, reconstructive and maxillofacial surgery	Lyophilization	rabbit bone marrow-derived mesenchymal stem cells	New Zealand white rabbits	[131]
gelatin/ chitosan	bone tissue engineering strategies.	Crosslinking and freeze-drying	-	mature male Wistar rats	[119]
Alginate/ Gelatin	Scaffolds may be candidates for bone tissue engineering applications.	Freeze drying	Mouse mesenchymal stem cells		[132]
Gelatin/ Hyaluronic acid/ Alginate	Composite matrix has a potential use for in vivo MSC-based bone regeneration.	Lyophilization	Bone marrow-derived human mesenchymal stem cells	Mice	[133]
Hyaluronic acid/PLGA	Bone regeneration.	Multihead deposition system (MHDS)	MC3T3-E1 preosteoblast cells	Sprague Dawley rats	[134]
PCL/PLLA	The scaffold can be applicable in the field of bone tissue engineering.	Salt leaching method	MG63 osteoblast-like cells	Adult male New Zealand white rabbits	[135]
PCL/PMMA	The scaffolds can be used for bone tissue regeneration.	Electrospinning	MG-63 osteoblast cells	Male Sprague Dawley rats	[136]
Polystyrene/ PCL	Bone regeneration.	Electrospinning	Human osteoblasts MG-63 and rabbit	Rat specimens	[137]

			mesenchymal stem cells		
PLGA/ chitosan	Custom-shaped bone regeneration tool for both basic research into osteogenesis and for development of therapeutic application	Particulate-leaching technique followed by crosslinking	KUSA/A1 cells	Female C3H/He mice	[138]
PU/PLA	Filler material for healing facilitation across critical-sized bone defects.	Phase inverse salt leaching method	7F2 mouse osteoblast	New Zealand white rabbits	[139]
PEG/PLA	Potential for broad application in bone tissue engineering.	Electrospinning	Rat bone marrow MSCs	Sprague Dawley rats	[140]
PLLA/PEG	Promising substrates for bone tissue engineering.	Supercritical carbon dioxide foaming technique	Mouse embryonic fibroblast cells	New Zealand white rabbits	[141]
PPF/PLGA	*In vivo* bone formation	Thermal crosslinking	-	Female New Zealand white rabbits	[142]
PLGA/PVA	Improve the hydrophilicity and cell compatibility of the scaffolds for tissue engineering applications.	Melt-molding particulate-leaching	Immortalized human costal chondrocyte cell line C-28/I2	Skeletally mature male New Zealand white rabbits	[143]

Besides all the possibilities covered in tables 4 and 5, polymers can also be combined with inorganic materials (table 6), since a single polymer does not hold the ideal properties for all applications [68,112]. The examples present on the tables 4, 5 and 6 are related to experiments that contain the materials mentioned in the first column as the main component(s) of the scaffold. However, some additional components may be present and are not mentioned on the tables (as explained before in the section of ceramic-based scaffolds), such as organic compounds, cations, proteins, loaded bioactive molecules and drugs, and polymeric binders to help the printing process. This highlights the high versatility of this type of scaffolds.

Table 6 - Natural and synthetic polymers used (in combination with inorganic materials) as scaffolds for bone applications.

Scaffold's composition	Applicability	Scaffold Fabrication method	In vitro	In vivo	Ref.
Collagen/ Apatite	Scaffold for improved bone repair and regeneration.	Freeze-casting	Mouse Calvarial osteoblasts (COBs) cells	Transgenic mice	[144]

Collagen/ CaP	Biomaterials that can promote effective healing of a critical-sized rat cranial defect.	Freeze-drying	Rat mesenchymal stem cells	Young-adult male Wistar rats	[129]
SF/CaP	Promote newly formed bone volume being a good candidate for bone implantation and provide a feasible therapeutic approach for treating patients with bone defects.	Polymer sponge template	MC3T3E-1 cells	New Zealand white rabbits	[145]
SF/HA	Initial screening tool to identify the most suitable pore size ranges/morphologies with which to pursue more detailed studies of tissue-related outcomes.	Direct-Write Assembly	Human bone marrow derived mesenchymal stem cells and human mammary microvascular endothelial cells	-	[146]
Chitosan/ Gelatin/ Graphene oxide	Application in bone tissue regeneration.	Freeze-drying	Rat calvarial osteoprogenitor cells	Male albino-Wistar rats	[147]
Chitosan/ Gelatin/ BG	Attractive to be assessed for bone reconstruction in future clinical trials.	Freeze-drying	Dental pulp stem cells DPSCs	Adult Sprague-Dawley rats	[148]
Gelatin/HA	Tissue-engineering applications.	Cryogelation	L929 mouse fibroblast cells	Female Sprague-Dawley rats	[149]
PCL/gelatin/ BCP	Bone tissue regeneration and local delivery of biomolecules.	Electrospinning	mice Preosteoblast MC3T3-E1 cells	Male Sprague-Dawley rats	[150]
Chitosan/ CaP	Bone regeneration purposes, such as some applications in dentistry.	Enzymatically-induced gelation of chitosan followed by Ice segregation induced self-assembly	Mouse C2C12 cell line	Male New Zealand rabbits	[151]
Chitosan/HA	Bone tissue engineering applications in the clinical setting.	Freeze gelation	-	Chinchilla rabbits	[152]
Chitosan/ PCL/Sr(II)	Application in bone tissue engineering such as the treatment of craniofacial	Casting/ solvent evaporation technique	MG-63 osteoblast-like cells and human bone marrow	Male albino Wistar rats	[153]

	regeneration, as well as on the active regeneration of other bone tissues.		mesenchymal stem cells		
Gelatin/ Alginate/ PVA/HA	Preliminary data to expect the suitability of the developed material for bone tissue engineering applications.	Freeze-thaw method	Human osteoblast cells and MC3T3-E1 preosteoblast cells	-	[154]
Alginate/HA	Bone tissue engineering application.	3D plotting	Human bone-marrow-derived mesenchymal stem cells (hBMSC)	-	[155]
PCL/HA	Synthetic substitute for bone tissue engineering.	Solvent casting and particulate leaching techniques	Primary human bone cells	Male ICR Mouse	[156]
PLGA/TiO2	Novel scaffold for bone tissue engineering.	Sintered microsphere method	G-292 and SaOS-2 cells	New Zealand white rabbits	[157]
PLA/ PLGA/HA	Treat segmental bone defects in the canine long bone.	Electrospinning and 3D printing	-	Beagle dogs	[158]
PLGA/HA	Treatment of bone defects.	Gas forming and particulate leaching method	Rat calvarial osteoblasts	Female athymic mice (BALB/c-nu)	[159]
PLGA/HA	Bone tissue regeneration.	Gas foaming and particulate leaching method	Osteogenic cells derived from human embryonic stem cells and primary bone-derived cells	Female immunodeficient mice (BALB/c-nu)	[160]
PLLA/HA	Bone substitute for bone tissue engineering applications.	Solid–liquid phase separation	Rat mesenchymal stem cells	-	[161]
PLA/Magnesium/Zinc/ HA/PEO/ Xenetic	Potential applications for bone implant.	Solvent casting	-	Dogs	[162]
PU/HA	Potential scaffold for bone regeneration applications.	Copolymerization and simultaneous foaming	Rat bone marrow derived mesenchymal stem cells	Male nude mice	[163]
PPF/HA	Induce the osteoblastic differentiation of	Salt leaching	Rat bone marrow stromal cells	-	[164]

	transplanted rat BMSCs.				
PPF/ß-TCP and PFF/BCP	Promising platform for the functional restoration of large bone defects.	Stereolithography	Rabbit bone marrow stromal cells	Adult female New Zealand White rabbits	[165]
PCL/PVA/HA	Potential scaffold for bone tissue engineering application.	Electrospinning	MG-63 osteoblast cells and NIH 3T3 fibroblast cells	-	[166]

3.3.1. Konjac Glucomannan-based scaffolds

Konjac glucomannan (KGM) is a natural polysaccharide (non-ionic and linear), similar to agarose, that has a backbone chain of ß-1,4-linked D-mannose and D-glucose (figure 12). The mannose to glucose ratio is 1.6:1 and the monosaccharide residues can be randomly distributed with 5–10% acetyl-substituted residues. It is one of the main components of *Amorphophallus konjac* C. Koch (Araceae) tubers, that are produced and used in China, south-east Asia and Japan. The molecular weight of KGM ranges from 200 to 2000 kDa, depending on the cultivars, origin, producing methods and storage time [167,168].

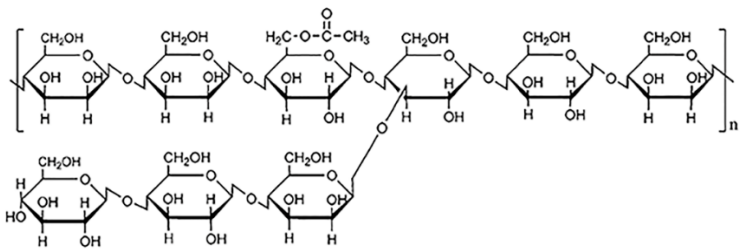

Figure 12 - The proposed chemical structure of Konjac glucomannan. Adapted from [167].

Two key features of KGM are its high viscosity and gelling properties. In addition, it is water soluble being the solution formed extremely viscous. This polymer has both hydrophilic and hydrophobic groups, but it is insoluble in organic solvents (such as methanol, ethanol, acetone or ether). It is known that the two major factors involved in the mechanism of gelation are the hydrogen bonds and the hydrophobic interactions between the KGM molecules [167]. Given that, under heating and alkaline pH conditions, KGM can become an elastic, strong and heat-irreversible gel and stable hydrogels can be formed by heating konjac flour in the presence of alkali substances [167,168].

Due to the high biocompatibility and biodegradability of KGM gels, they have been widely used for several applications, such as food, pharmaceutical carriers, tissue scaffolds and absorbing materials (figure 13) [169].

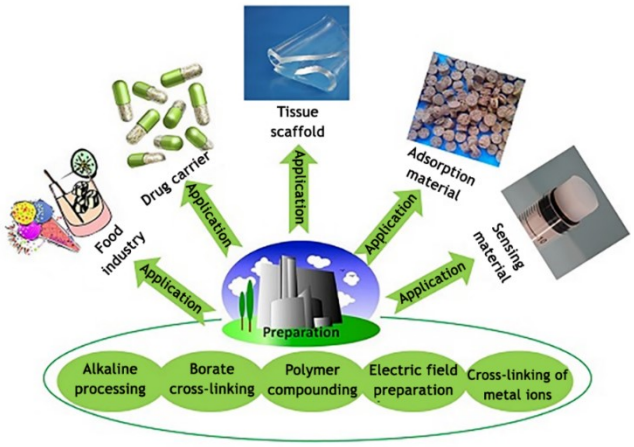

Figure 13 - Konjac glucomannan application areas. The gelation capability enables the application of KGM gels in several areas, such as food, chemical, pharmaceutical, materials, and other fields. Adapted from [169].

In the biomedical field, KGM-based gels are considered to be a potential carrier for specific bioactive protein drug delivery systems [167,169]. For example, they can be used for the design of colon-specific drug delivery systems, where KGM acts as an adjuvant, since it can be degraded in the colon but not in the small intestine. The drug release effect can be affected by the KGM category and degree of acetylation, where different profiles of this polymer and different degrees of acetylation can lead to different swelling rates and drug release effects on the prepared tablets [170]. Another biomedical application of KGM, is its use to prepare controlled release beads. KGM can be combined with chitosan (CS) and alginate (ALG) to prepare controlled release beads with KGM wrapped within, where the KGM can help increase the drug payload [171].

Besides acting as drug delivery system, KGM-based materials can be used in scaffolds for tissue engineering applications, namely in wound dressings. For example, KGM/CS were blended in a film that could be used for wound healing and haemorrhage control. The microporous structure of the film allowed it to absorb water from the blood and trap blood cells [172]. Films based on KGM/CS were found to be nontoxic, biofunctional, biodegradable, biocompatible and to having antimicrobial properties [173]. Moreover, KGM could significantly improve mechanical properties of CS as a wound dressing material, and the breaking elongation and tensile strength were improved in about 40% and 30% respectively [174]. Besides that, the addition of KGM improved the biocompatibility of CS materials [175].

3.4. Other agents

Besides the usual ceramic-polymeric materials that can be used to develop bone substitutes, other agents can be used to enhance the properties of such systems. Between them, polydopamine (PDA) can be highlighted due to its photosensitive properties. PDA is a dopamine derived synthetic eumelanin polymer which in the past few years has gained attention in the field of coating materials [176]. The main advantages of PDA are its ability in attach to almost all material surfaces, including metal, oxides, ceramics and polymers, and

their properties as biocompatible materials [177]. Other interesting aspects are their fluorescence quenching and photothermal conversion abilities, which arouses interest in the use of these agents in a wide range of applications such as biomedicine [178].

For that reason, when looking for a bi-functional material to be used in bone tissue engineering applications, PDA sounds a promising agent to be included on such systems. In fact, dopamine-based materials have been used for diagnosis and cancer therapy and also as theranostic agents (an agent with both therapeutic and diagnostic applications) [178]. In terms of cancer therapy, photothermal therapy has arising as an effective technique due to its high selectivity and minimal invasiveness. The process consists in applicating a localized near infrared (NIR) laser (650-950 nm) that can increase the temperature of the photothermal therapeutic agent that is located on the tumor sites. Thus, this increase of temperature is high enough to kill cancer cells by photothermal effects. Besides that, this approach functions in a spatiotemporal manner, without damaging the healthy cells and surrounding tissues [179].

In conclusion, since the already established use of PDA in combination with ceramic materials that can be used for photothermal cancer therapy [180], the inclusion of this agent in hybrid polymeric-ceramic scaffolds sounds promising.

3.5. Scaffolds production - Additive manufacturing

Addictive manufacturing (AM) refers to a series of techniques characterized by blending materials, either by fusion, binding or solidifying materials (such as liquid resin and powders) [181], creating objects in a layered fashion. The layers are formed under computer's control in order to develop 3D products [182,183] meaning that the tree-dimensional (3D) geometric information of the designed object is determined by computer-aided design (CAD) models of the object parts, or by scanning objects in two dimensions and processing the acquired data into a 3D model. Afterwards, the sample is fabricated from a powder or from a sheet material [71]. Other terminologies can be used to describe AM processes, such as 3D printing (3DP), rapid prototyping (RP), direct digital manufacturing (DDM), rapid manufacturing (RM), and solid freeform fabrication (SFF) [181].

This kind of technique is a better approach when compared with traditional strategies, since a superior structure-function relationship is observed, when an object is 3D printed and forms composites with a controlled spatial heterogeneity [184]. This feature has made 3D printing an extremely useful tool, both in the fields of biomedical research and tissue engineering, due to the capability of replicate the intrinsic architecture and the cellular heterogeneity of tissues and organs. In terms of bone grafting, the ability to print biocompatible, patient-specific geometries with controlled macro- and micro-pores, creating personalized implants, and the possibility to incorporate drugs and proteins, has made this technology ideal for orthopaedic applications [184]. Besides that, other advantages include the reduced time and cost of making sample implants or physical models, one at a time or even in small batches, and the improvement of doctor-patient communication, helping surgeons to

have a better preoperative assessment of the condition, allowing the design of more reasonable operation plans [71].

In terms of tissue engineering, some AM techniques currently available for bone scaffold fabrication are 3D printing, various forms of direct writing, such as direct write assembly/robocasting, Selective laser sintering (SLS) , Stereolithography (SLA) and Fused deposition modelling (FDM) [71,185]. Figure 14 presents the most commonly techniques employed in tissue engineering and several examples are given for the field of bone tissue engineering.

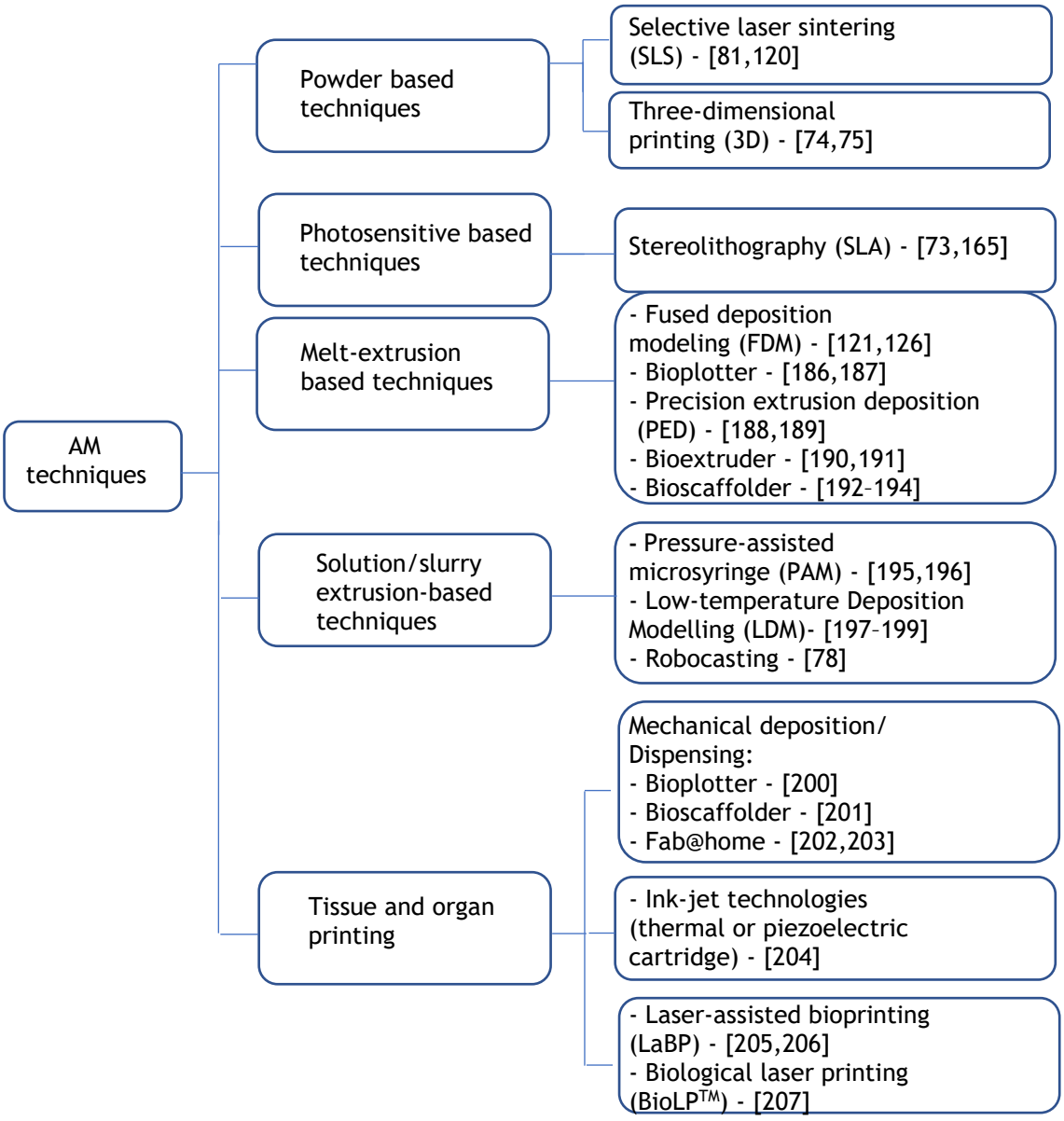

Figure 14 - Some of the most commonly used AM techniques for tissue engineering and their classification. Examples of bone tissue applications are given in each technique. Adaped from [208].

The principal AM techniques are described on figure 15. The Stereolithography technique (figure 15-A) is based on a low power but highly focused UV laser, used to trace out successive cross-sections of a three-dimensional object, in a vat of liquid photosensitive polymer [209].

The fused deposition modelling technique (figure 15-B) uses a plastic or wax material, that is heated and extruded through a nozzle that traces the object cross sectional geometry, layer by layer [210]. Regarding the selective laser sintering (figure 15-C), this technology uses a moving laser beam to trace and selective sinter the desired material into successive cross-sections of a three-dimensional part, that is built upon a platform. This platform adjusts its height as equal to the thickness of the layer being built [211]. On the 3D printing process (figure 15-D), that is an ink-jet printing-based technology, the head of the ink jet prints a liquid binder onto thin layers of powders, based on object profiles that have been generated by a software [75]. Finally, the robocasting technique (figure 15-E) consists on the robotic deposition of highly concentrated colloidal suspensions, that are capable of supporting their own weight during assembly. For that reason, an ink with appropriate rheologic properties is necessary for printing with this technique [212], as it will addressed in the next section.

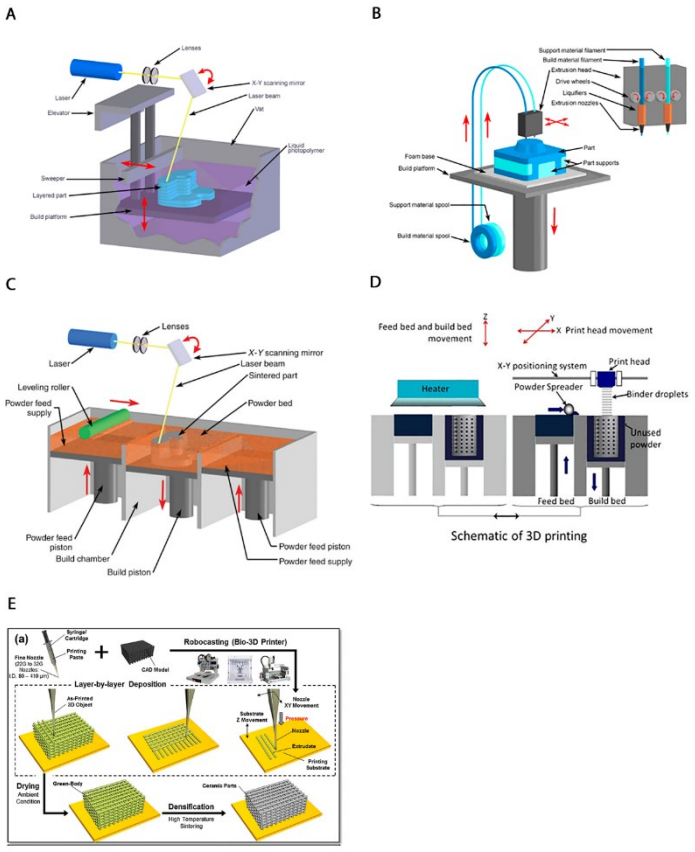

Figure 15 - Representation of the most used AM techniques for tissue engineering. (A) Stereolithography. (B) Fused deposition modelling. (C) selective laser sintering. (D) 3D printing. (E) Robocasting. All these AM techniques feature different characteristic and specifications, that distinguish them from one another and allow a broader range of applications that can be achieved with additive manufacturing. Adapted from [75,209–211,213].

3.5.1. Robocasting

Robocasting is often referred to or included in the definition of Direct Ink Writing (DIW), Direct-Write Assembly (DWA) or Microrobotic Deposition. It is an additive manufacturing

technology that is based on a robotic deposition of colloidal suspensions at high concentration (inks), that are able to support their own weight during the assembly [214]. In this way, lines of ink are laid down in a controlled manner to build up a 3D structure in a layer-by-layer fashion, following a computer-aided design (CAD) model, that is used to control the movements of the robocaster (figure 15-E). Comparing this technique with other AM processes, robocasting allows the building of ceramic scaffolds using water-based inks with minimal organic content (<1wt.%) and it does not need a especial support material or mould [215]. One of the main advantages of this technique is the mechanical quality of the produced material and the flexibility of technology in printing different materials.

Until now, different studies have shown the possibility of developing calcium phosphate-based scaffolds through robocasting, using ß-TCP [214], HA [216], Biphasic calcium phosphates (HA/ß-TCP) [217] and even ceramic/polymeric composites (Table 7). Besides that, robocasting is also able to produce metallic [218], polymeric [219], graphene [220] and ferroelectric [221] inks.

Table 7 – Examples of several studies using different ceramic/polymeric scaffolds fabricated by robocasting.

Main components	Aim	Ref.
Si-doped HA/Gelatine	Optimize the processing conditions to fabricate, by rapid prototyping, composite scaffolds with a high content of ceramic and without the addition of any sort of additive, by means of a simple, fast and low-cost procedure.	[222]
ß-TCP/PLA or PCL/Darvan® C (dispersant)/ hydroxypropyl methylcellulose/PEI (flocculant)	Study the effect of polymer infiltration on the compressive strength of ß-tricalcium phosphate scaffolds fabricated by robocasting.	[223]
HA/PLA or PCL and 6P53B glass/PLA	Show how hybrid organic/inorganic scaffolds of various chemical compositions with well controlled architecture and porosity can be built using robotic assisted deposition at room temperature	[224]
45S5 Bioglass/carboxymethyl cellulose (additive)/ poly(methylvinyl ether) (additive)	Overcome the difficulties of producing scaffolds from 45S5 Bioglass by Direct-writing fabrication techniques	[225]
13-93 bioactive glass/PLA or PLC/carboxymethyl cellulose (additive)	Study the effect of polymer infiltration on the mechanical properties of 13–93 bioactive glass scaffolds fabricated by robocasting	[226]
HA or ß-TCP or BCP /Pluronic	Design a flexible ink formulation approach to print a wide range of calcium phosphates	[227]
Aluminium oxide/ PAA (dispersant)/PEI(flocculant)/ Methylcellulose(thickening agent)	Study the rheological behaviour of Al2O3 suspensions containing polyelectrolyte complexes for direct ink writing	[228]
HA/ß-TCP/Pluronic F-127	investigate the porosity, mechanical property, and degradation of the scaffolds.	[229]

The key factors for robocasting are the properties and composition of the inks. They must be homogeneous, free of air bubbles entrapped, have a high-volume fraction of ceramic powder and the correct properties of flow. This allows both the extrusion and the ability of holding the

shape after printing. Several studies demonstrate that the ink used must be highly shear thinning in order to allow the extrusion through fine nozzles, while being capable of retain a degree of strength and stiffness to be self-supporting after printing [230].

3.6. Drug Delivery

In bone tissue engineering, scaffolds are important not only to the bone regeneration and formation, but also, they show an enormous potential in the field of drug delivery systems. By loading drugs into scaffolds, it is possible to treat bone disorders or to act on the surrounding tissues, using an adequate therapeutic concentration level and during a specific/desired time [231]. This method brings several advantages when comparing with the systemic administration of the drugs, since it can minimize the side effects and the risk of over dose, as well as having the capacity of improve the bioavailability of the drug with the appropriate therapeutic concentration at the target site [232]. In addition, the direct delivery of biomolecular agents (such as growth factors or therapeutic agents) from the scaffold can enable the protection against the extracellular barriers that could reduce their therapeutic efficacy, by protecting them from being attacked by the immune system [232]. When it comes to 3D scaffolds, they have shown the capacity to deliver therapeutic drugs in a controlled manner [233].

Both bioactive ceramics and biodegradable polymeric materials can be used in bone tissue engineering as drug delivery vehicles. However, in the case of bioactive ceramic materials, the drug delivery patterns observed are difficult to control and, regarding the biodegradable polymeric materials, they show impaired osteoconduction and they can also provoke an adverse response due to inflammation that occurs as a result of acidic degradation [234,235]. The possibility of combining bioceramics (CaP, silicate BGs and HA) with biodegradable polymers is a promising approach because not only should improve the degradability of the inorganic material, it should also help to achieve more controlled drug release profiles when compared to pure ceramics [233].

Virtually all the types of drugs can be incorporated on the 3D scaffolds, with literature showing many examples of antimicrobial agents, anti-inflammatory drugs and other type of drugs [233]. Antimicrobial agents are important to treat bacterial infections, that can occur on scaffolds and medical implants. Levofloxacin is a quinolone antibiotic that has shown antimicrobial effects against planktonic and biofilm forms of *Staphylococcus aureus*. It is able to penetrate into both trabecular and cortical bone and can minimize the risk of bacterial resistance. Levofloxacin can also be incorporated on 3D meso-macroporous scaffolds based on nanocomposites making these scaffolds suitable for the treatment and prevention of osteomyelitis [236,237]. Regarding anti-inflammatory drugs, ibuprofen is one of many examples that can be incorporated on biodegradable scaffolds to reduce wound inflammation and patients' pain [238].

3.6.1. Strategies for drug incorporation

When loading an agent into a 3D scaffold, it is important to consider both its encapsulation efficiency and its sustained release rate in order to allow an effective therapeutic dose during the desired time. They can be loaded into a scaffold either by attachment to the material surface or by entrapment within the scaffold [232]. Some of the most used approaches to load biomolecular agents into the scaffolds are (figure 16):

A. Adding the molecular agent/drug directly into the polymer solution or emulsion that will be used subsequently to fabricate the scaffolds [239];

B. Immerse a prefabricated scaffold into a drug-containing solution, to allow the drug adsorption into the scaffold surface or to get a polymer coating with better ability to control drug release [240].

C. Load micro/nanospheres that contain the agent into the scaffold. The incorporation of the nano/microspheres can be done after the scaffold fabrication [241], or before [132];

D. Incorporate functional groups into scaffolds' surface (surface functionalization), allowing specific interactions between the agents and the scaffolds' surface [242].

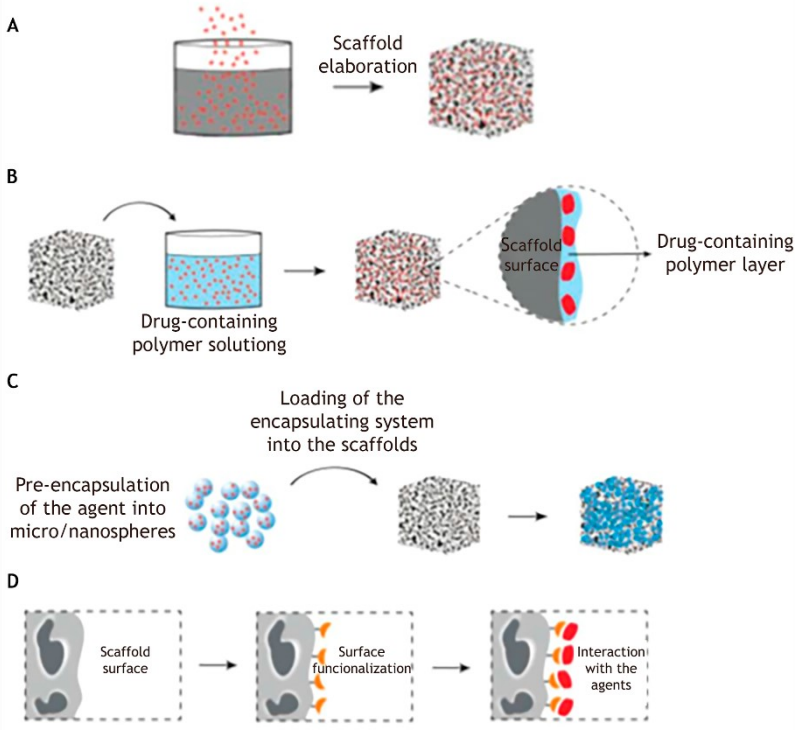

Figure 16 - Schematic representation of different approaches for loading drugs into scaffolds. (A) In this method a molecular agent is added to the polymer solution or emulsion before the scaffold fabrication; (B) a scaffold is immersed in a drug containing solution to allow the drug adsorption into the scaffold; (C) shows a pre-encapsulation of the agent using micro/nanospheres that are subsequently loaded into the scaffold and (D) uses a specific interaction, through the introduction of a functional group into the scaffold surface, to achieve a better control of the bond between the scaffold and the agent. Adapted from [232].

Despite the advantages of each method, drug-containing micro/nanospheres loaded into a scaffold seems to bring some advantages over the other methods. Since the encapsulation system and the scaffold can be made from different biomaterials, it is possible to provide

interesting and different composite alternatives to be used in each specific condition. By combining a biodegradable polymer for the drug encapsulation system (to obtain a fast degradation rate and sustained release of the entrapped drug) with a composite material with lower degradation rate and robust mechanical properties, it is possible to manufacture a scaffold that fits the requirements for bone tissue engineering applications. In addition, by encapsulating a drug, a physical barrier is created to prevent the diffusion of the agent before the encapsulation system has been sufficiently degraded [232]. As such, by modifying the composition of the encapsulation system, it is possible to tune its degradation rate and the subsequent release of the entrapped drug, which allows maintaining the therapeutic dose for the required period of time [243]. Moreover, by using drug-containing micro/nanospheres, it is possible to obtain a better control of the drug release, since the encapsulation system can be studied and optimized independently, before its incorporation on the scaffold [244]. Additionally, the possibility of loading two (or even more) biomolecular agents into nano/microspheres, with different degradation profiles and to be released at different time-points is being studied [245].

Since drug-containing nanoparticles (nanomedicines) are gaining attention as non-invasive therapeutic devices [246], this was the elected method to develop a drug loading scaffold in this work. After the drug incorporation into the nanoparticles (and before its loading into the scaffold), it is necessary to verify how much drug is effectively encapsulated within the nanoparticle, once variations in drug encapsulation can alter the therapeutic activity of the encapsulated drug (even if the number of particles is the same) [246]. The most used techniques to access this parameter are HPLC (High performance liquid chromatography) and Ultraviolet-visible (UV-Vis) spectroscopy and the choice between both will be based on the type of drug that was encapsulated.

High-performance liquid chromatography is a separation technique (figure 17), that can be applied to analyse compounds of different samples and it is possible to select the type of HPLC, depending on the nature, chemical structure, and molecular weight of the analytes [247].

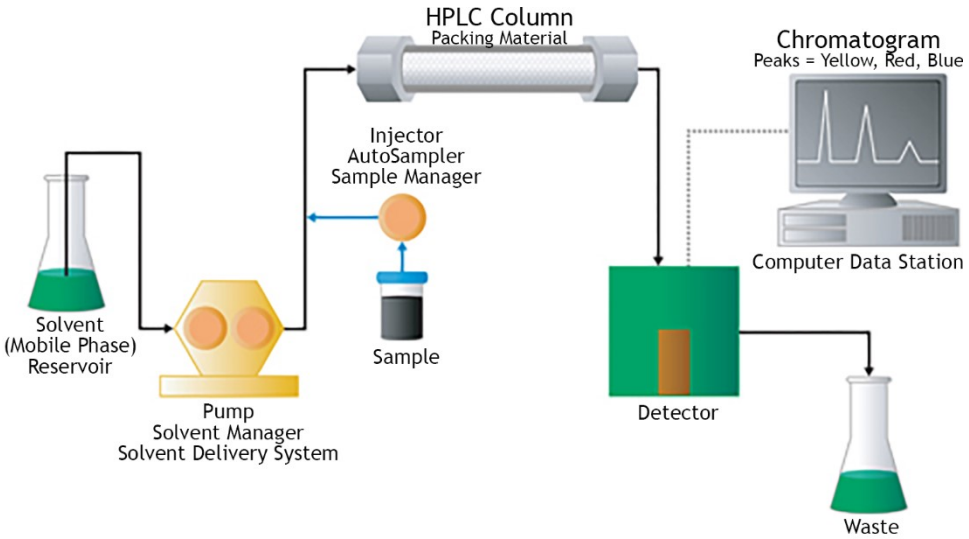

Figure 17 - Diagram illustrating the components of a basic high-performance liquid chromatography. The solvent (mobile phase) is hold on a reservoir and a high-pressure pump is used to generate a specific flow rate of this mobile phase. After, an injector introduces the sample into the continuously flowing mobile phase stream, carrying the sample into the HPLC column that contains the chromatographic packing material (stationary phase) needed do perform the separation. The use of a detector is the necessary to see the bands of the separated compound, as they elute from the HPLC column. Afterwards, the mobile phase exits the detector and is sent to waste (or collected). Adapted from [248].

The UV-vis spectrophotometry is a quantitative analytical technique based in the absorption of near ultraviolet (180-390 nm) or visible (390-780 nm) radiation by chemical species in solution or in the gas phase. The energy that gives rise to the electronic transitions are provided by the near-ultraviolet and the visible regions of the electromagnetic spectrum (figure 18) [249]. It is a very rapid, simple and low cost method and there are spectrophotometers available virtually at any laboratory [250].

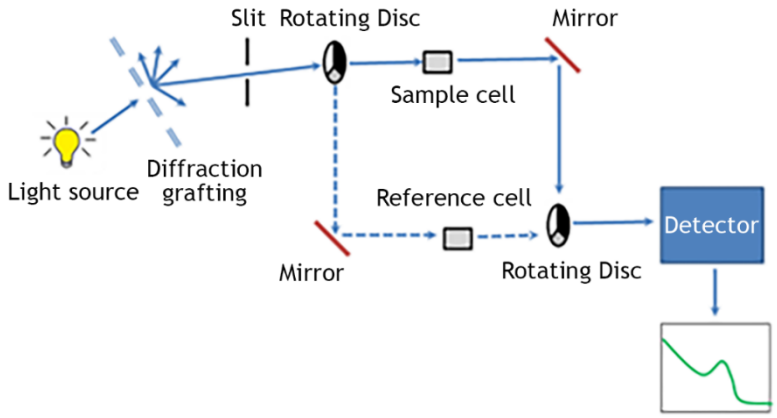

Figure 18 - Schematic of an UV-visible spectrophotometer. A beam from the UV/visible light source is separated into its component wavelengths by a diffraction grafting and the light from the slit falls onto a rotating disc. After, if the light hits the transparent section of the rotating disc, it goes straight through the sample cell, it is reflected by a mirror, hits the mirrored section of a second rotation disc and then is collected by the detector. However, if the light hits the mirrored section of the first rotation disc, it passes through the reference cell, hits the transparent section of a rotating disc and then is collected by the detector. Finally, the detector converts the light into a current signal that can be read by a computer. Adapted from [251].

There are some studies comparing these two techniques. One of them, related with the encapsulation of Lychnopholide (a sesquiterpene lactone isolated from Lychnophora trichocarpha) in a nanocapsule, revealed that the UV-spectrophotometry was appropriated to determine the encapsulation efficiency and drug loading; however the HPLC-DAD (high-performance liquid chromatography-diode array detection) was more sensitive to quantify the entrapped agent in dissolution/release studies, in which very small amount of drug is released over time [252]. Another work, related with the determination of repaglinide (a miglitinide class of antidiabetic drug) in tablets, demonstrated that the quantitative determination of the drug was more accurate and precise when using HPLC, over the UV method. However, the UV method brings the advantage of not needing the elaboration of treatments and procedures usually associated with the chromatographic method and it is less time consuming and

economical [253]. Finally, another study revealed that these two methods applied to determine doxorubicin in pH-Sensitive Nanoparticles, have showed non-significant differences; however, they have chosen the HPLC technique to determine not only the drug encapsulation efficiency but also to measure the in vitro release of the drug and to perform degradation kinetic studies, which suggests the versatility of the technique [172].

3.6.2. Drug release

Controlled release drug delivery systems seem to have great advantages over conventional dosage forms, such as the ability of performing a localized drug delivery, a reduction in the dosing frequency and enhanced patient compliance, a decreasing in the *in vivo* fluctuation of the concentration of the drug and the possibility of maintaining the drug concentration in a desired range, providing a therapeutic action for an extended period of time (figure 19), as well as fewer side effects. In this way, this is one of the most desired features when develop a system for drug delivery [254,255].

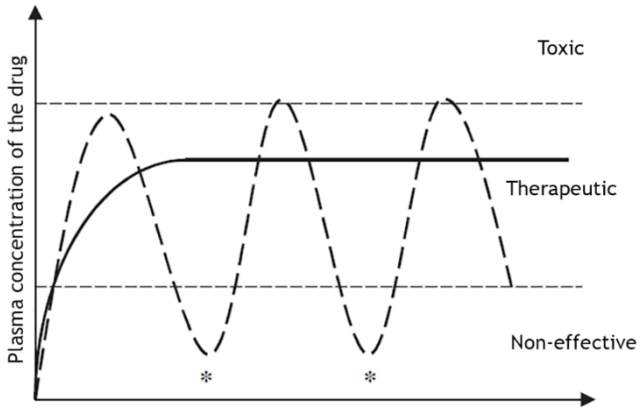

Figure 19 - The plasma concentration of drug in the patient represented as a function of time after administration. The dashed line represents traditional delivery systems with repetitive administration (*). The continuous line represents prolonged delivery system. The prolonged drug delivery system is characterized by the release of the drug in a controlled way, to maintain an appropriate and therapeutic plasma concentration for a long period of time. Adapted from [255].

Among all type of materials, biodegradable polymers are gaining an exponential interest in the field of controlled drug release. In fact, is has been shown that by incorporating the therapeutic agent into a biodegradable polymeric vehicle, the agent is continuously released as the polymer degrades [255,256]. This process can be achieved following 3 phases. First, the erosion of the polymer is the triggering step, where the drug molecules entrapped will be liberated and released as the matrix is degraded; then the diffusion of the drug particles through the matrix takes place, being the concentration gradient the driving force of this process; and finally, there is the dissolution of the drug into the surrounding medium [255] (figure 20).

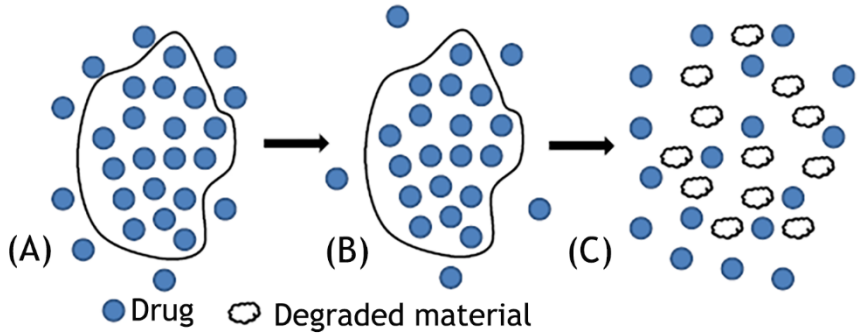

Figure 20 - Schematic representation of the degradation-controlled drug release mechanism in polymeric materials. (A) the drug is released from the matrix surface or pores that are connected to the surface. (B) A little degradation of the matrix takes place, being the remaining drug entrapped (C) the entrapped drug is rapidly released when the matrix disintegrates. Adapted from [257].

To ensure the quality and performance of a product, several *in vivo* and/or *in vitro* experiments need to be conducted. Since the *in vivo* experiments need human subjects/animals are expensive and are labour-expensive, *in vitro* release tests are gaining more relevance as surrogate tests to assess the product performance, where they can be used as predictors of the in vivo behaviour. Generally, these tests are performed at the physiological temperature (37 ºC). In terms of nanoparticles, the drug release from these nano-sized dosage forms, can be evaluated using one of the 3 methods: sample and separate (SS), dialysis membrane (DM) and continuous flow (CF) [258] (figure 21). In SS (figure 21 – A) the nanoparticles are introduced into the release media that is maintained at a constant temperature and the drug release is assessed by sampling of the nanoparticles' release media (supernatant or filtrate) [258]. The release media is selected based in the drug solubility and stability over the duration of the release study. Moreover, the size of container, agitation speed and sampling methods can be adjusted accordingly with each experiment [257]. In the DM method (figure 21 – B), the utilization of a dialysis membrane allows a physical separation between the dosage form and the bulk media and the drug release is assessed, generally, from the outer bulk over time. This method is considered to be is the most versatile and popular for assess drug release from nano-sized dosage forms [258,259]. The CF method (figure 21 – C) is characterized by an apparatus consisting of a flow-through cell that holds the sample, a pump and a water bath in a closed or open ends system. The drug release occurs since the buffer or media is constantly circulating in the column that contains the drug-loaded particles and is monitored by collecting the eluent at periodic intervals [258,259].

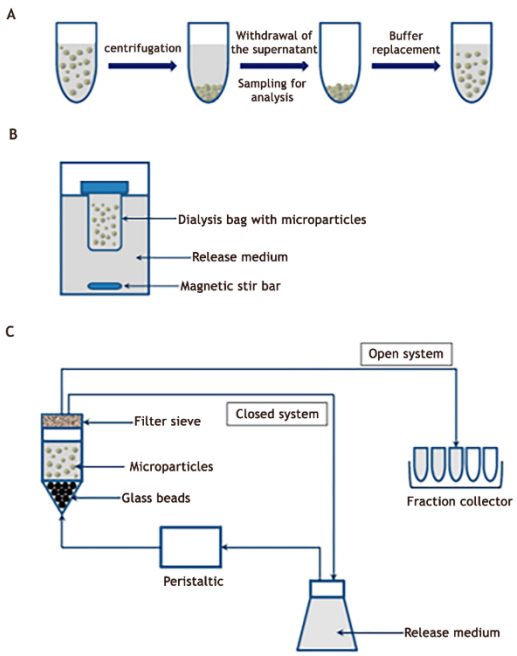

Figure 21 - Schematic representation of the methods used to determine the in vitro drug release profiles from nano-sized dosage forms. (A) Sample separation method; (B) dialysis membrane method; (C) continuous flow method. Adapted from [259].

The ultimate goal of these methods is to prepare the samples to assess the drug release. In this way, HPLC is a suitable and validated quantitation method that can determine released drug concentrations from nano pharmaceutical formulations. It is one of the most common techniques used for this purpose and it can be applied in different physical conditions, over different periods of time [260–263].

Moreover, there are many types of HPLC methods that depend on the type of column and detector, being sometimes difficult for the researches to choose the most suitable method for their nano drug delivery system, as well as a simple, fast and validated HPLC technique [264]. However, there are still several studies that use UV-vis spectrophotometry technique [265–267].

After assessing the drug release from the nanoparticles, it is necessary to evaluate the effective drug release from the scaffolds. This feature can be controlled by choosing the type of scaffold material that is used, the amount of drug that is loaded, the formulation factors and the fabrication process. The mechanisms follow by this process can be divided into three categories: solvent-controlled, diffusion-controlled, and degradation controlled. The latter is usually the mechanism adopted by biodegradable scaffolds, while the nondegradable scaffolds typically follow the diffusion and/or solvent controlled mechanism. However, the desired release profiles, such as constant, pulsatile and controlled behaviours within the specific site, can be accomplish by an appropriate combination of these mechanisms [257]. In respect to the quantitative analysis of the drug/bioactive agent released from de scaffolds (that containing the drug/bioactive agent encapsulated on a nanoparticle), as suggested in the literature, the preferred method to assess this parameter seems to be the same used to evaluate the drug release from the nanoparticles [261,265,268] but, in several cases, the quantification is only

performed once, after the nano system is incorporated into the scaffold [266,267,269]. Either way, the HPLC and UV-Vis spectrophotometry were, once more, the preferential choices.

3.6.3. Challenges in developing drug release scaffolds for BTE

Despite the recent advances in the development of bioactive bone tissue engineered scaffolds with a further drug-delivery capability, it seems that there are still challenges needed to be addressed in this field, such as controlling the effective and sustained release of the drug, prolonging the drug stability and activity, and avoid cell toxicity [236,270]. Moreover, a large breakthrough is still needed regarding the biological information available in this subject [233]. It is extremely important to fully understand both *in vitro* and *in vivo* performance of this unique type of scaffold but, by reviewing the literature, it is hinted that there is a lack of biological data (such as *in vivo* studies) regarding some important aspects in this field. One aspect that still needs more studies is the relationship between the specific drug concentration needed and the local microenvironment, and how this is affected by the interaction between the new tissue and the scaffold [233]. In addition, the vascularization process in the scaffolds needs to be further investigated due to the insufficient vascularization, which in turn reduces the survivability of the cells especially when dealing with large bone defects, that may be responsible for slowing the progress of this kind of scaffolds in clinical circumstances [232]. Regarding the scaffolds processing parameters and their effect on scaffold microstructure and on the resulting drug-release profiles, biodegradation behaviours and scaffold's mechanical and physical properties need further investigation [233]. Other challenges within this field include a better understanding of the connection between the variables that determine the scaffold-processing conditions and the stability of the incorporated drug in the nanoparticles. In this way, it is necessary to achieve an accurate control over time and space of specific quantities of the drug (in specific applications) and evaluate the interactions between the drug and the scaffold, the solubility of the drug and the amount of drug loaded that is effectively available to be delivered [233]. Moreover, one of the major challenges for developing composite scaffolds with a drug delivery function, is the incorporation of such function with sufficient complexity, in order to induce the release profiles that may be necessary not only for an effective vascularization, but also for an appropriate osseointegration and bone regeneration [232].

To overcome some of these challenges, scientific efforts are being directed to the design of 3D scaffolds than can contribute simultaneously to the regeneration process, by promoting integration, angiogenesis and osteoconduction and to the delivery of drugs [236,271–274]. In the field of 3D scaffolds production, as seen in a previous section, robocasting seems to be the preferential choice when choosing a method to print 3D ceramic-based scaffolds and some studies reveal also its applicability in develop scaffolds for both bone applications and drug delivery [222,236,275]. However, even this promising approach brings challenges, such as the necessity of including a sintering step at high temperatures (1100-1200 ºC) after printing the scaffolds, in order to achieve adequate mechanical properties. This hampers the incorporation of temperature sensitive bioactive molecules in the extrudable ink before the sintering step

and this process can also lead to shortcomings in the resulting scaffold, which is translated in unexpected crystallizations, unstable mechanical properties due to shrinkage and low biofunctional performance. Alternatively, the bioactive molecules can be added after sintering but this process may result in a low adsorption efficiency and insufficient clinical effects, as well as discontinues release [275,276]. Moreover, the impregnation process limits the amount of the biomolecules that are incorporated, the capacity of the scaffold adsorption, as well as their surface properties. This means that it is required a high concentrated solution to incorporate only a small amount of drug in the scaffold [275]. Therefore, a good way to surpass this problem can rely on the production of sintering-free scaffolds, which holds a great promising of develop multifunctional ceramic based scaffolds for bone tissue engineering [275,276]. In this work, this will be the approach used to introduce the drugs/bioactive molecules on the 3D scaffolds, which will be printed by robocasting.

4. Aim of the thesis

The main goal of this thesis is to develop a sintered-free 3D system, fabricated by robocasting, that can function as a multi-functional material for bone tissue engineering applications. Initially, the strategy designed to achieve this goal was the incorporation of nanoparticles loaded with levofloxacin in our 3D scaffolds of KGM/bTCP-nanoHA in other to not only promote bone regeneration but also be able to treat bone infections. The nanoparticles were produced but due to operational issues and equipment unavailability, the drug incorporation into the NPs was not achieved and we could not optimizer further this process. For that reason, we were not able to test the incorporation of LEVO-NPs on the 3D scaffolds produced by AM.

As a result, a second strategy was developed with the resources that were available. Our alternative approach consisted on the incorporation of polydopamine particles in our KGM/bTCP-nanoHA 3D scaffolds. The goal is making our 3D scaffold bi-functional, allowing it not only to promote bone regeneration, but also making it suitable to kill tumor cells by hyperthermia.

Accordingly, the specific goals of the thesis include:

1. The development of alternative scaffolds than the ones previously used in the scope of the project in which this thesis is inserted. The in-house produced powders were substitute for commercial powders given the lower reproducibility of the former.
2. Study the rheological behaviour of the scaffolds' inks, in order to conclude about their suitability for robocasting printing.
3. Assess the mechanical and structural properties of both type of scaffolds to infer about their suitability for bone applications.
4. Perform *in vitro* tests on our "base" material (composed by KGM and a mixture of HA and ß-TCP powders), previously develop in the scope of the project in which

this thesis is inserted. The objective is to infer the ability of these scaffolds in promote bone regeneration, by seeding them with MSCs.

5. Production of polymeric-levofloxacin loaded nanoparticles with the rationale of using this system to develop a scaffold with controlled drug release features.
6. Inclusion of PDA particles (previously developed in the scope of the project in which this thesis is inserted) on KGM/bTCP-nanoHA 3D scaffolds material to infer about their potential in killing cancer cells. For that reason, *in vitro* studies were conducted:
    - using hMSC to test the biocompatibility and the ability to differentiate onto the osteogenic lineage
    - osteosarcoma cell-line to study their behaviour on our 3D systems. The use of this type of cells will be needed to demonstrate that, under hyperthermia conditions, the scaffolds might induce cancer cell death in future studies.
    - An SBF assay to assess the scaffolds ability in predict the *in vivo* bone bioactivity of a material, by analysing the formation of apatite on their surface.

Materials and Methods

1. Materials

To produce the Levofloxacin nanoparticles, Levofloxacin (LFX) powder was purchased from Sigma-Aldrich (USA), pluronic was purchased from Merck (Germany), PLGA (PURASORB PDLG 5002A) was acquired from Corbion (Netherlands)

For the synthesis of polydopamine particles, dopamine hydrochloride was purchased from Sigma-Aldrich (USA); 25 % (v/v) ammonia solution was purchased from Merck (Germany) and 96% ethanol was purchased from Valente e Ribeiro (Portugal).

To prepare the simulated body fluid (SBF), sodium chloride (NaCl), calcium chloride (CaCl2) and Tris-hydroxymethyl aminomethane ((HOCH2)3CNH2) (Tris), were purchased from VWR, (USA); sodium hydrogen carbonate (NaHCO3) was purchased from Sigma-Aldrich (USA), potassium chloride (KCl), di-potassium hydrogen phosphate trihydrate (K2HPO4.3H2O) and magnesium chloride hexahydrate (MgCl2.6H2O) were purchased from Merck (Germany), sodium sulfate (Na2SO4) was purchased from PanReac AppliChem ITW Reagents (Germany).

To produce the KGM-BCP and KGM-BCP-PDA scaffolds, KGM was purchased from Prozis (Portugal). ß-Tricalcium phosphate (ß -TCP, with a phase purity of 100%, a specific surface area of 80 m^2/g and a particle size (d50) of 5.2 µm) and Hydroxyapatite (HA, with a phase purity of 100%, a specific surface area of 133 m^2/g and a particle size (d50) of 2.5 µm) were purchased from Fluidinova (Portugal). The Polydopamine particles were previously prepared at our lab, having a spherical shape with a diameter of around 150 nm (TEM characterization).

2. Levofloxacin-loaded nanoparticles

Levofloxacin (LFX) was encapsulated in PLGA nanoparticles (NPs) according to the double emulsion method (figure 22), According to this technique, polymers are dissolved in organic solvent, EA. The hydrophobic solution is then emulsified with an aqueous phase containing the drug to be encapsulated or water, in case of empty NPs. The first created emulsion is added to a surfactant, to form the w/o/w emulsion using sonication. This emulsion is left under magnetic agitation for 3 h at 300 rpm to evaporate the organic solvent. After the 3 h, the NPs formed are separated from the surfactant and non-encapsulated drug by centrifugation. Briefly, PLGA was dissolved in ethyl acetate for a final concentration of 1 % (w/v) and a solution of 1% Poloxamer 407 in ultrapure water was placed under stirring (at 300 rpm). After, a 4 % (w/v) LFX solution was added to PLGA solution and this first emulsion was homogenized by quickly vortex the tube (max speed) for 30 seconds. To proceed to the 2nd emulsion, 10 mL of the Poloxamer 407 solution was added to the Levofloxacin-PLGA mixture and sonicated on ice (70% amp) for 60 seconds and it was stirred (at 300 rpm) overnight (ON). The same procedure was applied to the same amount of water to serve as control). Nanoparticles were retrieved and

washed using a protocol of repeated centrifugations. Nanoparticles were concentrated by centrifugation (4,300 rpm/3,490×*g*, 4°C, 10-15 min) using Amicon centrifuge filters (100 kDa MWCO) and resuspended in ultrapure water (ddH_2O). This process was repeated twice. NPs were stored at 4ºC at a concentration of 1mg/mL until further use. In addition, NPs were lyophilised, and the supernatant was collected after the first concentration by centrifugation of the in other to be further analysed by an indirect method. All the samples were studied to assess their drug content.

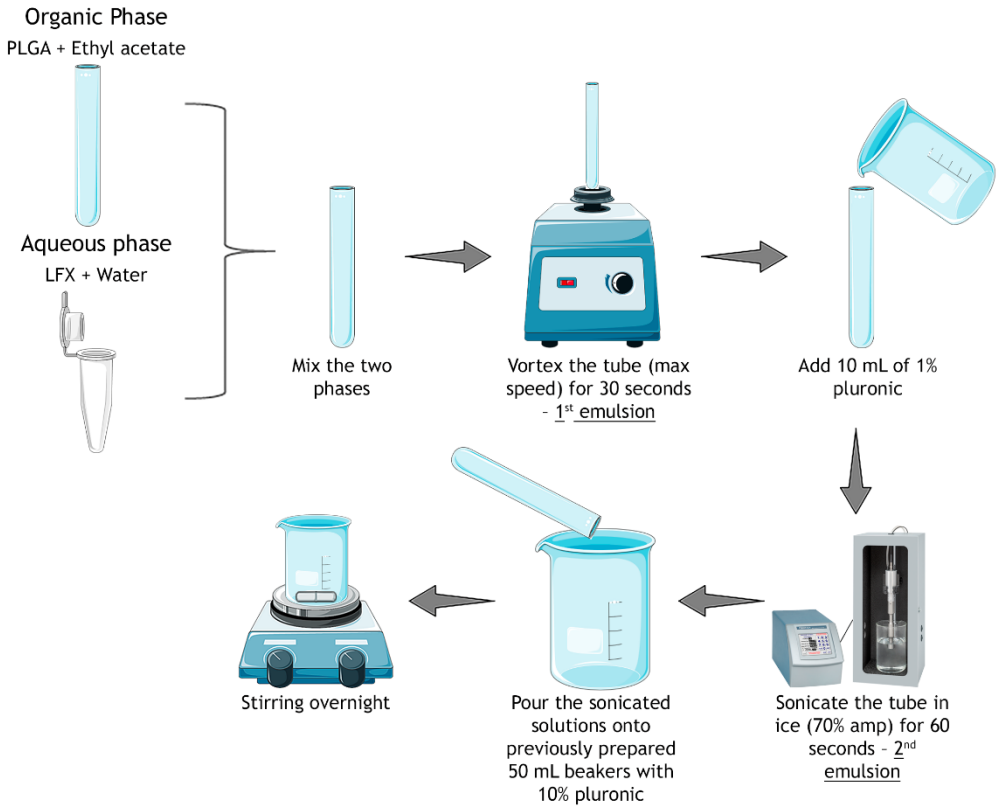

Figure 22 - Schematic representation of the double emulsion method used to prepare the LFX-loaded PLGA nanoparticles. The same process was applied to produce the nanoparticles loaded with water (control) and after this procedure they were washed following a specific protocol of repeated centrifugations. At the end, nanoparticles were stored at 4°C, with a concentration of 1mg/mL.

2.1. Nanoparticles characterization

NPs were characterized for their hydrodynamic diameter and polydispersity index (PdI) through dynamic light scattering (DLS) method. Zeta potential was measured by electrophoretic light scattering (ELS). Both methods were performed using the Malvern Zetasizer Nano ZS instrument (Malvern Instruments, UK). The samples were diluted 1:100 in sodium chloride (NaCl) 10 mM solution at pH 7.4.

2.2. Assessment of Drug Encapsulation Efficiency via HPLC

To assess the LFX encapsulation efficiency, both direct and indirect analysis were conducted. The samples were named as NP-0 and NP-LFX; Liof-0 and Liof-LFX; Ind-0 and Ind-LVX for the nanoparticles loaded with water (control) and LFX respectively; NP lyophilized and loaded with water and LFX, respectively and NP analysed using the indirect method, loaded with water and LFX, respectively.

On the direct method, both lyophilized and non-lyophilized samples were used. To prepare them for analysis, 10 µL of the nanoparticle's suspension was diluted in 990 µL of acetonitrile (ACN), in order to obtain a final concentration of 10 µg/mL. After, they were assessed for drug content by HPLC (Merck-Hitachi HPLC) and the encapsulation efficiency was calculated according to the following equation:

$$Encapsulation\ efficiency\ (\%, w/w) = \frac{Amount\ of\ drug\ encapsulated\ (mg)}{Amount\ of\ drug\ initially\ taken\ to\ prepare\ the\ nanopartucles\ (mg)} * 100$$

On the indirect method, the supernatant was collected after the washing procedure of the PLGA NPs, being after assessed for they drug content by HPLC.

The HPLC system used was a Merck-Hitachi HPLC system with UV detector and the drug was analysed using a C18 column. The assay was performed at 35ºC and two mobile phases were used, one consisting of a solution of 25mM potassium phosphate (KH_2PO_4) at pH 3 adjusted with HCl, and other of ACN. The flow rate and volume of injection were 1 mL/min, and 10 µL, respectively. The run time was 15 min and the detection wavelength (UV) was 220 nm. The stock solutions and standard concentrations were prepared in mobile phase. The standard curve was linear in a concentration range of 0 – 50 µg/mL (R^2 = 0.9985) and the standard concentrations (P0 – P7) are shown on table 8.

Table 8 – **Standards and their respective concentrations used to make the standard curve.**

Standards	Concentration (µg/mL)
P0	0
P1	1
P2	5
P3	10
P4	20
P5	30
P6	40
P7	50

3. Synthesis of Polydopamine particles

The reaction medium was prepared by mixing 2.9 mL of 25% (v/v) ammonia solution, 52 mL of 96% vol. ethanol and 117 mL of deionized water under mild stirring at 30 °C. After 30 min, a solution of dopamine hydrochloride (0.65g; 0,005 mol) in dH2O (13 mL) was added and the reaction allowed to proceed for 24 h at 30 ºC. The colour of this solution immediately turned to pale yellow and gradually changed to dark brown, indicating polymerization of dopamine (figure 23) [277]. The resultant suspension was centrifuged at 25 000 rpm and the pellet washed with water (3x). The precipitate was resuspended in water and freeze-dried, giving a black powder (220 mg).

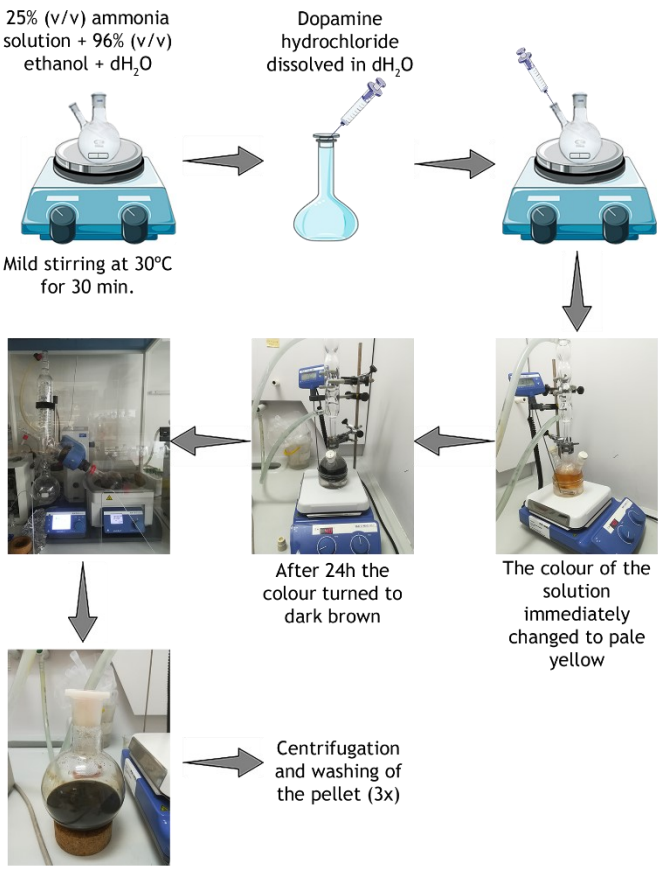

Figure 23 - Schematic representation of the synthesis of polydopamine particles. The process started by injecting a solution of dopamine hydrochloride and water, in a mixture of ammonia, ethanol and water, creating a reaction that lasted for 24h. The colour exchange of the solution trough time (from transparent to pale yellow and finally dark brown), indicate the successful polymerization of dopamine [278].

4. Preparation of the KGM-BCP and KGM-BCP-PDA inks for robocasting

4.1. KGM-BCP and KGM-BCP-PDA inks

A KGM solution with a concentration of 2 % (w/v) was prepared using deionized water (dH_2O) by overnight stirring (1400 rpm) at room temperature (RT), using an Eppendorf termomixer (Eppendorf thermomixer comfort). This concentration was previously optimized in order to have the adequate viscosity to be printed later by robocasting, and it was used for the ink of the two types of scaffolds (KGM-BCP and KGM-BCP-PDA).

For the production of the printable inks, four different components were required, namely the 2 % (w/v) KGM polymer, the ß-TCP and HA powders and Polydopamine (PDA) particles. The process consisted in successive blends of these primary materials. First the KGM solution was mixed (alone) using a planetary centrifugal mixer (ARE-250, Thinky Corp., Tokyo, Japan). Afterwards, the BCP ceramics (HA and ß-TCP) and PDA powders were added to the polymer gradually and mixed in the planetary centrifugal mixer, in order to obtain a final concentration of 52.7 % (w/v) of BCP ceramic powders (KGM-BCP ink). On the KGM-BCP-PDA inks, 1 % (w/v) of polydopamine was added after the addition of the BCP powders. At the end, the KGM-BCP scaffolds had a concentration in powders of 52.7 % (w/v) (70.9% ß-TCP + 29.1% HA) and the KGM-BCP-PDA scaffolds had a concentration of 53.7 % (w/v) in powders (69.6 % ß-TCP + 28.6 % HA + 1.9 % PDA).

5. Robocasting of the KGM-BCP and KGM-BCP-PDA scaffolds

The 3D scaffolds were produced layer-by-layer by DWA, using a robotic deposition device (figure 24-C) (3-D Inks, Stillwater, OK). The process was sequential, as explained in figure 24, starting by inserting the ink prepared previously (figure 24-A) in a cylindrical deposition nozzle (figure 24-B) (EFD Inc., East Providence, RI), that had a diameter of 410 µm, a volume of 3 mL, and printed at a speed of 10 mm s^{-1}. After, the desired position of the nozzle was adjusted on the software, which was then run, according to specific inputs previously defined. Finally, the structures were printed (figure 24-D) and immediately placed for 1h in an ethanol bath (figure 24-E) to allow their assembly. Subsequently the samples were incubated overnight at 37°C with controlled humidity (80%) (figure 24-G). The final structures consisted of grids (figure 24-H), which were then cut in smaller structures - 9 individual scaffolds.

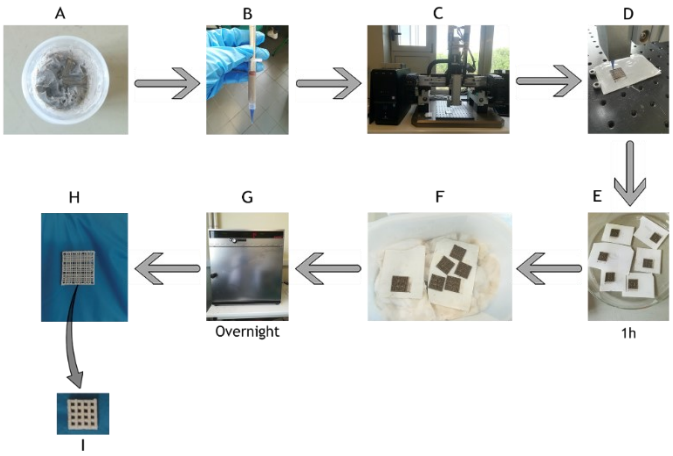

Figure 24 - Representation of the sequential process involved on the production of the KGM-BCP-PDA scaffolds. The KGM-BCP scaffolds were produce following the same process. **(A) Final printable ink formulation; (B) Cylindrical deposition nozzle with a diameter of 410 µm, a volume of 3 mL and a speed of printing of 10 mm s-1, containing the ink that is introduced on the robocaster (C); (D) Printing of the structures that are then placed on ethanol bath for one hour (E) and then placed in a specific recipient (F) inside an incubator at 37°C with controlled humidity (G); (H) Final grid that is composed of 9 individual scaffolds (I).**

6. Characterization of the KGM-BCP and KGM-BCP-PDA scaffolds

6.1. Characterization of the KGM-BCP and KGM-BCP-PDA printable inks

Rheological measurements of the ink and KGM solution were made using a Kinexus Pro Rheometer (Malvern, Pennsylvania, USA). The apparent viscosity of the ink, as well as of the KGM solution, was measured in viscometry mode using a cone and plate sensor system (4°/40 mm) and 150 µm gap size. Samples were placed in the bottom plate geometry and analysed in manual viscometry mode applying different shear stress (0.1, 1, 5, 10, 20, 50, 75, 100, 200 and Pa).

6.2. Characterization of the KGM-BCP and KGM-BCP-PDA scaffolds

6.2.1. Analysis via Scanning Electron Microscopy / Energy Dispersive X-Ray Spectroscopy (SEM/EDS)

The samples, that were immerse in basal medium for 28 days without cells, were collected and analysed by SEM/EDS at timepoints 0 and 28. To prepare them for analysis, first they were fixed for 15 min in a paraformaldehyde (PFA, EMS, Pennsylvania, USA) solution (4 % (w/v) and then, to visualize them, they were placed with a carbon tape, in adequate supports for SEM visualization. Before visualization, the samples were coated with palladium gold. The micro and macroporosity of the scaffolds were assessed through SEM using a High resolution (Schottky) Environmental Scanning Electron Microscope with X-Ray Microanalysis and Electron Backscattered Diffraction analysis: Quanta 400 FEG ESEM / EDAX Genesis X4M.

6.2.1. Confocal Raman micro spectroscopy

Confocal Raman micro spectroscopy analyses were performed using a LabRAM HR 800 confocal Raman microscope system (Horiba Jobin Yvon, Tokyo, Japan) comprising a spectrometer and a fully integrated Olympus BX41 confocal microscope (Olympus Iberia, S.A.U., Lisboa, Portugal). Raman spectra were collected using a 515.5 nm laser and for the characterization of the samples, the regions from 400 to 1800 cm^{-1} and 2700 to 3700 cm^{-1} were analysed. All spectra were acquired using an Olympus LMMPlanFL N 50X objective (N.A. 0.50, Olympus, Japan), and a pinhole of 100 µm using the LabSpec 5 software (version 5.25.15, Horiba Jobin Yvon, Tokyo, Japan). Spectra were taken from randomly selected points in the fibers and at the surface of the materials, with an integration time of 30 s and 2 accumulations. The scattered light was dispersed by a grating with 1800 lines/mm (Jobin-Yvon) at 4 cm^{-1} spectral resolution. Spectra were processed using the LabSpec5 software for baseline correction and smoothing.

6.2.2. X-ray computed microtomography (microCT)

CT images were acquired from samples stored in 70% ethanol in polypropylene tubes using a SkyScan 1276 microCT (Bruker, Kontich, Belgium) at the Bioimaging Scientific Platform from i3S. Projection images were obtained using the SkyScan software version 1.0.11 (Bruker, Kontich, Belgium), with a resolution of 3 x 3 x 3 µm. X-ray tube potential was 40 KV and tube current 100 µA, with exposure time of 800 ms. A total of 1801 projection images were acquired over 360 degrees with a rotation angle of 0.2 degrees and average of 4 projections.

Tomographic images (3D datasets) were obtained by reconstructing the projection images using the NRecon software (version 1.7.4.2, Bruker, Kontich, Belgium). This software uses a filtered back-projection algorithm developed by Feldkamp and co-workers (Feldkamp 1984). For the reconstruction the image alignment with respect to the actual center of rotation was specifically chosen to each sample. While for every sample, the ring artifact reduction chosen was 19 and the beam hardening compensation of 35%.

Further visualization and inspection of the reconstructed 3D datasets was performed using the softwares DataViewer (version 1.5.6.2, Bruker, Kontich, Belgium) and CTVox (version 3.3.0r1383, Bruker, Kontich, Belgium). The DataViewer software was used to extract the images for the constructing the figures for this thesis while the CTVox software was used for the preparation of the videos and images of the 3D dataset.

6.2.3. Mechanical properties - Compressive strength

The compressive strength was determined by performing uniaxial tests on scaffolds with approximately 4 x 4 x 1.7 mm. Tests were carried out in air using a universal testing machine (AG-IS 200N, Shimadzu Corpor., Kyoto, Japan) in the perpendicular direction of the printing plane at a constant speed of 0.5 mm min^{-1}. The compressive strength of the structures was calculated by the maximum applied load divided by the measured square section of the sample and a minimum of 5 samples were tested for each composition (KGM-BCP and KGM-BCP-PDA), to obtain statistically reliable values.

6.2.4. Biomineralization assay with simulated body fluid (SBF)

The SBF solution was prepared according to a method described on [279]. The scaffolds were soaked in specific volumes of SBF solution, at 36 ºC, according to the equation: Vs = Sa/10, where Vs represents the volume of SBF (ml) and Sa is the surface area of the sample (mm^2). Also, an extra amount off SBF solution was added (20% in each scaffold), since the specimens analysed were porous. At different timepoints (T0, T3, T7 and T21) the scaffolds were collected to assess the formation of apatite on the samples' surface. Briefly, at each timepoint, the samples were washed three times with dH_2O for 30 min, placed on an oven overnight at 36ºC, to dry, and then stored at a desiccator until their analysis by Confocal Raman micro spectroscopy.

7. *In vitro* studies on KGM-BCP and KGM-BCP-PDA scaffolds

7.1. Cell culture

Human mesenchymal stem cells (hMSCs) were purchased from Lonza. Cells were thawed and maintained in culture at 37°C in a humidified atmosphere with 5% v/v CO_2 in air and were expanded in an Expansion Medium (EM) before being seeded on the scaffolds. EM consisted of

α-Minimum Essential Medium (α-MEM, Gibco, California, USA), 10 % vol of heat-inactivated Mesenchymal Stem Cell Fetal Bovine Serum (MSC FBS, Gibco, California, USA) and 1 % v/v Penicillin/Streptomycin (P/S, Biowest). To expand the cells, they were cultured on T75 flasks, with a concentration of 0.4×10^6 cells/mL. After reaching 70-80% confluence, cells were trypsinized.

At the second part of this work, an osteosarcoma cell line (U2OS) was used. U2OS cells were cultured in Dulbecco's Modified Eagle Medium (DMEM, Invitrogen) with 10 % v/v FBS, 1 % v/v Penicillin/Streptomycin (P/S) and 1 % v/v Amphotericin B. U2OS were trypsinized when 70-80% confluence was reached.

7.2. Seeding test

A seeding test was performed to infer the optimum number of cells that should be seeded on the scaffolds. On the first part of this work, only 3.0×10^4 of cells were seeded on the material, but given the results obtained on the *in vitro* tests, we performed a seeding test with a higher number of cells (hMSCs). The number of cells tested was 5.0×10^4 and 10.0×10^4, per scaffold, and the procedure to seed them is represented on figure 25. Briefly, the scaffolds were pre-incubated with BM for 1h and then the cells were seeded. After, they were incubated for 1h and then BM medium was added, being changed every 2 days for 28 days. Samples were collected at different timepoints to be further analysed with immunostainings

7.3. hMSCs and U2OS cell culture on KGM-BCP and KGM-BCP-PDA scaffolds

Prior to cell seeding, the scaffolds were sterilized using 70% vol. ethanol for at least 15 min and were washed three times with ultrapure water. First, hMSCs were seeded on the Konjac Glucomannan-Biphasic calcium phosphate scaffolds (KGM-BCP) initially by placing a droplet of 10 µL per scaffold, containing 3.0×10^4 cells. On a second approach the number of cells seeded increased to 1.0×10^5. In addition, two experiences were conducted: one had a seeding process as explained above and other underwent a pre-incubation period of 7 days in both basal and osteogenic mediums before cell seeding

For Konjac Glucomannan-Biphasic calcium phosphate-Polydopamine scaffolds (KGM-BCP-PDA scaffolds), hMSCs were seeded by placing a droplet of 10 µL per scaffold containing 1.0×10^5 cells. hMSCs were allowed to adhere before adding 300 µL of Basal Medium (BM) per well. Basal Medium is composed by α-MEM (Gibco, California, USA), 10%vol of heat-inactivated fetal bovine serum (FBS, Gibco, California, USA) and 1% v/v Penicillin/Streptomycin (P/S).

After 7 days in BM, in half of the scaffolds the culture medium was switched to Osteogenic Medium (Figure 25). Osteogenic medium is composed of BM supplemented with 5×10^5 M Ascorbic

Acid (Sigma, Missouri, USA), 0.1 µM of dexamethasone (Sigma, Missouri, USA) and 0.01M of ß-glycerophosphate (Sigma, Missouri, USA).

Medium was changed every 2 days for up to 28 days on both scaffolds.

U20S osteosarcoma cell line was seeded on KGM-BCP and KGM-BCP-PDA scaffolds after scaffolds sterilization, by placing a droplet of 20 µL per scaffold containing 1.0 x 10^5 cells. U20S cells were allowed to adhere before adding DMEM medium, which was changed every 2 days for up to 10 days in culture.

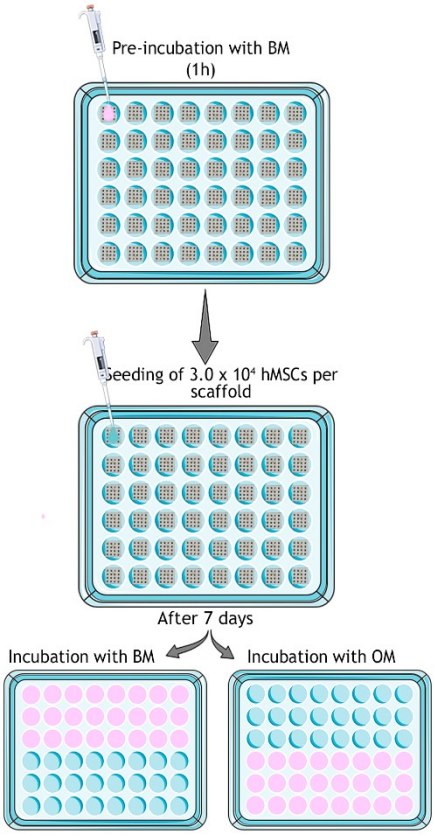

Figure 25 - Schematic Illustration of hMSCs culture on the 3D KGM-BCP and KGM-BCP-PDA scaffolds. The cells were seeded on top of scaffolds with a drop of 10 or 20µL. After promoting the attachment of the cells to the scaffolds, 300µL of Basal medium was added to the wells. After 7 days the osteoinduction was initiated. In half of the samples the basal medium was changed to an osteogenic medium – basal medium enriched with dexamethasone, ß-glycerophosphate and ascorbic acid.

7.4. Metabolic activity of hMSCs and U20S cells

The Metabolic activity of the cells, for both type of scaffolds, was estimated using a resazurinbased assay. At different time-points, the culture medium was removed from the wells and fresh medium with resazurin (20 % (v/v), Sigma) was added (300µL/well). Samples were incubated (37ºC, 5 % (v/v) CO2) for 3h, after which 100µL/well were transferred to a black 96 well plate and the fluorescence signal was measured (λex ≈ 530 nm, λem ≈ 590 nm) using a micro-plate reader (Synergy MX, BioTek).

7.5. Immunostainings

To perform immunostainings in each time point, the samples were transferred into new wells and washed three times with HBSS. After, each sample was fixed for 15 min in a paraformaldehyde (PFA, EMS, Pennsylvania, USA) solution (4 % (w/v) in HBSS). PFA solution was removed, the samples were washed again three times with HBSS and permeabilized with Triton X-100 (CALBIOCHEM, San Diego, USA) (0.1 % (v/v) in HBSS) for 5 min. Then the samples were washed 3 times with HBSS and incubated for 30 min with a bovine serum albumin (BSA, VWR International, Pennsylvania, USA) solution (1 % (w/v) in HBSS). Afterwards, the 1 % BSA solution was removed from the scaffolds and they were incubated overnight at 4ºC with primary antibodies, diluted in BSA 1 % (table 9). On the day after the solution of the primary antibodies was removed from the samples, washed 3 times with HBSS and incubated for 45 min with a secondary antibody diluted also in the 1 % BSA solution (table 9). Subsequently, the samples were washed 3 times with HBSS and DNA was counterstained with a solution of 4',6-diamidine-2′-phenylindole dihydrochloride (DAPI) (0.1 mg/ml) in anti-fading mounting medium (VECTASHIELD, Vector Laboratories) 10 min before confocal microscope visualization (CLSM, Leica SP5, Leica Microsystems, Wetzlar, Germany) using LCS software (Leica Microsystems, Wetzlar, Germany). The scanned Z-series were projected onto a single plane and pseudo-colored using ImageJ.

Table 9 - Combination of antibodies used for the immunostainings.

	Antibodies	Manufactures	Dilution
Primary	Rabbit Fibronectin Polyclonal Antibody	Invitrogen	1:400
	Flash Phalloidin™ Green 488	BioLegend	1:100
Secondary	Alexa Flour ™ 594 (fragment of goat anti-rabbit)	Invitrogen	1:1000

7.6. SEM visualization

The samples were placed, with a carbon tape, in adequate supports for SEM visualization. Before the visualization the samples were coated with palladium gold. The micro and macroporosity of the scaffolds were assessed through SEM using a High resolution (Schottky) Environmental Scanning Electron Microscope with X-Ray Microanalysis and Electron Backscattered Diffraction analysis: Quanta 400 FEG ESEM / EDAX Genesis X4M. Images were acquired but due to service constrains were not available to include in this version of the thesis

Results and discussion

1. Hybrid 3D KGM-BCP scaffolds

Since KGM shows high biocompatibility and biodegradability and can act as drug delivery system [169], this polymer can be a great promising when combined with BCPs. Both β-TCP and HA are naturally present on a normal and healthy bone, so they are important assets when developing successful bone substitutes [280–282]. Despite the existing controversies in the literature regarding the optimum composition ratio of β-TCP/HA, it is considered that a higher ratio of β-TCP results in a higher biodegradation rate of the BCP material [283] and in the formation of more apatite agglomerates on the material's surface, which indicates a better bioactivity [284]. Given that, it is possible to control the material resorption rate and bioactivity by modifying the percentage ratio of β-TCP/HA within it. Taking all this into consideration, composites of BCPs and KGM are expected to be excellent biomaterials for bone tissue engineering applications. On the first part of this work, only scaffolds composed by KGM and BCPs where used, with the aim of comparing them with the previously developed scaffolds (in another work inserted within this project) and optimize them to improve the outcomes related with the material's bone regeneration induction ability.

1.1. Characterization of the KGM-BCP and KGM-BCP-PDA printable ink

Two of the most important characteristics for printing in robocasting are the properties and composition of the inks. They need to be homogenous, free of air bubbles, they must have a high-volume fraction of ceramic powders, to assure their mechanical properties, and they need to be able to flow through a fine deposition noozle, while maintaining their shape after printing. For that reason, robocasting relies more on rheology rather than solidification in order to print a self-supporting material [230].

Therefore, to characterize our inks, first it was evaluated their shear viscosity with time, when applying different shear stresses (figure 26). It was possible to conclude that the viscosity of both inks increased with time, in every different shear stress applied and it increased until a value of shear stress of 100 Pa (figure 26 A and C). When comparing the two types of inks, it was possible to conclude that unlike what happened in the KGM-BCP-PDA scaffolds (figure 26 C), in the KGM-BCP scaffolds (figure 26 D), for all the values of shear stress applied, the shear viscosity reached a plateau. This might be explained by the fact that, in polymeric systems, at a certain point, the population of macromolecules achieve a state of maximum disentanglement and the viscosity stops changing with time. This is called the plateau value of infinite shear viscosity and is characteristic of shear-thinning fluids [285].

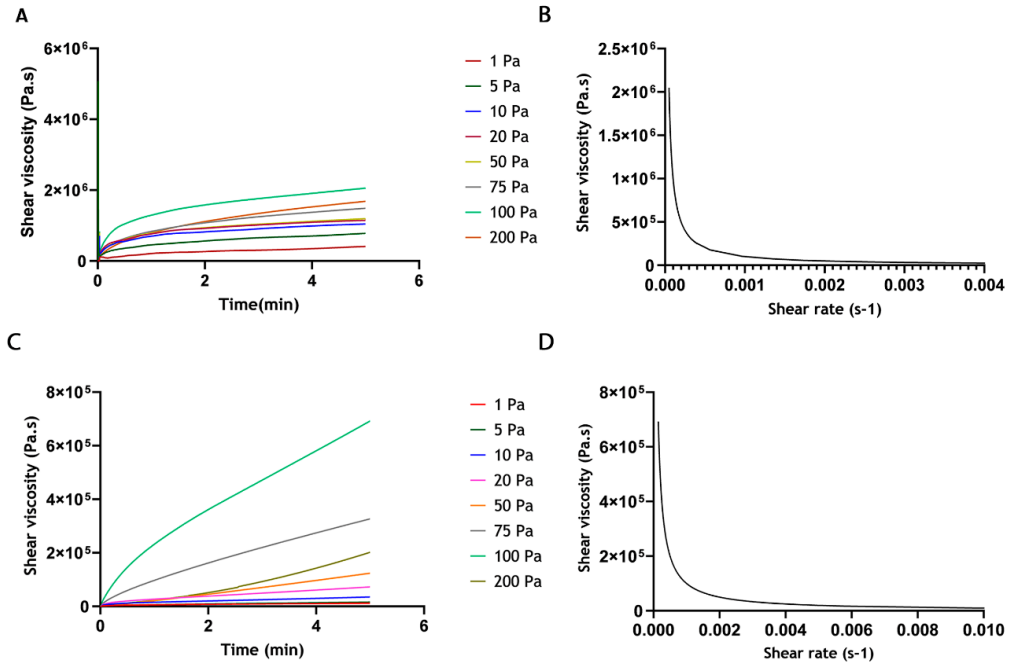

Figure 26- Rheological characterization of the KGM-BCP and KGM-BCP-PDA inks. (A) and (C): Evaluation of shear viscosity with time for different shear stress values applied on the (A) KGM-BCP and (C) KGM-BCP-PDA inks. (B) and (D): Evaluation of the shear viscosity versus shear rate for the (B) KGM-BCP and (D) KGM-BCP-PDA inks. The shear thinning behaviour is confirmed by the decrease of viscosity with shear rate and by achieving a plateau value of infinite shear viscosity.

After, the viscosity of both inks *versus* shear rate was analysed, in order to confirm their shear thinning behaviour (Figure 26 B and D). The graphics represent the behaviour of the inks when submitted to a shear stress of 100 Pa, since this is the maximum value of pressure that the ink will be submitted during the printing process on the robocasting system but all other values of shear rate (1, 5, 10, 20, 50, 75 and 200 Pa) showed the same behaviour (data not shown). On both inks it is possible to perfectly see their shear tinning behaviour of the inks, since it is verified the decrease of viscosity with shear rate, making them suitable for robocasting printing. The shear tinning behaviour will facilitate the deposition of the ink through the robocaster needle [286].

1.2. Preparation and characterization of the scaffolds

The scaffolds developed in this work, composed by KGM and BCP powders were produced as explained in the materials and method section, having a concentration in powders of 52.7 % (w/v) (70.9% β-TCP + 29.1% HA).

The previously developed KGM-BCP scaffolds had a composition of 3 % (w/v) KGM with 40 % (w/v) of ceramic solids (BCPs). According to the literature, to obtain a sintered-free scaffold that is able to keep its 3D structure after printing, a high percentage of solids is required since they can decrease the shrinkage levels during drying, avoiding shape distortions [287]. Also, it is reported in a study that tested different polymeric/ceramic mass ratios in a composite, that the highest values of bending and compressive strength occured when the percentage of

ceramic solids was ~60 % wt [288] . Moreover, since most bones are composed by approximately 60-70% of mineral part, of its dry mass [289], the ink formulation used for this work was optimized to 2 % (w/v) KGM with 52.7 % (w/v) BCPs, from this corresponding 70.9% to ß-TCP and 20.1% to HA. The scaffolds where prepared following a DWA technique, as explained previously, and the ink formulation and the scaffolds were characterized regarding their structural and physicochemical properties. The polymer characterization was not performed, since it was made previously [278]

1.3. Structural characterization of the scaffolds

The structural characterization of KGM-BCP and KGM-BCP-PDA scaffolds was assessed by Micro-CT (micro-computed tomography). This is a modern preclinical imaging method that allows the non-destructive visualizations and structural analysis of the material in study, in a resolution of a few micrometres [290]. Micro-CT can be a complementary method to conventional analysis, such as SEM, that will be performed later.

The use of this type of analysis in the developed scaffolds is important to evaluate their structural parameters, such as their macropore size, which is a very important aspect when designing structures for bone tissue engineering apllications. Due to time constrains we were only able to perform a preliminary analysis and full analysis in ongoing.

The 3D micro-CT reconstructed the images are showed in figure 27. These images show the well-organized macroporous arrangement of the developed 3D scaffolds, which highlights their adequate structure for bone tissue engineering applications. The use of porous structures in this work relies on the fact that the porosity is a key factor when developing bone substitutes, playing a key role in the possible osteoconductivity of the material. To a bone regenerate with the help of a scaffold, *in vivo*, it is necessary the recruitment and penetration of cells that surround the bone tissue, along with the vascularization, which can enhance osteogenesis. Consequently, these processes take place in structures with high porosity [291].

The porosity parameters of the scaffolds will be determined later from these 3D micro-CT images.

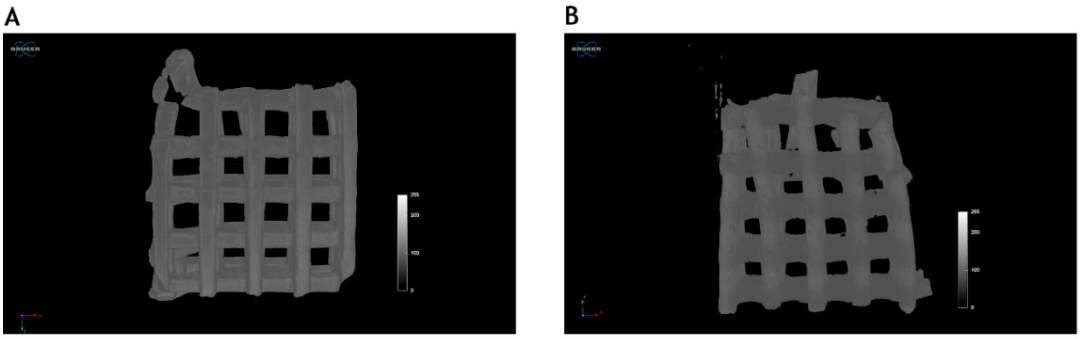

Figure 27 - 3D micro-CT reconstruction images of the (A) KGM-BCP and (B) KGM-BCP-PDA scaffolds. It is possible to see the characteristic pores of these scaffolds that were design with a macropore size of 500 µm.

1.4. Mechanical characterization of the scaffolds

After printing the scaffolds with an adequate ink, it is necessary to evaluate the mechanical properties of the material. Since we are looking for a bone substitute, and its mechanical properties are crucial to the movement of our skeletons and provide protection to our vital organs, it is necessary to evaluate the compressive strength of the scaffolds. This analysis will predict the overall strength of our material and evaluate if it can support as much compressive strength as the real bone. Both cortical and cancellous bone have different values for the compressive strength since the porosity can affect this property [292]. Cortical and trabecular bone have a compressive strength around 130-200 MPa and 0.1-16 MPa, respectively [293].

To calculate the compressive strength of both KGM-BCP and KGM-BCP-PDA scaffolds, first it is necessary to have the maximum applied load on each sample. These values were taken from a graphic which evaluates the strength applied to the scaffold versus its shift (figure 28 A and B), and is marked with an arrow, that represents the maximum load that the scaffold can bear. After, the maximum applied load on each sample was divided by the measured square section of the samples to obtain the compressive strength of the scaffold. The results, for each type of scaffold, on average, are present on figure 28 C.

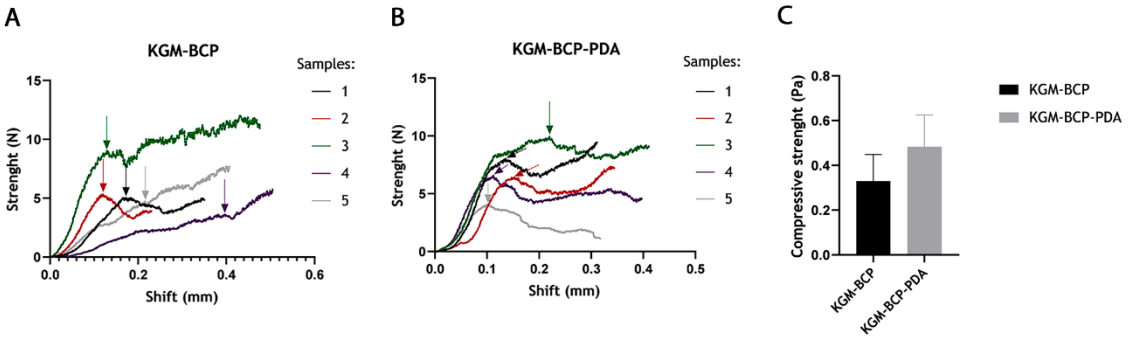

Figure 28 - Compressive strength of the KGM-BCP and KGM-BCP-PDA scaffolds. (A) and (B) - strength applied on the KGM-BCP and KGM-BCP-PDA scaffolds versus their shift, with the arrows representing the maximum applied load on each sample. (C) – compressive strength of the two types of scaffolds, showing the better mechanical properties of the KGM-BCP-PDA scaffolds.

As seen by figure 28 C, the compressive strength of both scaffolds is far below of the desired, even with the KGM-BCP-PDA scaffolds showing better results, that might be due to the higher solid content in this formulation. A strategy to enhance this property could be the reduction of the material's pore size, since it has been reported that scaffolds with higher pore sizes show diminished mechanical properties [287,293,294]. However, higher pore sizes (>300 μm) allow new bone formation, greater bone ingrowth and the formation of capillaries [293], since it enables an effective release of proteins, genes or cells and provide good substrates for nutrient exchange. Besides that, some studies have reported that a better osteogenesis occurs with a pore size of (>300 μm) [295]. For that reason, a balance must be established between

the mechanical and mass transport functions of the scaffolds. Additionally, the addition of more ceramic content could improve the compressive mechanical properties of the scaffolds and their coating with nanocomposites, such as SiO2/MgO may also be advantageous [296,297]

1.5. Biomineralization assay with simulated body fluid (SBF)

Simulated body fluid (SBF) is a solution having an ion concentration close to that of human blood plasma that can predict the in vivo bone bioactivity of a material, occurring through the formation of an apatite layer on its surface. In vivo bioactivity is provided by osteoblasts, which proliferate and differentiate to produce apatite and collagen recognized by the surrounding bone. Following that reasoning, a material which forms apatite can also bind to the living bone, through the formation of a tight chemical bond between the apatite layer and the bone [279]. Therefore, several researchers have been using this assay to assume that the in vitro ability to form apatite, measured by SBF, is a strong predictor of in vivo bioactivity [298–300]. In this work, this assay was performed in the hybrid organic-inorganic scaffolds and the formation of an apatite-like layer was investigated by Confocal Raman micro spectroscopy) at different timepoints (T0, T3, T7, T14 and T21). The Raman spectrum provides information for the identification of functional groups present in the samples, where it is expected to see the formation of an amorphous calcium-phosphate layer that can later convert to crystalline hydroxyapatite.

1.5.1. Characterization of the scaffold's components

Before proceeding to the analysis of the scaffolds, it is important to understand the structural composition of their components, namely the KGM polymer, the β-TCP and HA powders, and the particles of PDA. All the spectra were analysed in the wavenumber range of 400–1800 cm^{-1} and 2700-3600 cm^{-1}.

The spectrum of KGM (figure 29) exhibit weak peaks at 3197,3445 and 3648 cm^{-1} corresponding to the O-H stretching vibrations from the hydroxyl groups present in monomeric glycosidic units, whereas the intense peak at 2902 cm^{-1} corresponds to the C-H stretching vibrations of aliphatic methylene groups. The weak peak at 1600 cm^{-1} corresponds to the vibration of carbonyl (C=O) which together with the peak at 1461 cm^{-1} characteristic of the vibration of methyl (–CH3) evidences the presence of acetyl groups. The peaks at appearing at lower wavenumbers, 1116 cm^{-1} and 1086 cm^{-1}, can be assigned to the C-O-C vibration from the glycosidic units of KGM [301]. Furthermore, there are also peaks appearing at 532 cm^{-1} , 435 cm^{-1} , and 473 cm^{-1} that should correspond to C-H deformation vibrations [302]. Finally, the peak at 900 cm^{-1} is characteristic of the presence of mannose units composing the KGM polymer chain [303].

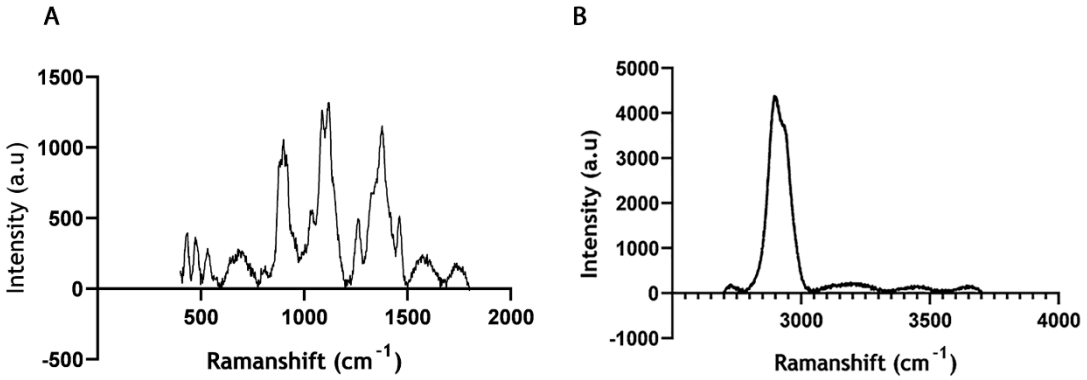

Figure 29 - Raman Spectrums of Konjac Glucomannan (KGM), taken from two different regions. (A) – 800-1400 cm-1 region. (B) 2700-3600 cm^{-1} region. In both spectra it is possible to see the appearance of peaks that are characteristic of functional groups present in the structure of KGM.

The spectra of B-TCP and HA (figure 30) present high similarity with each other, exhibiting the same peaks with varying intensity. The peaks that appear in the range of 500-1400 cm-1 correspond to the vibration bands of PO_4 groups. In this range it is possible to observe the symmetrical stretching vibration mode of PO_4 groups (v1), that appears at 960 cm^{-1} and correspond to the peak with the highest intensity for both materials. It could also be observed the symmetrical bending (v2) peak appearing at 426 cm^{-1}, the antisymmetric bending (v4), usually appearing at 588 cm^{-1} and the antisymmetric stretching vibrations (v3) associated with the 1045 cm^{-1} peak. On the B-TCP spectrum it is important to highlight the splitting of the peak at v3 (1000 cm-1), which is not present on the HA spectrum [304–306]. Additionally, the low intensity peak at 3570 cm^{-1} corresponds to the bending mode of O–H group [304], that is more intense on the HA spectrum due the presence in its structure (figure 30-D).

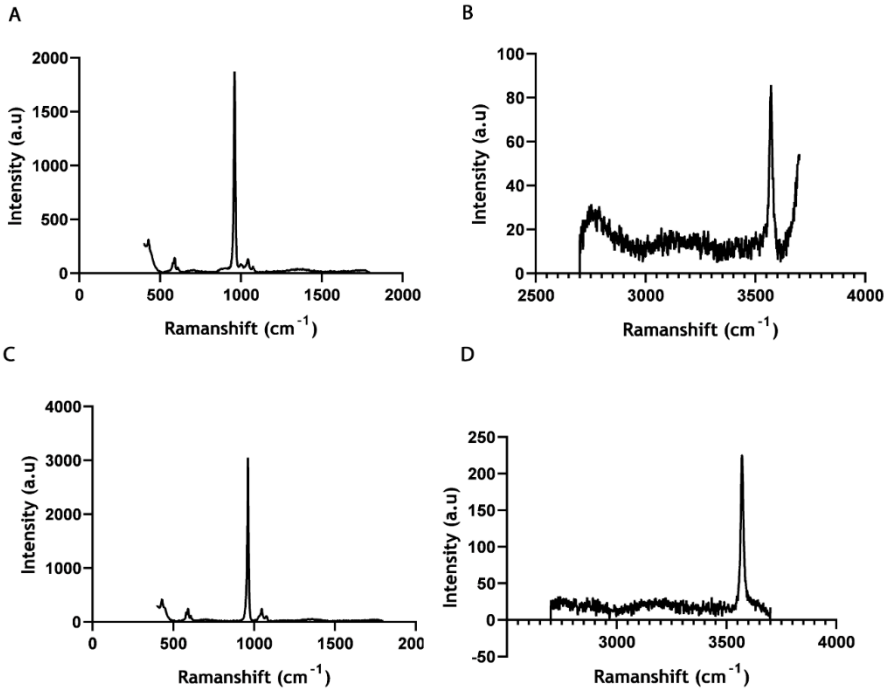

Figure 30 - Raman Spectrua of ß-TCP and HA powders. (A) ß-TCP spectrum in the 800-1400 cm^{-1} region. (B) B-TCP spectrum in the 2700-3600 cm^{-1} region. (C) HA spectrum in the 800-1400 cm^{-1} region. (D) HA spectrum in the 2700-3600 cm^{-1} region.

Regarding the polydopamine particles (figure 31), the more characteristic peaks are revealed at 1353 and 1596 cm-1, which are associated with the stretching of C-O in the catechol group and with the C=C stretching in the aromatic ring, respectively [307]. A low-intensity peak is also observed at 698 cm-1, which together with the broad peak appearing at 3000–3400 cm^{-1} indicate the presence of aromatic O-H moieties [308].

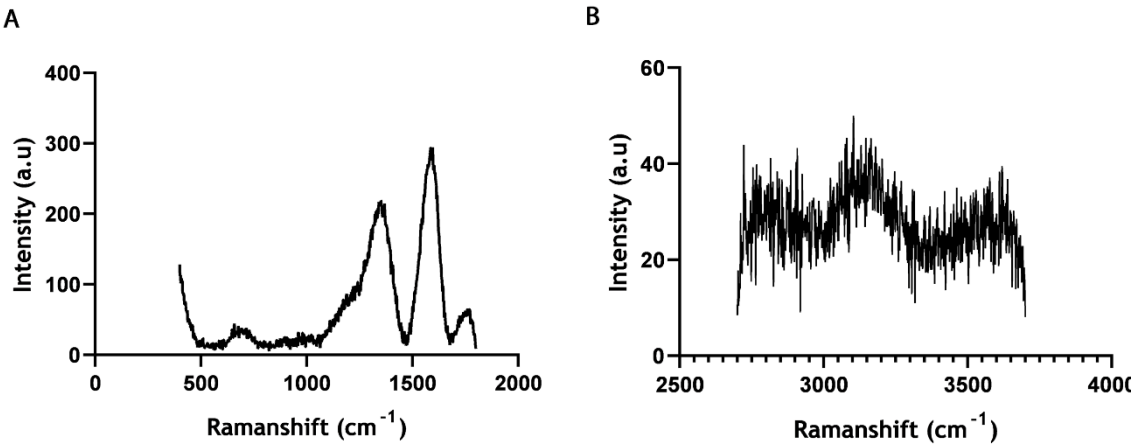

Figure 31 - Raman spectra of PDA particles. (A) PDA spectrum in the 800-1400 cm^{-1} region. (B) PDA spectrum in the 2700-3600 cm^{-1} region.

1.5.2. Characterization of the KGM-BCP and KGM-BCP-PDA scaffolds after immersion in SBF

After analysing their individual components, the KGM-BCP and KGM-BCP-PDA scaffolds were analysed both at their surface and inside their fibres, obtaining the corresponding spectra in the range of 400–1800 cm^{-1} and 2700-3600 cm-1. The KGM-BCP scaffolds were analysed at day 0, 3, 7, 14 and 21 after immersion in the SBF solution and the KGM-BCP-PDA scaffolds where only analysed at day 0, 7 and 14, since these were the days that showed more significant differences throughout the experience.

Regarding the analysis of the scaffolds' fibres (figure 32), it is possible to conclude that both KGM-BCP (figure 32- A and B) and KGM-BCP-PDA scaffolds (figure 32 – C and D) showed characteristics peaks from the spectra of their individual components. More specifically, In the range of 3600-3700 cm-1, besides the characteristic peak of the bending vibration of O–H from the inorganic powders (at 3570 cm-1), it was also possible to see the peaks corresponding to the KGM polymer at 2900 cm-1, and from polydopamine nanoparticles at 1353 and 1596 cm-1 in the spectrum of KGM-BCP-PDA scaffolds. This highlights the successful incorporation of all components in the material. The intensity of these bands is different in each day but since there is not a correlation with the number of days and the intensity of peaks, these differences may be related with the zone that the spectra were acquired rather than with the deposition

of a calcium-phosphate layer on the materials surface. However, by comparing the two kind of materials, it is possible to see that the peaks of the KGM-BCP-PDA scaffolds are much more intense when comparing the peaks obtained for the KGM-BCP scaffolds. The intensity of the peaks is higher not only in the region of the phosphates (form 540 cm-1 to 1165 cm-1) but also at higher wavenumbers (2900-3550 cm-1) characteristic of the vibrations from aliphatic and hydroxyl groups from thepolymer and HA, respectively. However, also here there is not a clear relation of the increasing intensity with the days of experiment, meaning that this feature may be intrinsic to the material.

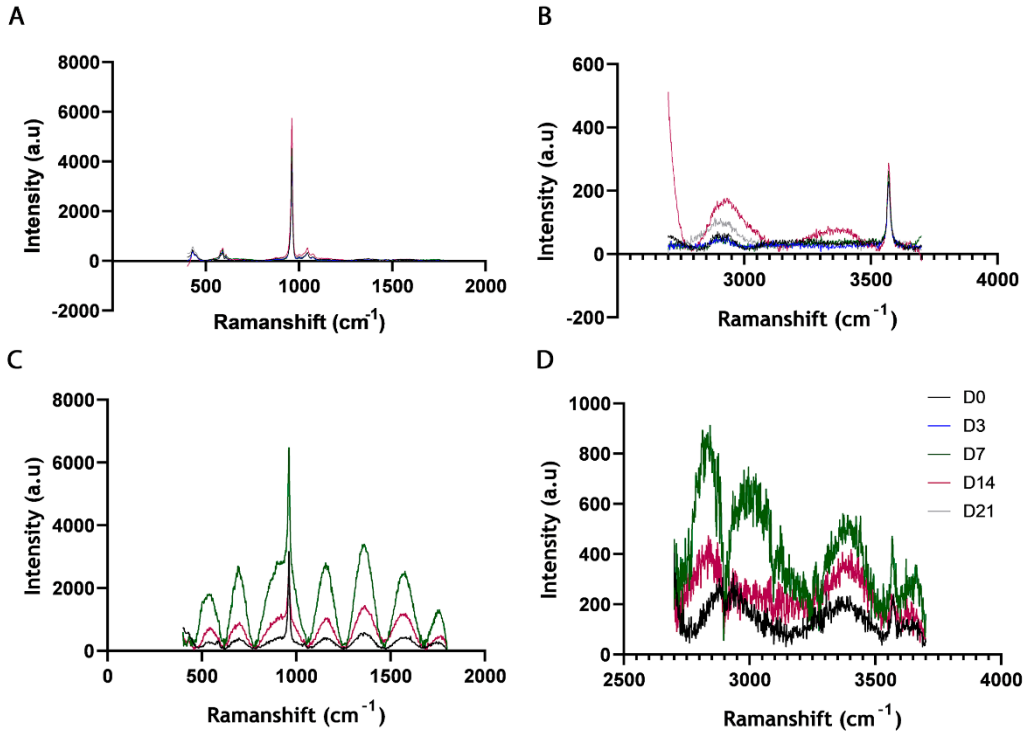

Figure 32 - Raman spectra of KGM-BCP and KGM-BCP-PDA fibres. (A) KGM-BCP spectrum in the 800-1400 cm^{-1} region. (B) KGM-BCP spectrum in the 2700-3600 cm^{-1} region. (C) KGM-BCP-PDA spectrum in the 800-1400 cm^{-1} region. (D) KGM-BCP-PDA spectrum in the 2700-3600 cm^{-1} region.

The surface of the scaffolds was analyzed to evaluate the formation of an apatite-like Ca-P layer. Pictures were taken at the surface of the scaffolds following local acquisition of the raman spectra to assess its structural composition. The acquired images showed the presence of some deposited structures along the surface of the KGM-BCP scaffolds at days 7 and 14, whose size seems to increase with time (figure 33).

It was possible to see what looks like crystals deposited on the surface of the material and their size seems to increase with time, until day 14. This may suggest the deposition of an apatite like layer on the scaffolds' surface, supporting the bioactivity of the hybrid organic-inorganic biomaterial. However, regarding the KGM-BCP-PDA scaffolds these crystals were not observed at similar timepoints, meaning that the presence of these particles mixed in the

hybrid organic-inorganic phase of KGM and HA/ß-TCP may impair the ion exchanges between the inorganic phase of the scaffolds and SBF solution, retarding the formation of this layer.

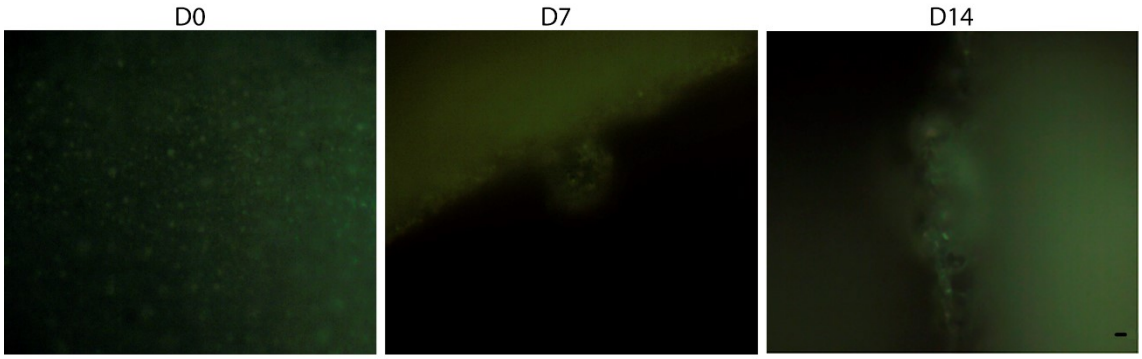

Figure 33 - Photos taken by confocal Raman micro spectroscopy at the KGM-BCP scaffolds' surface. It is possible to see some structures deposited on the scaffolds, which is thought to be HA crystals. Scale bar: 2µm.

The raman spectra were acquired at the surface of the scaffolds, preferentially, whenever possible, in the region where the deposited crystals have been detected at different timepoints (figure 33), and compared with the spectrums observed for the scaffolds' fibres (Figure 32). In the case of the KGM-BCP-PDA scaffolds, the analysis was made in a region where the crystals should have been detected, based on what has been observed for scaffolds without PDA.

Regarding the KGM-BCP scaffolds, the Raman spectra acquired at the surface of the material (Figure 34) revealed some differences when comparing with the spectra obtained for the materials' fibres (Figure 32). Between them, it is important to highlight the presence of peaks in the region of 1400 cm^{-1}, attributed to the presence of carbonates that precipitate from SBF solution forming a carbonated apatite layer. Moreover, the intensity of these peaks increases form day 0 to day 14, which may suggest the in vitro ability of the material to form an apatite-like layer. These ions are involved in the biological mechanism of apatite formation, being associated with the transition of the amorphous calcium phosphate into the crystalline hydroxyapatite phase [309,310]. In addition, the intensity of the peaks at 1045 cm-1 (characteristic of phosphates) increases from day 0 to day 14, supporting the formation of a Ca-P layer at scaffold surface. As the Ca^{2+} ions from present in SBF accumulate with time, the surface of the scaffolds becomes positively charged and therefor it attracts the negatively charged phosphate ions also present in SBF, forming an amorphous calcium phosphate. This is a metastable phase that eventually may latter transform into a stable crystalline apatite [311]. In the region corresponding to higher wavenumbers, 2700-3600 cm^{-1}, the raman spectra did not revealed significant differences when compared with the ones from scaffolds' fibres, meaning that the peaks detected in that region are characteristic of scaffold components.

The KGM-BCP-PDA scaffoldsdid not show considerable differences when comparing the scaffolds' fibres, except on the intensity of the detected peaks. The intensity of the peaks on

day 7 is much lower than the one registered at day 14 and at the scaffold's fibre on day 7. In addition, the peaks located in the region 2700-3600 cm-1 also decreased in their intensity, and the characteristic peak of carbonates (~1400 cm-1) did not appear in the spectrum. For that reason, the increase of the peaks intensity from day 7 to day 14 at the surface of these scaffolds may not be related with the deposition of a Ca-P layer. Probably these variation in intensity may arise from the higher heterogeneity of the scaffolds caused by the presence of PDA nanoparticles in the composition.

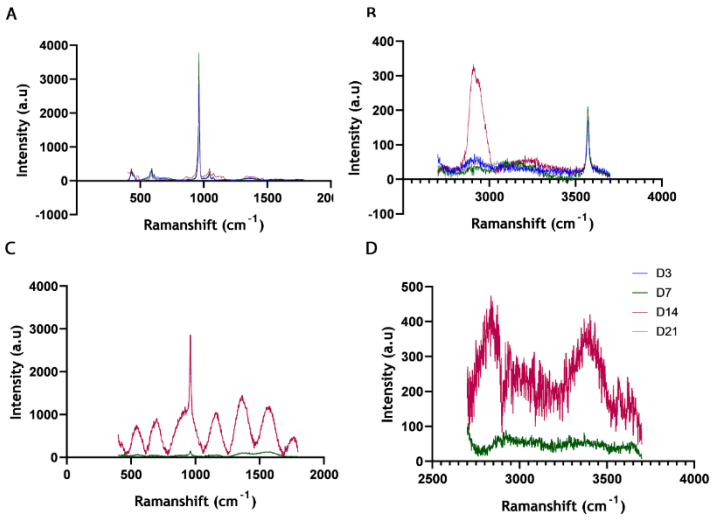

Figure 34 - Raman Spectrums of KGM-BCP and KGM-BCP-PDA surface. (A) KGM-BCP spectrum in the 800-1400 cm^{-1} region. (B) KGM-BCP spectrum in the 2700-3600 cm^{-1} region. (C) KGM-BCP-PDA spectrum in the 800-1400 cm^{-1} region. (D) KGM-BCP-PDA spectrum in the 2700-3600 cm^{-1} region.

Taking together all these results, the KGM-BCP scaffolds demonstrated bioactivity through the formation of a carbonated apatite-like layer on their surface, which is a strong predictor of their in vivo bone bioactivity. Regarding the KGM-BCP-PDA scaffolds, it appears that the presence of PDA may retard the formation of such layer. However, the inclusion of SEM images complemented with an energy dispersive spectroscopy (EDS) is needed, to effectively conclude if the "crystals" at the KGM-BCP scaffolds represent the deposition of crystalline apatite.

1.6. *In vitro* assessment of the metabolic activity and morphology of hMSCs seeded on the KGM-BCP scaffolds

After the production of the 3D KGM-BCP scaffolds, we studied some *in vitro* parameters in order to simulate the complex interactions between cells and scaffolds in a relatively controlled

environment. The in vitro studies included the metabolic activity assessment of a cell population (hMSCs) and the morphologic evaluation of the cells on the developed scaffolds, to investigate the possibility of these scaffolds support a long-term cell attachment and proliferation. The choice in using hMSCs is due to their intensive and establish use in the study of osteogenic differentiation on CaP scaffolds for bone applications [312–314], since these cells are important for making and repairing skeletal tissues, such as bone, cartilage and fat.

The *in vitro* studies in this part of the work were performed following two different experiments. On the first (experiment A) before hMSCs seeding, the scaffolds were pre-incubated for 7 days with both basal and osteogenic medium with the aim to evaluate if a pre-incubation time with OM is advantageous over a pre-incubation with BM. It is reported in the literature that more cell proliferation and attachment occur as the pre-incubation time increases, which might happen because of the long term increase of protein adsorption after the incubation [315]. On the second experiment (experiment B) a "normal" seeding process was realized as described in the "materials and methods section" (figure 25).

To assess the metabolic cell activity of hMSCs on the KGM-BCP scaffolds, a resazurin-based method was used after collecting the samples at specific timepoints (T0, T7 and T28 for experiment A and T0, T7, T14 and T28 for experiment B). Although the absence of statistical analysis, on experiment A (figure 35-A) it is possible to observe an overall increase of the hMSCs' metabolic activity from day 0 to day 28 in both conditions, and this increase seems to be more significant on the cells that were pre-incubated with osteogenic medium. Also, in both conditions, the increase of the metabolic activity of the cells seemed to be more significant from day 0 to day 7. A (slightly) decrease was detected form day 7 to day 28 on the cells that were maintained in the basal medium through the entire experience. These results indicate that hMSCs remained viable and metabolically active until the end of the experience, being able to proliferate. Also, they reveal that a pre-incubation period with osteogenic medium seems advantageous.

To confirm these results, the morphology of the hMSCs on the scaffolds was assessed by CSLM visualization (figure 35-B). The images show the presence of cells until the 28th day of experiment. However, it is not possible to verify a difference on the cell number throughout the time they were in culture. In all the images it is possible to observe the presence of fibronectin, an ECM protein. This glycoprotein is crucial not only for attaching cells to matrices but also for guiding cell migration, being also able to interact with several extracellular processes. The actin filaments are also very visible on T7 of the cells that were pre-incubated with osteogenic medium. This protein is essential to maintain the cell stability and morphogenesis, being involved in many crucial processes, such as cell division, endocytosis, and cell migration. Cells presented a normal morphology as can be observed by the cytoskeleton visualization (f-actin). Cells are able to adhere and spread over the scaffold fibers along time.

Taking all together these results, despite the resazurin based assay not being in agreement with the confocal images, it is possible to confirm that the cells were able to adhere to the scaffolds throughout the entire time in culture and a typical hMSC morphology, a

polygonal shape with a multiple contact points with the scaffolds. These results also indicate that resazurin assay may not be the ideal technique to assess the metabolic activity either due to limits of detection (thus, the assay must be optimized for our system), or due to problems with the diffusion of resazurin solution to the interior of the scaffold.

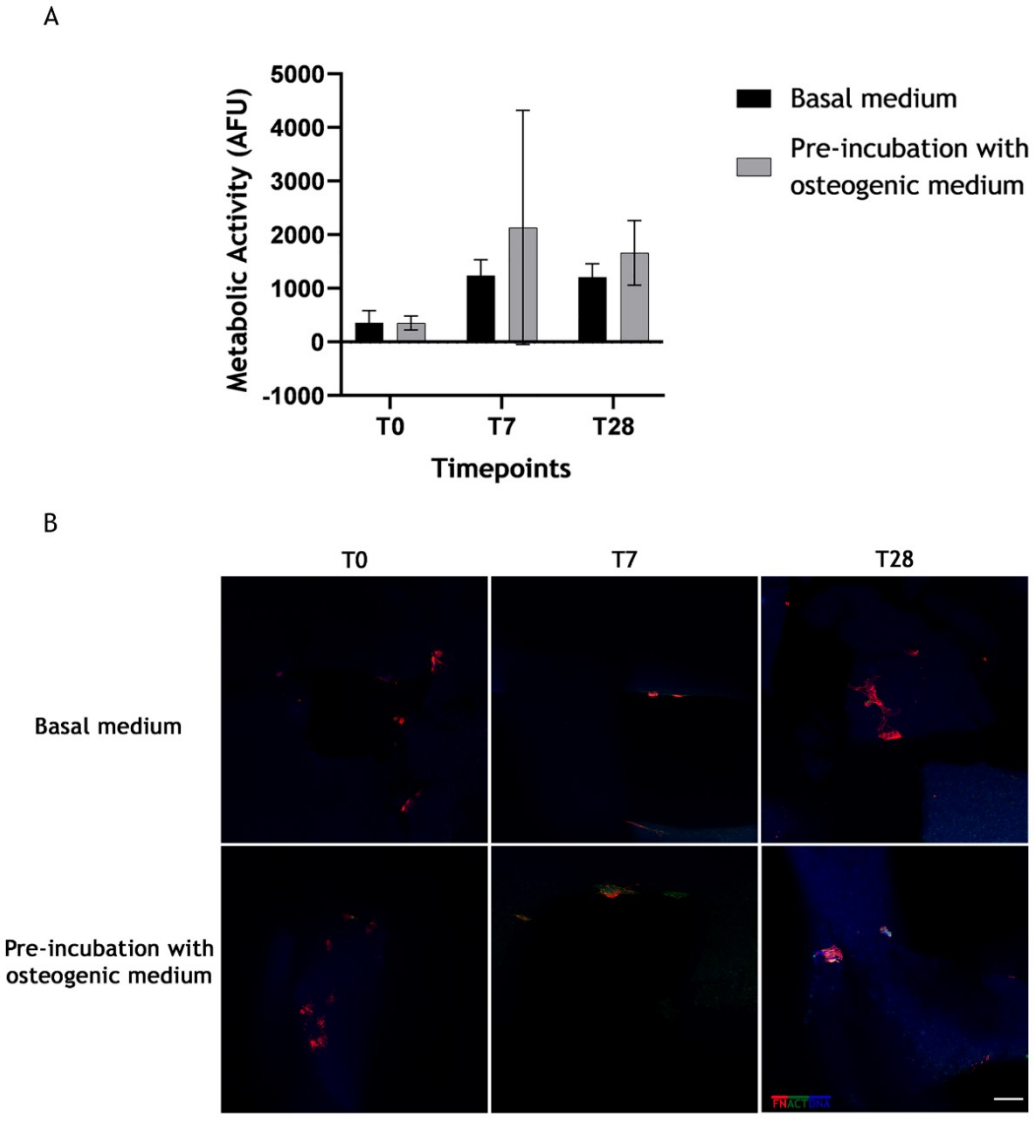

Figure 35 - Metabolic activity and morphology of hMSCs on the KGM-BCP scaffolds (experiment A) (A) From day 0 to day 28, an increase of the metabolic cell activity if verified both basal and osteogenic conditions. Outlier values were excluded from this analysis. (B) Confocal microscopy images to assess the morphology of hMSCs throughout the entire experience, stained for nuclei (blue), F-actin (green) and fibronectin (red). Scale bar: 100 µm.

On experiement B, the resazurin-based assay showed negative values (after normalization with blank values) on the metabolic activity of the cells (figure 36-A), which indicates that the cells may not be alive or, at least, are not metabolic active. However, when looking for the confocal images (figure 36-B), it is possible to see that are present both fibronectin and actin filaments, as happened in experiment A. Also, we can observe once again the prevalence of fibronectin on the scaffolds and a typical hMSC morphology is even observed until the later

culture timepoints. The discrepancy between the resazurin assay and the confocal images may be due to the low number os cells present on the scaffolds, that did not allow their detection on the resazurin assay. The number of cells present in the scaffold can be on the limit of detection of the resazurin assay. Future experiments should adress this issue. Limits in the difusion are also an hypothesis and could be solved with agitation during the resazurin assay incubation period.

Moreover, these in vitro results are not in agreement with what is reported on the literature as it was expected an increase of the cells' metabolic activity in both conditions (basal and osteogenic) from day 0 to day 28, and this increase should have been more emphazied on the basal medium. Regarding the osteogenic medium, the metabolic activity of the cells should have been lower than on basal medium [316,317].

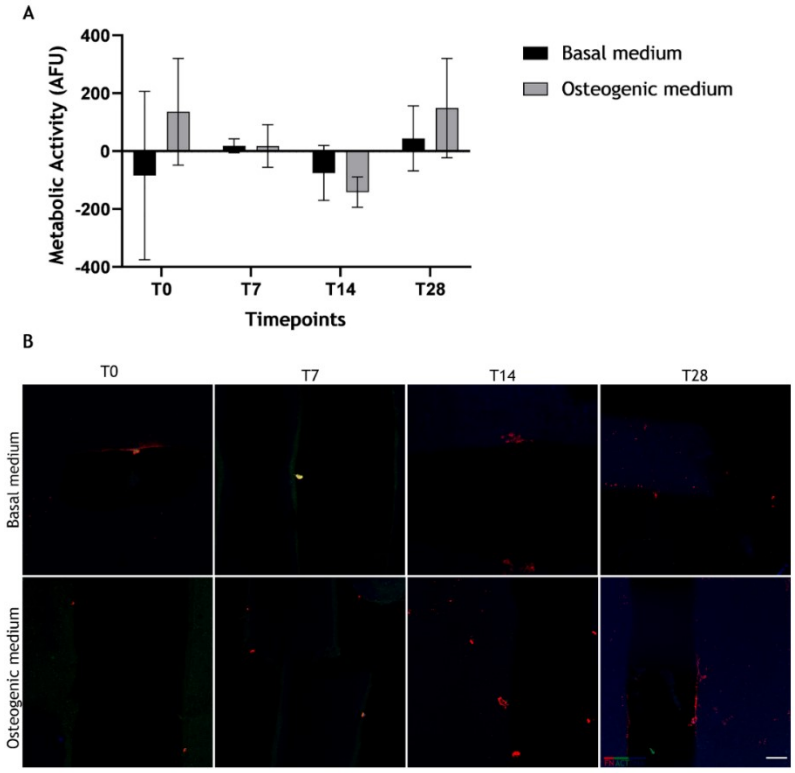

Figure 36 - Metabolic activity of hMSCs and their morphology on the KGM-BCP scaffolds (experiment B) (A) – Metabolic Cell Activity during the differentiation assay for basal and osteogenic conditions. (B) - Confocal microscopy images to assess the morphology of hMSCs throughout the entire experience, stained for nuclei (blue), F-actin (green) and fibronectin (red). Scale bar: 100 µm.

2. Hybrid 3D KGM-BCP scaffolds with drug-delivery properties

In order to develop scaffolds that allow bone and also with the capability of treating infections (bi-functional scaffold), we intend to develop nanoparticles loaded with levofloxacin

(LFX), able of being incorporated on the scaffolds (figure 37). This drug has been reported to be effective eradicating S. aureus bacterial biofilm while allowing bone regeneration at the same time, once incorporated on a hierarchical mesomacroporous 3D scaffold [236]. PLGA nanoparticles were selected to load the drug since it is reported in the literature its efficacy and capability of promoting a sustained release of the drug [260,318]. The NPs were produced according to the doble-emulsion method and they were stored at 4ºC with a final volume of 1mL and a LFX concentration of 1mg/mL.

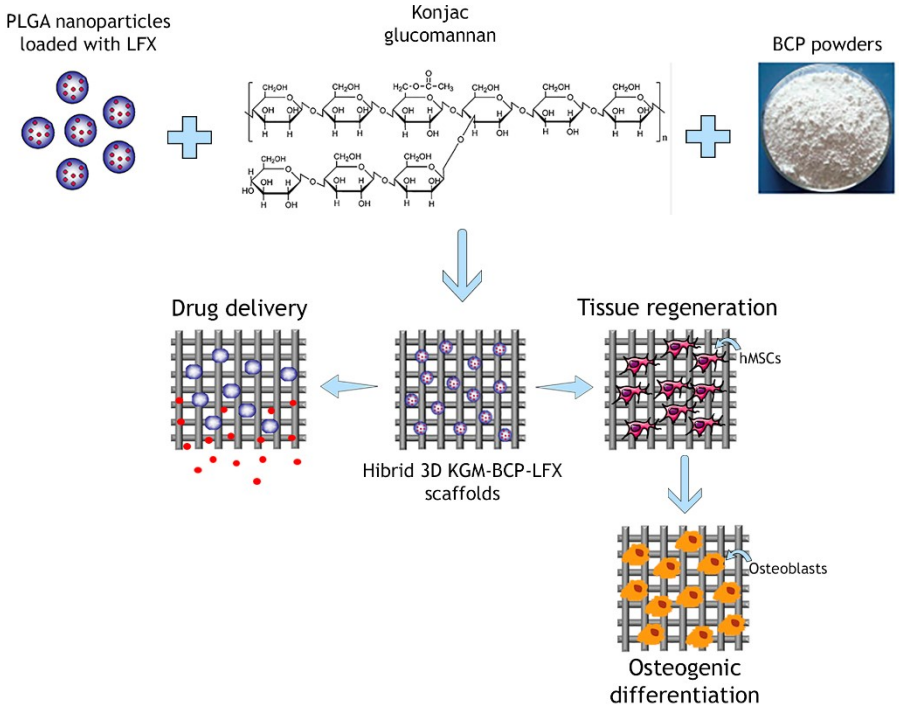

Figure 37 - Representative scheme regarding the incorporation of levofloxacin on the 3D KGM-BCP scaffolds to produce a bi-functional scaffold. The inclusion of levofloxacin-loaded nanoparticles aims to give the scaffolds the feature of drug delivery, whereby the nanoparticles can be incorporated during the ink preparation. Besides that, bone tissue regeneration ability is also desired.

2.1. Preparation and characterization of the levofloxacin-loaded nanoparticles

The w/o/w double emulsion technique was the method used to produce empty and LFX-loaded PLGA NPs. All NPs formulations were characterized after production regarding particle size, PdI and surface charge (Table 10). Mean particle size (Z-average or hydrodynamic radius) and surface charge (Zeta potential) are the two most commonly studied factors that are responsible for a range of biological effects of NPs. They were measured by DLS and ELS, respectively. Zeta potential is the potential at the slipping/shear plane of a colloid particle moving under electric field, and its widely used to assess the surface charge of NPs. PdI was

used to characterize the NP size distribution, where small values of PdI (near to zero) confirm the uniformity of size distribution.

Table 10 - Nanoparticles characterization regarding their Average size, Polydispersity index and Zeta potential.

	LFX-NPs	Control-NPs
Average Size (nm)	89.59	97
Polydispersity Index	0.133	0.143
Zeta Potential (mV)	-4.71	-7.1

These results are slightly different with the ones reported on the literature, since it is reported in the literature that using the same method to prepare these kind of NPs the average size of the NPs is around 424 nm, the PdI is around 0.35 and the zeta potential -33 mV [318], which is not in accordance with the developed nanoparticles.

It is known that the size of polymeric nanoparticles can range between 10 nm and 1 μm [319] and both particle size and size distribution are a major characteristic of nanoparticles. They determine the in vivo distribution of these delivery systems, and also their biological fate, toxicity and targeting ability. Moreover, they can influence drug loading, drug release and the stability of the nanoparticles. Smaller nanoparticles, by having a larger surface area-to-volume ratio, allow the drug to be incorporated near or at the particle surface, which leads to a faster drug release and, on the other hand, the larger core of bigger nanoparticles, allows the encapsulation of more drug per particle and have a slower release [320]. The PdI can measure the heterogeneity of a sample based on the size, since it is a representation of the distribution of size populations within a given sample. It is stablished, according to International standards organizations (ISOs), that PdI values < 0.05 are characteristic of monodisperse samples, while values > 0.7 are assigned to a broad size (e.g., polydisperse) distribution of particles (ISO standards ISO 22,412:2017 and ISO 22,412:2017). In polymer-based nanoparticle materials, values of 0.2 and below are considered to be the most acceptable [321,322]. Regarding the zeta potential, its value is affected by the chemistry of the NP surface, particle concentration, size of particle, pH of the medium, temperature and ionic strength [321]. This parameter indicates the stability of the NP suspension, since a higher electric charge on the surface of the NPs will prevent aggregation of the NPs in a buffer solution. In fact, it is established that absolute values above 30 mV provide good stability and above 60 mV excellent stability. In contrast, if the zeta potential falls below a certain level, the emulsion droplets or colloids will aggregate as a result of the attractive forces, so a ZP about 20 mV provides only short-term stability and values in the range -5 mV to +5 mV indicate fast aggregation [323]. Since we obtained a zeta potential that falls into this range, the fast aggregation of the nanoparticles

may be the cause of the size reduction of the nanoparticles after drug incorporation, when compared with the NPs loaded with water (control).

2.2. Levofloxacin Encapsulation Efficiency

In order to assess the amount of drug that was efficiently loaded into the nanoparticles, levofloxacin-loaded samples were analysed by HPLC. The chromatograms showed that the characteristic peak of the levofloxacin, which appears approximately on min 7 (figure 38-A) [324] appeared only on the samples obtained using the indirect method (Ind-LVX) (figure 38-B), which reveals that the drug was not incorporated on the NPs and remained only on the supernatant (that was collected after the first concentration of the NPs suspension, using Amicon filters). Moreover, there are no significant differences between the chromatograms obtained on the drug-loaded NPs and their controls (data not shown). Regarding the amount of drug that appeared on the supernatant, by using the standard curve equation ($y = 104741x + 48749$), it was possible to conclude that the supernatant had a levofloxacin concentration of 14 µg/mL. Given that the initially concentration of the drug was 88.9 µg/mL (2 mg of levofloxacin in a final volume solution of 22.5 mL), the efficiency of the process was very low (15,7 %), which demonstrates that a lot of drug was lost during the NPs fabrication process.

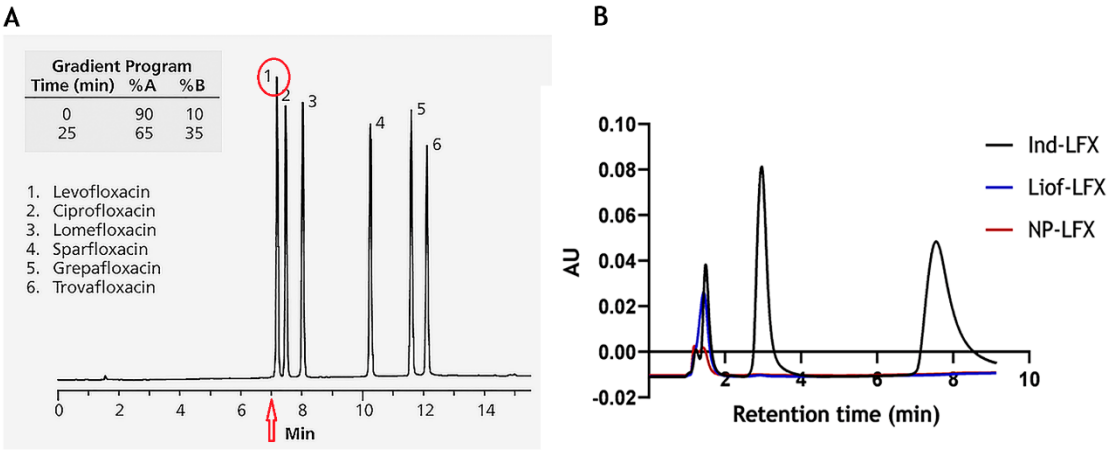

Figure 38 - HPLC analysis of Antibiotics and chromatograms obtained to assess the levofloxacin (LFX) encapsulation. (A) Fluoroquinolones chromatograms. The retention time of LFX is at, approximately, 7 min [324]; (B) HPLC chromatograms correspondent to the vial nº1 of the samples obtained by the direct method (NP-LFX), the indirect method (Ind-LVX), and after NPs lyophilization (Liof-LFX). It is possible to observe that levofloxacin is only detected on the Ind-LFX samples.

To a nanodelivery system be successful, it should have a high drug-loading capacity, in order to reduce the quantity of dose administrations. The drug solubility in the excipient matrix (solid polymer or liquid dispersion agent) it is a parameter than can affect both drug loading and entrapment efficiency. It is related with the matrix composition, molecular weight, the presence of end functional groups in either the drug or matrix and drug-polymer interactions [320]. According to a study reported on the literature that used a PLGA nanoparticle to

incorporate a polar model drug (Rose Bengal), a low drug loading can be attributed to several factors. First, if the drug is hydrophilic, it can happen a significant loss of the drug to the external aqueous phase during the production process. Second, if the particle has a small size, as said before, the drug will be incorporated near or at the nanoparticle's surface, allowing it to be readily release during the nanoparticle production or during the removal of unincorporated drug [325]. Other aspects that may influence the absence of drug incorporation in the delivery system develop during this work can be the potential zeta of the nanoparticles and the nanoparticle's time of storage. The low potential zeta shows a low stability of the system and combining that with the long period of storage and low size of the particles, it may have result on drug loss before it was possible to quantify it. Besides that, by using a biodegradable polymer, it is possible to infer that the polymer could have started to degrade during the long period of storage, allowing the drug to be released. It is also known that the release of NPs produced through PLGA 50:50, used in the present work, achieve a complete degradation profile after two months [326].

Taking all this into consideration, and in order to obtain a more reasonable explication about the absence of drug incorporation, the characterization of the nanoparticles should have been done also after their storage (and before HPLC analysis). This could verify if the parameters of average size, polydispersity index and zeta potential have changed and, if so, they might have explained the results.

Since the nanoparticles did not show any incorporation of the drug, we did not proceed to the assessment of its encapsulation efficiency, as reported in the materials and methods section. Moreover, we did not perform the incorporation of the PLGA-LFX NPs on the scaffolds as planned in the beginning of this thesis.

3. Hybrid 3D KGM-BCP scaffolds with hyperthermia properties

On the first part of this work, only scaffolds composed by KGM and BCPs where used, with the aim of comparing them with the previously developed scaffolds (in another work inserted within this project) and optimize them to improve the outcomes related with the material's bone regeneration ability. On the second part, we tried to develop a scaffold with drug delivery properties but, due to some technical constrains, it was not possible to accomplish that purpose. Finally, the third strategy to develop a bi-functional scaffold relied on the incorporation of polydopamine particles within the scaffold (during the ink preparation, as explained in the materials and methods section), that could have the capability of killing tumor cells by hyperthermia (figure 39). The use of polydopamine is due to its properties as a photosensitive agent, being considered as a therapeutic agent in the field of photothermal therapy to treat cancer cells [178]. It is reported in the literature that using a laser irradiation

of 808 nm, nanospheres of PDA can increase the temperature hight enough on the region affected with tumor cells, being even able to kill them [327].

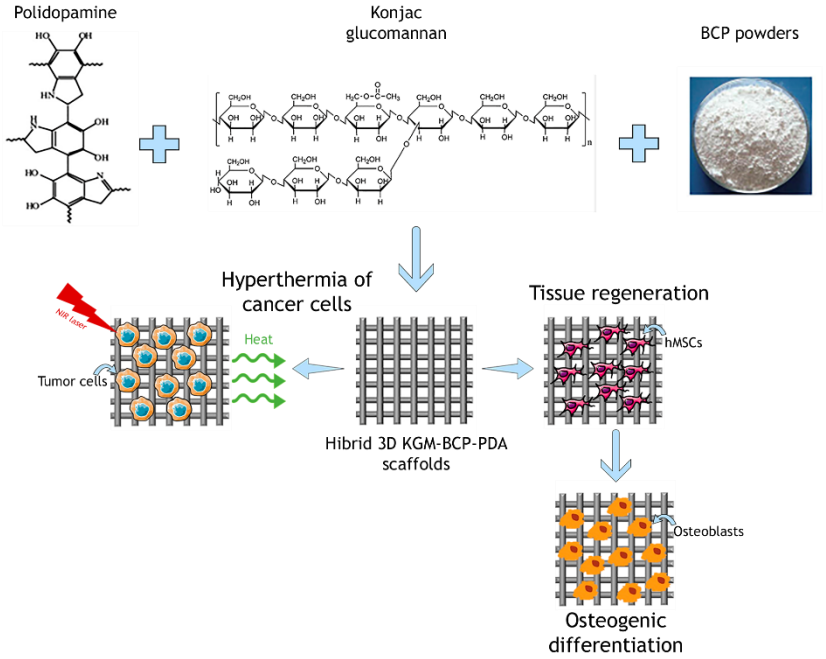

Figure 39 - Second strategy adopted to produce a bi-functional scaffold. The goal is to develop scaffolds that are capable of treating bone cancer cells. To achieve that, polydopamine particles were added during the ink preparation of the scaffolds, since they have showed an optical absorption in the NIR region. Once again, bone tissue regeneration is also desired.

The polydopamine particles were developed previously by our lab, by a alkaline polymerization of dopamine hydrochloride (figure 40-A) and did show promise results upon their characterization, especially by having a strong optical absorption in the NIR region (600 to 1000 nm) (figure 40-C) [278]. Also, this is a continuation of a work develop within this project, which goal is to develop scaffolds with photosensitive properties, to be applied in the treatment of bone cancers.

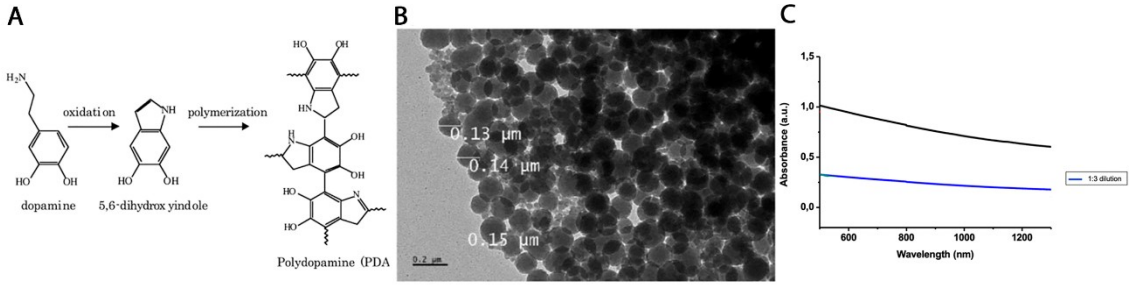

Figure 40 - Characterization of the previously prepared polydopamine particles that were used to fabricate the KGM-BCP-PDA scaffolds. (A) synthesis reaction of polydopamine from dopamine [328]. (B) SEM characterization of polydopamine particles that show their spherical shape and a diameter around 150 nm [278]. (C) Uv-vis spectrum of polydopamine particles, showing their good absorbance in the Near infrared region (NIR) [278].

3.1. In vitro studies on the 3D KGM-BCP and KGM-BCP-PDA scaffolds

3.1.1. Metabolic activity and morphology of hMSCs seeded on the KGM-BCP and KGM-BCP-PDA scaffolds

To assess the metabolic cell activity of hMSCs on the KGM-BCP and KGM-BCP scaffolds, the parameters assessed were the same as the ones in the previously in vitro experiments. Accordingly, first a resazurin-based method was used after collecting the samples previously seeded on the scaffolds, at specific timepoints (T1, T7, T14 and T28). On figure 41-A, it is possible to observe an increase of the hMSCs' metabolic activity from day 1 to day 28 but this increase is not constant with time. However, by looking to the confocal images taken on the same timepoints (figure 41-B) it is possible to see a high number of cells attached and spread over the scaffolds, even on timepoints that have showed very low metabolic activity (such as on T14). It is possible to see that on the scaffolds that have showed less autofluorescence (T1 of KGM-BCP scaffolds on basal medium and T1 and T7 of KGM-BCP scaffolds on osteogenic medium) the nuclei of cells are visible, confirming that the intense signal of the scaffolds might have obscured the signal of the nuclei. When comparing the two type of scaffolds, the confocal images always show a higher number of cells on the KGM-BCP-PDA scaffolds, being this difference more significative on the cells incubated with osteogenic medium. These results are consisting with the ones reported on the literature, as it is reported that the inclusion of PDA in scaffolds allow a better adhesion and proliferation of hMSCs, , when comparing with the same materials without PDA [329]. Regarding the basal medium, this conclusion is only verified on T1 and T7. Cytoskeleton visualization indicates that the cells present the expected morphology.

When comparing the influence of the type of medium where the cells were incubated, regardless the type of scaffold, the confocal images indicate that the osteogenic medium seems to have allowed the growth, attach and spread of a higher number of cells, when comparing to the basal medium (figure 41-B). However, this tendency is not verified for every timepoint on the resazurin assay (figure 41-A).

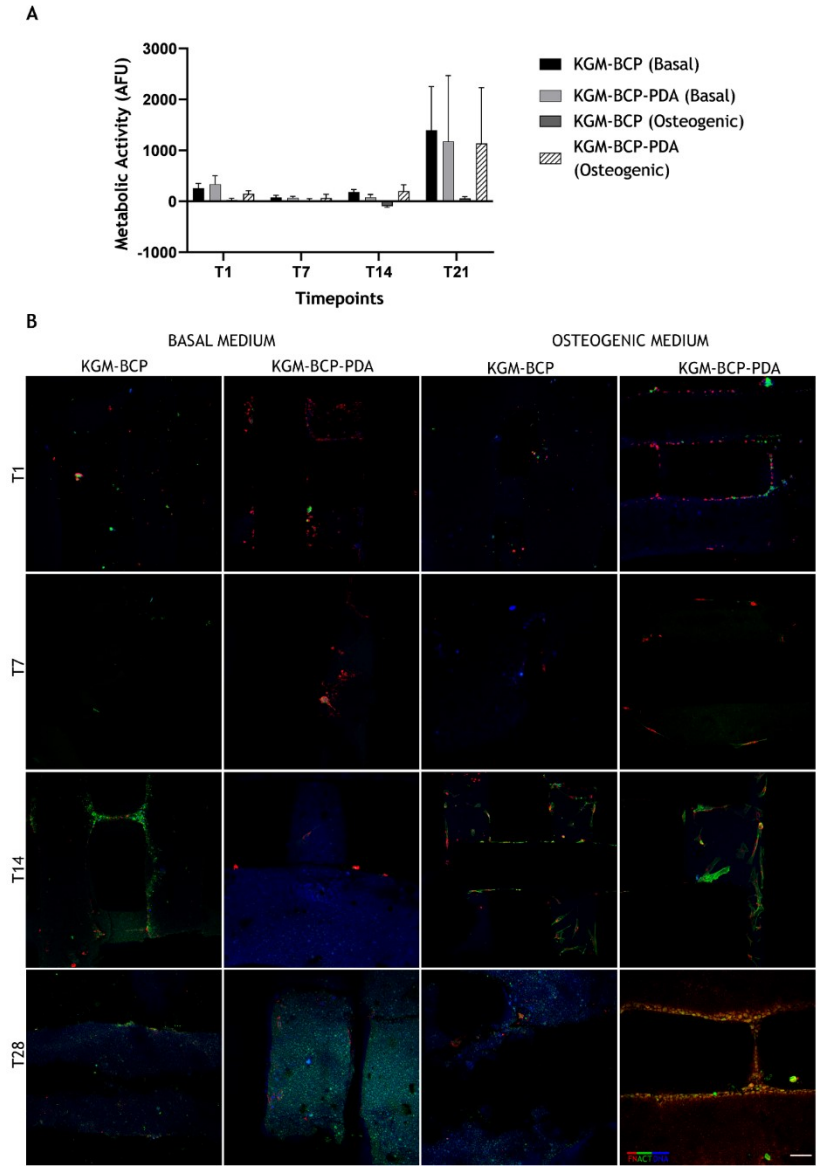

Figure 41 - Metabolic activity of hMSCs and their morphology on the KGM-BCP and KGM-BCP-PDA scaffolds. (A) From day 0 to day 28, an increase of the metabolic cell activity if verified both basal and osteogenic conditions, that is not constant with time. Outlier values were excluded from this analysis. (B) - Confocal microscopy images to assess the morphology of hMSCs throughout the entire experience, stained for nuclei (blue), F-actin (green) and fibronectin (red). Scale bar: 100 µm.

3.1.2. Metabolic activity and morphology of U20S osteosarcoma cell line on the KGM-BCP and KGM-BCP-PDA scaffolds

To assess the metabolic cell activity of U2OS cell line on the KGM-BCP and KGM-BCP scaffolds, the parameters assessed were the same as the ones in the previously in vitro experiments. On figure 42-A it is possible to see that the cells maintain their metabolic activity constant through all the time in culture, when seeded on KGM-BCP scaffolds but, on the KGM-BCP-PDA scaffolds, their activity increases from day 1 to day 10. The confocal images confirm

the analysis done for the resazurin based assay on the KGM-BCP-scaffolds (figure 42-B), but on the KGM-BCP-PDA type of scaffolds a higher number of cells in only observed on T1 indicating higher initial seeding efficiency. The images of the scaffolds regarding T10 were lost and thus they are not present on this work. The analysis of these results leads us to conclude that osteoblasts proliferate better, when seeded on KGM-BCP scaffolds than on KGM-BCP-PDA scaffolds. The morphology of these cells is different from hMSCs, showing a more spherical form as expected.

Unlike what happened for hMSCs, the inclusion of PDA on the KGM-BCP scaffolds does not seems to bring advantages for the adhesion and proliferation of osteoblasts and the causes should be addressed in future experiments. However, as reported on the literature, these cells should have showed a better adhesion, spread and proliferation when seeded in a material with PDA [330]

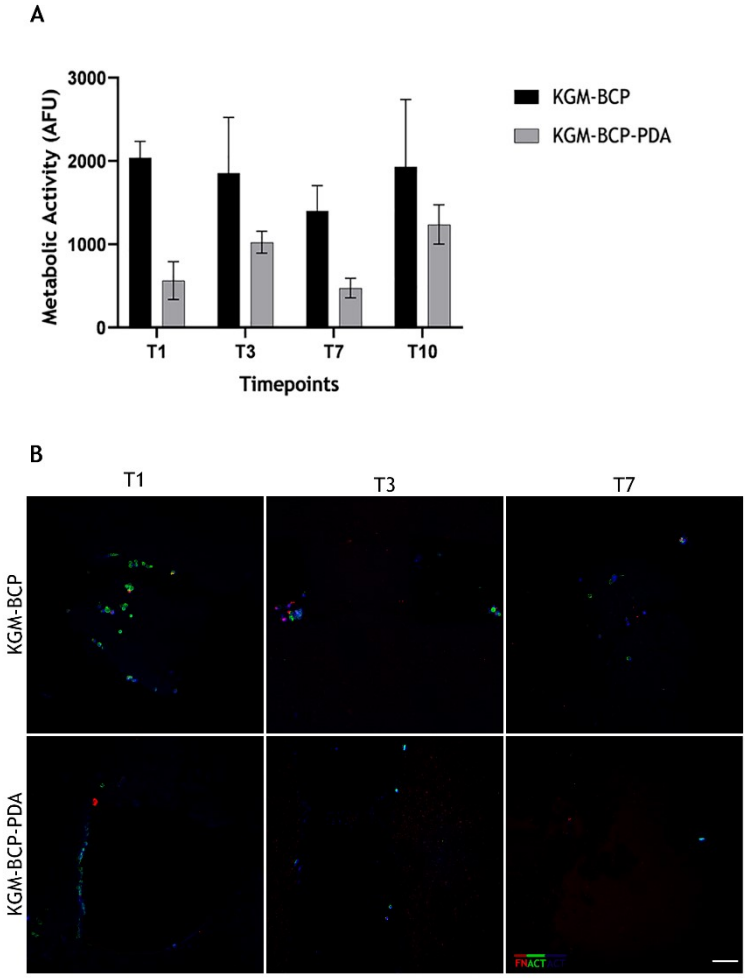

Figure 42 - Metabolic activity of U20S and their morphology on the KGM-BCP and KGM-BCP-PDA scaffolds. (A) From day 1 to day 7 the cells on KGM-BCP scaffolds maintain their metabolic activity constant. Outlier values were excluded from this analysis. (B) - Confocal microscopy images to assess the morphology of the U20S cells throughout the entire experience, stained for nuclei (blue), F-actin (green) and fibronectin (red). Scale bar: 100 µm.

Conclusions and Future Work

On the first part of this work, the KGM-BCP scaffolds validated the hypothesis of being a material that can support cell attachment and proliferation of hMSC. Cells were able to adhere to the scaffolds throughout the entire time in culture but, to infer about their capacity in promoting bone regeneration, further studies are necessary. They include the assessment of the hMSCs' ability to differentiate into the osteogenic lineage, which can be done, for example, through ALP enzymatic assays and gene expression tests. Additionally, the inclusion of additional experiments is also fundamental to rule out out possible experimental errors that led to controversial results, especially when comparing the results obtained in the assay of metabolic cell activity and confocal images.

Regarding the second part, the aim was to develop a bi-functional scaffold that could, simultaneously promote bone regeneration and treat bone infections. However, despite the successful production of PLGA nanoparticles, HPLC assays revealed that the drug (LFX) was not incorporated on the NPs, possibly due to the high period of incubation time. Unfortunately, due to time constraints, no additional advances were made regarding this part of the work.

Finally, a different approach was developed to produce bi-functional scaffolds. The production of the new KGM-BCP-PDA scaffolds was conducted by robocasting, as in our base material (KGM-BCP scaffolds). Both developed inks were characterized regarding their rheological properties and it was revealed that both had a shear thinning behavior that is essential for printing in robocasting. The characterization of the scaffolds proceeded with the assessment of their mechanical properties, by evaluating their compressive strength. Both KGM-BCP and KGM-BCP-PDA scaffolds showed a very low compressive strength (far below the one in the real bone). A strategy to overcome this problem can be the reduction of the pore size of the material, keeping in mind that a balance must be established. The size of the pores needs to be relatively small in order to increase the mechanical properties of the scaffolds but sufficiently high to allow new bone formation. Finally, when it comes to the characterization of these systems, a SBF assay was performed in order to infer about the *in vivo* bone bioactivity of the scaffolds. The confocal Raman micro spectroscopy of the samples showed the possibility of apatite formation on the surface of the scaffolds but further analysis (such as SEM/EDS) should be conducted to confirm this hypothesis. Further characterizations, such as degradation studies, and viscoelastic properties measurements in dry and wet states are also important to have into consideration.

These new hybrid systems were also assessed for their *in vitro* ability to support cell attachment and proliferation of two types of cells: hMSCs and U20S osteosarcoma cell line. The KGM-BCP-PDA scaffolds showed a better adhesion and proliferation of hMSCs when comparing with the same materials without PDA but the opposite happened when using U20S cells.

From this thesis we can conclude that the use of KGM-BCP-PDA scaffolds is a promising tool when looking for bi-functional scaffolds capable of regenerating bone and, at the same time,

kill cancer cells. However, a major assessment still needs to be performed - The evaluation of the hyperthermic potential of these scaffolds under laser irradiation, to further confirm their suitability for cancer treatment applications. Only after this study, more conclusive statements can be done regarding the bi-functionality of the developed scaffolds

References

[1] R. Florencio-Silva, G.R.D.S. Sasso, E. Sasso-Cerri, M.J. Simões, P.S. Cerri, "Biology of Bone Tissue: Structure, Function, and Factors That Influence Bone Cells," *Biomed Res. Int.* , vol. 2015, 2015

[2] A.R. Costa-Pinto, R.L. Reis, N.M. Neves, "Scaffolds based bone tissue engineering: The role of chitosan," *Tissue Eng. - Part B Rev.* , vol. 17, pp. 331–347, 2011

[3] Y. Mahsut Dinçel, "Bone Graft Types," in: Bone Grafting - Recent Adv. with Spec. Ref. to Cranio-Maxillofacial Surg., IntechOpen, , 2018

[4] U. Ranjan Dahiya, S. Mishra, S. Bano, "Application of Bone Substitutes and Its Future Prospective in Regenerative Medicine," in: Biomater. Tissue Reconstr. or Regen., IntechOpen, , 2019

[5] P.A. Downey, M.I. Siegel, "Bone biology and the clinical implications for osteoporosis," *Phys. Ther.* , vol. 86, pp. 77–91, 2006

[6] K.M. Alghazali, Z.A. Nima, R.N. Hamzah, M.S. Dhar, D.E. Anderson, A.S. Biris, "Bone-tissue engineering: Complex tunable structural and biological responses to injury, drug delivery, and cell-based therapies," *Drug Metab. Rev.* , vol. 47, pp. 431–454, 2015

[7] D. King, "Bone Remodelling," (Available at: http://www.siumed.edu/~dking2/ssb/remodel.htm. Accessed on: May 1, 2020), 2004

[8] M. Capulli, R. Paone, N. Rucci, "Osteoblast and osteocyte: Games without frontiers," *Arch. Biochem. Biophys.* , vol. 561, pp. 3–12, 2014

[9] M. Brickley, R. Ives, "Background to Bone Biology and Mineral Metabolism," in: Bioarchaeology Metab. Bone Dis., Elsevier, : pp. 21–40, 2008

[10] T.A. Franz-Odendaal, B.K. Hall, P.E. Witten, "Buried alive: How osteoblasts become osteocytes," *Dev. Dyn.* , vol. 235, pp. 176–190, 2006

[11] L.F. Bonewald, "The amazing osteocyte," *J. Bone Miner. Res.* , vol. 26, pp. 229–238, 2011

[12] G.Y. Rochefort, S. Pallu, C.L. Benhamou, "Osteocyte: The unrecognized side of bone tissue," *Osteoporos. Int.* , vol. 21, pp. 1457–1469, 2010

[13] F. Johannesdottir, M.L. Bouxsein, "Bone structure and biomechanics," *Encycl. Endocr. Dis.* , vol. 4, pp. 19–30, 2018

[14] N. Takahashi, Y. Kobayashi, N. Udagawa, "Osteoclasts," in: Princ. Bone Biol., Elsevier, : pp. 111–131, 2019

[15] F. Xu, S.L. Teitelbaum, "Osteoclasts: New Insights," *Bone Res.* , vol. 1, pp. 11–26, 2013

[16] C. Gentili/snm, >, R. Cancedda, "Cartilage and Bone Extracellular Matrix," *Curr. Pharm. Des.* , vol. 15, pp. 1334–1348, 2009

[17] A.K. Gaharwar, A. Arpanaei, T.L. Andresen, A. Dolatshahi-Pirouz, "3D Biomaterial Microarrays for Regenerative Medicine: Current State-of-the-Art, Emerging Directions and Future Trends," *Adv. Mater.* , vol. 28, pp. 771–781, 2016

[18] A.K. Nair, A. Gautieri, S.W. Chang, M.J. Buehler, "Molecular mechanics of mineralized collagen fibrils in bone," *Nat. Commun.* , vol. 4, pp. 1–9, 2013

[19] J.A. BUCKWALTER, M.J. GLIMCHER, R.R. COOPER, R. RECKER, "Bone Biology," *J. Bone Jt. Surg.* , vol. 77, pp. 1276–1289, 1995

[20] M.J. Yaszemski, R.G. Payne, W.C. Hayes, R. Langer, A.G. Mikos, "Evolution of bone transplantation: Molecular, cellular and tissue strategies to engineer human bone," *Biomaterials.* , vol. 17, pp. 175–185, 1996

[21] A.S. Mistry, A.G. Mikos, "Tissue engineering strategies for bone regeneration," *Adv. Biochem. Eng.*

Biotechnol. , vol. 94, pp. 1–22, 2005

[22] B. Clarke, "Normal bone anatomy and physiology.," *Clin. J. Am. Soc. Nephrol.* , vol. 3 Suppl 3, pp. S131, 2008

[23] T.M. Keaveny, E.F. Morgan, G.L. Niebur, O.C. Yeh, "Biomechanics of Trabecular Bone," *Annu. Rev. Biomed. Eng.* , vol. 3, pp. 307–333, 2001

[24] T.E. of E. Britannica, "Cancellous bone," *Encycl. Br.* (Available at: https://www.britannica.com/science/cancellous-bone. Accessed on: May 1, 2020), 2015

[25] N. Rucci, "Molecular biology of bone remodelling," *Clin. Cases Miner. Bone Metab.* , vol. 5, pp. 49–56, 2008

[26] H. Drissi, A. Sanjay, "The Multifaceted Osteoclast; Far and Beyond Bone Resorption," *J. Cell. Biochem.* , vol. 1756, pp. 1753–1756, 2016

[27] L.J. Raggatt, N.C. Partridge, "Cellular and molecular mechanisms of bone remodeling," *J. Biol. Chem.* , vol. 285, pp. 25103–25108, 2010

[28] R. Dimitriou, E. Jones, D. McGonagle, P. V. Giannoudis, "Bone regeneration: Current concepts and future directions," *BMC Med.* , vol. 9, pp. 66, 2011

[29] J.B. Chang, J.C. Lee, "Circulating Progenitor Cells in Regenerative Technologies: A Realistic Strategy in Bone Regeneration?," *Int. J. Stem Cell Res. Ther.* , vol. 3, 2016

[30] I. Pountos, P. V. Giannoudis, "Fracture healing: Back to basics and latest advances," in: Fract. Reduct. Fixat. Tech. Up. Extrem., Springer International Publishing, : pp. 3–17, 2018

[31] M. Majidinia, A. Sadeghpour, B. Yousefi, "The roles of signaling pathways in bone repair and regeneration," *J. Cell. Physiol.* , vol. 233, pp. 2937–2948, 2018

[32] "Bone fractures - Better Health Channel," (Available at: https://www.betterhealth.vic.gov.au/health/conditionsandtreatments/bone-fractures. Accessed on: April 30, 2020)

[33] T. Coughlan, F. Dockery, "Osteoporosis and fracture risk in older people," *Clin. Med. J. R. Coll. Physicians London.* , vol. 14, pp. 187–191, 2014

[34] K.N. Tu, J.D. Lie, C.K.V. Wan, M. Cameron, A.G. Austel, J.K. Nguyen, K. Van, D. Hyun, "Osteoporosis: A review of treatment options," *P T.* , vol. 43, pp. 92–104, 2018

[35] "WHO | 5. Population nutrient intake goals for preventing diet-related chronic diseases," *WHO.* (Available at: https://www.who.int/nutrition/topics/5_population_nutrient/en/index25.html. Accessed on: April 30, 2020) pp. 26, 2007

[36] "Facts and Statistics | International Osteoporosis Foundation," (Available at: https://www.iofbonehealth.org/facts-statistics#category-18. Accessed on: April 30, 2020)

[37] US Department of Health and Human Services, "Bone health and osteoporosis: a report of the Surgeon General," *US Heal. Hum. Serv.* pp. 437, 2004

[38] "Osteoporosis - Symptoms, Treatment, & Bone Health," *MSK Aust.* (Available at: https://www.msk.org.au/osteoporosis/. Accessed on: May 1, 2020)

[39] Jennifer Robinson, "Osteoporosis Guide: Brittle Bones, Treatments, and More," *WebMD.* (Available at: https://www.webmd.com/osteoporosis/ss/slideshow-osteoporosis-overview. Accessed on: May 1, 2020), 2018

[40] A. Ho-Shui-Ling, J. Bolander, L.E. Rustom, A.W. Johnson, F.P. Luyten, C. Picart, "Bone regeneration strategies: Engineered scaffolds, bioactive molecules and stem cells current stage and future perspectives," *Biomaterials.* , vol. 180, pp. 143–162, 2018

[41] P. V. Giannoudis, H. Dinopoulos, E. Tsiridis, "Bone substitutes: an update.," *Injury.* , vol. 36 Suppl 3, pp. S20–S27, 2005

[42] A. Misaghi, A. Goldin, M. Awad, A.A. Kulidjian, “Osteosarcoma: a comprehensive review,” *SICOT-J.* , vol. 4, 2018

[43] R. Rajani, C.P. Gibbs, “Treatment of Bone Tumors,” *Surg. Pathol. Clin.* , vol. 5, pp. 301–318, 2012

[44] A. Luetke, P.A. Meyers, I. Lewis, H. Juergens, “Osteosarcoma treatment - Where do we stand? A state of the art review,” *Cancer Treat. Rev.* , vol. 40, pp. 523–532, 2014

[45] Dr. Wittig, “Osteosarcoma (Conventional): Bone Tumor Cancer,” (Available at: http://www.tumorsurgery.org/tumor-education/bone-tumors/types-of-bone-tumors/osteosarcoma-conventional.aspx. Accessed on: May 1, 2020), 2014

[46] J.A. Ludwig, “Ewing sarcoma: Historical perspectives, current state-of-the-art, and opportunities for targeted therapy in the future,” *Curr. Opin. Oncol.* , vol. 20, pp. 412–418, 2008

[47] R.F. Riedel, N. Larrier, L. Dodd, D. Kirsch, S. Martinez, B.E. Brigman, “The clinical management of chondrosarcoma,” *Curr. Treat. Options Oncol.* , vol. 10, pp. 94–106, 2009

[48] A. Ibrahim, “3D bioprinting bone,” in: 3D Bioprinting Reconstr. Surg. Tech. Appl., Elsevier Inc., : pp. 245–275, 2018

[49] K. Nishitani, S.N. Bello-Irizarry, K.L. De Mesy Bentley, J.L. Daiss, E.M. Schwarz, “The Role of the Immune System and Bone Cells in Acute and Chronic Osteomyelitis,” in: Osteoimmunology Interact. Immune Skelet. Syst. Second Ed., Elsevier Inc., : pp. 283–295, 2016

[50] Y. Yang, L. Chu, S. Yang, H. Zhang, L. Qin, O. Guillaume, D. Eglin, R.G. Richards, T. Tang, “Dual-functional 3D-printed composite scaffold for inhibiting bacterial infection and promoting bone regeneration in infected bone defect models,” *Acta Biomater.* , vol. 79, pp. 265–275, 2018

[51] S. Miwa, T. Shirai, N. Yamamoto, K. Hayashi, A. Takeuchi, K. Tada, Y. Kajino, H. Inatani, T. Higuchi, K. Abe, Y. Taniguchi, H. Tsuchiya, “Risk factors for postoperative deep infection in bone tumors,” *PLoS One.* , vol. 12, pp. 1–9, 2017

[52] S. Steinmetz, D. Wernly, K. Moerenhout, A. Trampuz, O. Borens, “Infection after fracture fixation,” *EFORT Open Rev.* , vol. 4, pp. 468–475, 2019

[53] W.J. Metsemakers, R. Kuehl, T.F. Moriarty, R.G. Richards, M.H.J. Verhofstad, O. Borens, S. Kates, M. Morgenstern, “Infection after fracture fixation: Current surgical and microbiological concepts,” *Injury.* , vol. 49, pp. 511–522, 2018

[54] L.S. Jorge, A.G. Chueire, A.R. Baptista Rossit, “Osteomyelitis: a current challenge,” *Brazilian J. Infect. Dis.* , vol. 14, pp. 310–315, 2010

[55] A. Hasan, B. Byambaa, M. Morshed, M.I. Cheikh, R.A. Shakoor, T. Mustafy, H.E. Marei, “Advances in osteobiologic materials for bone substitutes,” *J. Tissue Eng. Regen. Med.* , vol. 12, pp. 1448–1468, 2018

[56] A.M. Pobloth, K.A. Johnson, H. Schell, N. Kolarczik, D. Wulsten, G.N. Duda, K. Schmidt-Bleek, “Establishment of a preclinical ovine screening model for the investigation of bone tissue engineering strategies in cancellous and cortical bone defects,” *BMC Musculoskelet. Disord.* , vol. 17, 2016

[57] B. Šebečić, V. Nikolić, P. Sikirić, S. Seiwerth, T. Šoša, L. Patrlj, Ž. Grabarević, R. Ručman, M. Petek, P. Konjevoda, S. Jadrijević, D. Perović, M. Šlaj, “Osteogenic effect of a gastric pentadecapeptide, BPC-157, on the healing of segmental bone defect in rabbits: A comparison with bone marrow and autologous cortical bone implantation,” *Bone.* , vol. 24, pp. 195–202, 1999

[58] R.P. Clark, P.M. Pham, F.S. Ciminello, R.J. Hagge, S. Drobny, G.B. Wong, “Nasal dorsal augmentation with freeze-dried allograft bone: 10-year comprehensive review,” *Plast. Reconstr. Surg.* , vol. 143, pp. 49E-61E, 2019

[59] J. Ma, F. Yang, S.K. Both, H.J. Prins, M.N. Helder, J. Pan, F.Z. Cui, J.A. Jansen, J.J.J.P. Van Den

Beucken, “Bone forming capacity of cell- and growth factor-based constructs at different ectopic implantation sites,” *J. Biomed. Mater. Res. - Part A.* , vol. 103, pp. 439–450, 2015

[60] G.R.J. Swennen, F. Schutyser, M.C. Mueller, F.J. Kramer, C. Eulzer, H. Schliephake, “Effect of platelet-rich-plasma on cranial distraction osteogenesis in sheep: Preliminary clinical and radiographic results,” *Int. J. Oral Maxillofac. Surg.* , vol. 34, pp. 294–304, 2005

[61] O. Brennan, B. Stenson, A. Widaa, D.M. O’Gorman, F.J. O’Brien, “Incorporation of the natural marine multi-mineral dietary supplement Aquamin enhances osteogenesis and improves the mechanical properties of a collagen-based bone graft substitute,” *J. Mech. Behav. Biomed. Mater.* , vol. 47, pp. 114–123, 2015

[62] M.S. Attia, H.M. Mohammed, M.G. Attia, M.A.A. El Hamid, E.A. Shoeriabah, “Histological and histomorphometric evaluation of hydroxyapatite-based biomaterials in surgically created defects around implants in dogs,” *J. Periodontol.* , vol. 90, pp. 281–287, 2019

[63] T. Lerner, V. Bullmann, T.L. Schulte, M. Schneider, U. Liljenqvist, “A level-1 pilot study to evaluate of ultraporous ß-tricalcium phosphate as a graft extender in the posterior correction of adolescent idiopathic scoliosis,” *Eur. Spine J.* , vol. 18, pp. 170–179, 2009

[64] T. Al Malat, M. Glombitza, J. Dahmen, P.M. Hax, E. Steinhausen, “The use of bioactive glass S53P4 as bone graft substitute in the treatment of chronic osteomyelitis and infected non-unions - A retrospective study of 50 patients,” *Z. Orthop. Unfall.* , vol. 156, pp. 152–159, 2018

[65] H.S. Sandhu, L.E.A. Kanim, J.M. Kabo, E.N. Zeegen, D. Liu, E.G. Dawson, L.L. Seeger, J.M. Toth, “Evaluation of rhbmp-2 with an opla carrier in a canine posterolateral (Transverse process) spinal fusion model,” *Spine (Phila. Pa. 1976).* , vol. 20, pp. 2669–2682, 1995

[66] T.B. Jensen, S. Overgaard, M. Lind, O. Rahbek, C. Bünger, K. Søballe, “Osteogenic protein-1 increases the fixation of implants grafted with morcellised bone allograft and ProOsteon bone substitute,” *J. Bone Jt. Surg. - Ser. B.* , vol. 89, pp. 121–126, 2007

[67] X. Du, S. Fu, Y. Zhu, “3D printing of ceramic-based scaffolds for bone tissue engineering: An overview,” *J. Mater. Chem. B.* , vol. 6, pp. 4397–4412, 2018

[68] K.S. Ogueri, T. Jafari, J.L. Escobar Ivirico, C.T. Laurencin, “Polymeric Biomaterials for Scaffold-Based Bone Regenerative Engineering,” *Regen. Eng. Transl. Med.* , vol. 5, pp. 128–154, 2019

[69] P. Zhou, Y. Xia, X. Cheng, P. Wang, Y. Xie, S. Xu, “Enhanced bone tissue regeneration by antibacterial and osteoinductive silica-HACC-zein composite scaffolds loaded with rhBMP-2,” *Biomaterials.* , vol. 35, pp. 10033–10045, 2014

[70] N. Eliaz, N. Metoki, “Calcium phosphate bioceramics: A review of their history, structure, properties, coating technologies and biomedical applications,” *Materials (Basel).* , vol. 10, 2017

[71] Y. Wen, S. Xun, M. Haoye, S. Baichuan, C. Peng, L. Xuejian, Z. Kaihong, Y. Xuan, P. Jiang, L. Shibi, “3D printed porous ceramic scaffolds for bone tissue engineering: A review,” *Biomater. Sci.* , vol. 5, pp. 1690–1698, 2017

[72] G. Liu, L. Zhao, W. Zhang, L. Cui, W. Liu, Y. Cao, “Repair of goat tibial defects with bone marrow stromal cells and ß-tricalcium phosphate,” *J. Mater. Sci. Mater. Med.* , vol. 19, pp. 2367–2376, 2008

[73] L. Wang, Y.-Y. Hu, Z. Wang, X. Li, D.-C. Li, B.-H. Lu, S.-F. Xu, “Flow perfusion culture of human fetal bone cells in large ß-tricalcium phosphate scaffold with controlled architecture,” *J. Biomed. Mater. Res. Part A.* , vol. 91A, pp. 102–113, 2009

[74] S.K. Nandi, G. Fielding, D. Banerjee, A. Bandyopadhyay, S. Bose, “3D-printed ß-TCP bone tissue engineering scaffolds: Effects of chemistry on in vivo biological properties in a rabbit tibia model,” *J. Mater. Res.* , vol. 33, pp. 1939–1947, 2018

[75] S. Tarafder, V.K. Balla, N.M. Davies, A. Bandyopadhyay, S. Bose, “Microwave-sintered 3D printed tricalcium phosphate scaffolds for bone tissue engineering,” *J. Tissue Eng. Regen. Med.* , vol. 7, pp. 631–641, 2013

[76] M. Nishikawa, A. Myoui, H. Ohgushi, M. Ikeuchi, N. Tamai, H. Yoshikawa, “Bone tissue engineering using novel interconnected porous hydroxyapatite ceramics combined with marrow mesenchymal cells: Quantitative and three-dimensional image analysis,” in: Cell Transplant., Cognizant Communication Corporation, : pp. 367–376, 2004

[77] G. Tripathi, B. Basu, “A porous hydroxyapatite scaffold for bone tissue engineering: Physico-mechanical and biological evaluations,” *Ceram. Int.* , vol. 38, pp. 341–349, 2012

[78] J.L. Simon, S. Michna, J.A. Lewis, E.D. Rekow, V.P. Thompson, J.E. Smay, A. Yampolsky, J.R. Parsons, J.L. Ricci, “In vivo bone response to 3D periodic hydroxyapatite scaffolds assembled by direct ink writing,” *J. Biomed. Mater. Res. Part A.* , vol. 83A, pp. 747–758, 2007

[79] Y. Huang, X. Jin, X. Zhang, H. Sun, J. Tu, T. Tang, J. Chang, K. Dai, “In vitro and in vivo evaluation of akermanite bioceramics for bone regeneration,” *Biomaterials.* , vol. 30, pp. 5041–5048, 2009

[80] A. Liu, M. Sun, X. Yang, C. Ma, Y. Liu, X. Yang, S. Yan, Z. Gou, “Three-dimensional printing akermanite porous scaffolds for load-bearing bone defect repair: An investigation of osteogenic capability and mechanical evolution,” *J. Biomater. Appl.* , vol. 31, pp. 650–660, 2016

[81] Z. Han, P. Feng, C. Gao, Y. Shen, C. Shuai, S. Peng, “Microstructure, mechanical properties and in vitro bioactivity of akermanite scaffolds fabricated by laser sintering,” in: Biomed. Mater. Eng., IOS Press, : pp. 2073–2080, 2014

[82] C. Wu, Y. Ramaswamy, H. Zreiqat, “Porous diopside (CaMgSi2O6) scaffold: A promising bioactive material for bone tissue engineering,” *Acta Biomater.* , vol. 6, pp. 2237–2245, 2010

[83] Q. Fu, M.N. Rahaman, B.S. Bal, K. Kuroki, R.F. Brown, “In vivo evaluation of 13-93 bioactive glass scaffolds with trabecular and oriented microstructures in a subcutaneous rat implantation model,” *J. Biomed. Mater. Res. Part A.* , vol. 95A, pp. 235–244, 2010

[84] C. Wu, Y. Luo, G. Cuniberti, Y. Xiao, M. Gelinsky, “Three-dimensional printing of hierarchical and tough mesoporous bioactive glass scaffolds with a controllable pore architecture, excellent mechanical strength and mineralization ability,” *Acta Biomater.* , vol. 7, pp. 2644–2650, 2011

[85] Q. Fu, M.N. Rahaman, B. Sonny Bal, R.F. Brown, D.E. Day, “Mechanical and in vitro performance of 13-93 bioactive glass scaffolds prepared by a polymer foam replication technique,” *Acta Biomater.* , vol. 4, pp. 1854–1864, 2008

[86] M. Asadi-Eydivand, M. Solati-Hashjin, S.S. Shafiei, S. Mohammadi, M. Hafezi, N.A.A. Osman, “Structure, properties, and in vitro behavior of heat-treated calcium sulfate scaffolds fabricated by 3D printing,” *PLoS One.* , vol. 11, 2016

[87] P. Lichte, H.C. Pape, T. Pufe, P. Kobbe, H. Fischer, “Scaffolds for bone healing: Concepts, materials and evidence,” *Injury.* , vol. 42, pp. 569–573, 2011

[88] J. Jeong, J.H. Kim, J.H. Shim, N.S. Hwang, C.Y. Heo, “Bioactive calcium phosphate materials and applications in bone regeneration,” *Biomater. Res.* , vol. 23, pp. 1–11, 2019

[89] A.J. Wagoner Johnson, B.A. Herschler, “A review of the mechanical behavior of CaP and CaP/polymer composites for applications in bone replacement and repair,” *Acta Biomater.* , vol. 7, pp. 16–30, 2011

[90] R.J. Dekker, J.D. De Bruijn, I. Van Den Brink, Y.P. Bovell, P. Layrolle, C.A. Van Blitterswijk, “Bone tissue engineering on calcium phosphate-coated titanium plates utilizing cultured rat bone marrow cells: A preliminary study,” *J. Mater. Sci. Mater. Med.* , vol. 9, pp. 859–863, 1998

[91] C.D. Friedman, P.D. Costantino, S. Takagi, L.C. Chow, “BoneSource™ hydroxyapatite cement: A

novel biomaterial for craniofacial skeletal tissue engineering and reconstruction," *J. Biomed. Mater. Res.* , vol. 43, pp. 428–432, 1998

[92] Z. He, Q. Zhai, M. Hu, C. Cao, J. Wang, H. Yang, B. Li, "Bone cements for percutaneous vertebroplasty and balloon kyphoplasty: Current status and future developments," *J. Orthop. Transl.* , vol. 3, pp. 1–11, 2015

[93] J.M. Bouler, P. Pilet, O. Gauthier, E. Verron, "Biphasic calcium phosphate ceramics for bone reconstruction: A review of biological response," *Acta Biomater.* , vol. 53, pp. 1–12, 2017

[94] D.Y. Cho, W.Y. Lee, P.C. Sheu, C.C. Chen, "Cage containing a biphasic calcium phosphate ceramic (Triosite) for the treatment of cervical spondylosis," *Surg. Neurol.* , vol. 63, pp. 497–503, 2005

[95] R. Cavagna, G. Daculsi, J.M. Bouler, "Macroporous calcium phosphate ceramic: A prospective study of 106 cases in lumbar spinal fusion," *J. Long. Term. Eff. Med. Implants.* , vol. 9, pp. 403–412, 1999

[96] C. Lindgren, A. Mordenfeld, C.B. Johansson, M. Hallman, "A 3-year clinical follow-up of implants placed in two different biomaterials used for sinus augmentation.," *Int. J. Oral Maxillofac. Implants.* , vol. 27, pp. 1151–62

[97] J. Delécrin, S. Takahashi, F. Gouin, N. Passuti, "A synthetic porous ceramic as a bone graft substitute in the surgical management of scoliosis: A prospective, randomized study," *Spine (Phila. Pa. 1976).* , vol. 25, pp. 563–569, 2000

[98] C. Gao, Y. Deng, P. Feng, Z. Mao, P. Li, B. Yang, J. Deng, Y. Cao, C. Shuai, S. Peng, "Current progress in bioactive ceramic scaffolds for bone repair and regeneration," *Int. J. Mol. Sci.* , vol. 15, pp. 4714–4732, 2014

[99] L. Nie, J. Suo, P. Zou, S. Feng, "Preparation and Properties of Biphasic Calcium Phosphate Scaffolds Multiply Coated with HA/PLLA Nanocomposites for Bone Tissue Engineering Applications," *J. Nanomater.* , vol. 2012, pp. 11, 2012

[100] A.L. Torres, V.M. Gaspar, I.R. Serra, G.S. Diogo, R. Fradique, A.P. Silva, I.J. Correia, "Bioactive polymeric-ceramic hybrid 3D scaffold for application in bone tissue regeneration," *Mater. Sci. Eng. C.* , vol. 33, pp. 4460–4469, 2013

[101] S.J. Florczyk, M. Leung, S. Jana, Z. Li, N. Bhattarai, J.I. Huang, R.A. Hopper, M. Zhang, "Enhanced bone tissue formation by alginate gel-assisted cell seeding in porous ceramic scaffolds and sustained release of growth factor," *J. Biomed. Mater. Res. Part A.* , vol. 100A, pp. 3408–3415, 2012

[102] L. Liu, J. Liu, M. Wang, S. Min, Y. Cai, L. Zhu, J. Yao, "Preparation and characterization of nano-hydroxyapatite/silk fibroin porous scaffolds," *J. Biomater. Sci. Polym. Ed.* , vol. 19, pp. 325–338, 2008

[103] S. Hasegawa, J. Tamura, M. Neo, K. Goto, Y. Shikinami, M. Saito, M. Kita, T. Nakamura, "In vivo evaluation of a porous hydroxyapatite/poly-DL-lactide composite for use as a bone substitute," *J. Biomed. Mater. Res. Part A.* , vol. 75A, pp. 567–579, 2005

[104] J.A. Inzana, D. Olvera, S.M. Fuller, J.P. Kelly, O.A. Graeve, E.M. Schwarz, S.L. Kates, H.A. Awad, "3D printing of composite calcium phosphate and collagen scaffolds for bone regeneration," *Biomaterials.* , vol. 35, pp. 4026–4034, 2014

[105] S.T. Becker, H. Bolte, O. Krapf, H. Seitz, T. Douglas, S. Sivananthan, J. Wiltfang, E. Sherry, P.H. Warnke, "Endocultivation: 3D printed customized porous scaffolds for heterotopic bone induction," *Oral Oncol.* , vol. 45, pp. e181–e188, 2009

[106] X. Guo, H. Gao, X. Liu, J. Diao, X. Shi, N. Zhao, Y. Wang, "Porous Li-containing biphasic calcium phosphate scaffolds fabricated by three-dimensional plotting for bone repair," *RSC Adv.* , vol. 7,

pp. 34508–34516, 2017

[107] K.A. Kwak, M.A. Jyoti, H.Y. Song, “In vitro and in vivo studies of three dimensional porous composites of biphasic calcium phosphate/poly ε-caprolactone: Effect of bio-functionalization for bone tissue engineering,” in: Appl. Surf. Sci., Elsevier B.V., : pp. 307–314, 2014

[108] L. Strobel, S. Rath, A. Maier, J. Beier, A. Arkudas, P. Greil, R. Horch, U. Kneser, “Induction of bone formation in biphasic calcium phosphate scaffolds by bone morphogenetic protein-2 and primary osteoblasts,” *J. Tissue Eng. Regen. Med.* , vol. 8, pp. 176–185, 2014

[109] K. Paul, A.R. Padalhin, N.T.B. Linh, B. Kim, S.K. Sarkar, B.T. Lee, “A study of BMP-2-loaded bipotential electrolytic complex around a biphasic calcium phosphate-derived (BCP) scaffold for repair of large segmental bone defect,” *PLoS One*. , vol. 11, 2016

[110] T.B.L. Nguyen, B.T. Lee, “A combination of biphasic calcium phosphate scaffold with hyaluronic acid-gelatin hydrogel as a new tool for bone regeneration,” *Tissue Eng. - Part A.* , vol. 20, pp. 1993–2004, 2014

[111] J.Q. Wang, B.J. Jiang, W.J. Guo, Y.M. Zhao, “Indirect 3D printing technology for the fabrication of customised ß-TCP/chitosan scaffold with the shape of rabbit radial head - An in vitro study,” *J. Orthop. Surg. Res.* , vol. 14, pp. 102, 2019

[112] C. Shi, Z. Yuan, F. Han, C. Zhu, B. Li, “Polymeric biomaterials for bone regeneration,” *Ann. Jt.* , vol. 1, pp. 27–27, 2016

[113] P.A. Gunatillake, R. Adhikari, N. Gadegaard, “Biodegradable synthetic polymers for tissue engineering,” *Eur. Cells Mater.* , vol. 5, pp. 1–16, 2003

[114] C. Dhand, S.T. Ong, N. Dwivedi, S.M. Diaz, J.R. Venugopal, B. Navaneethan, M.H.U.T. Fazil, S. Liu, V. Seitz, E. Wintermantel, R.W. Beuerman, S. Ramakrishna, N.K. Verma, R. Lakshminarayanan, “Bio-inspired in situ crosslinking and mineralization of electrospun collagen scaffolds for bone tissue engineering,” *Biomaterials.* , vol. 104, pp. 323–338, 2016

[115] P. Chen, J. Tao, S. Zhu, Y. Cai, Q. Mao, D. Yu, J. Dai, H.W. Ouyang, “Radially oriented collagen scaffold with SDF-1 promotes osteochondral repair by facilitating cell homing,” *Biomaterials.* , vol. 39, pp. 114–123, 2015

[116] G.Y. Du, S.W. He, C.X. Sun, L.D. Mi, “Bone Morphogenic Protein-2 (rhBMP2)-Loaded Silk Fibroin Scaffolds to Enhance the Osteoinductivity in Bone Tissue Engineering,” *Nanoscale Res. Lett.* , vol. 12, pp. 573, 2017

[117] A. Nisal, R. Sayyad, P. Dhavale, B. Khude, R. Deshpande, V. Mapare, S. Shukla, P. Venugopalan, “Silk fibroin micro-particle scaffolds with superior compression modulus and slow bioresorption for effective bone regeneration,” *Sci. Rep.* , vol. 8, pp. 1–10, 2018

[118] J. Kim, I.S. Kim, T.H. Cho, K.B. Lee, S.J. Hwang, G. Tae, I. Noh, S.H. Lee, Y. Park, K. Sun, “Bone regeneration using hyaluronic acid-based hydrogel with bone morphogenic protein-2 and human mesenchymal stem cells,” *Biomaterials.* , vol. 28, pp. 1830–1837, 2007

[119] A. Oryan, S. Alidadi, A. Bigham-Sadegh, A. Moshiri, “Comparative study on the role of gelatin, chitosan and their combination as tissue engineered scaffolds on healing and regeneration of critical sized bone defects: an in vivo study,” *J. Mater. Sci. Mater. Med.* , vol. 27, pp. 1–14, 2016

[120] J.M. Williams, A. Adewunmi, R.M. Schek, C.L. Flanagan, P.H. Krebsbach, S.E. Feinberg, S.J. Hollister, S. Das, “Bone tissue engineering using polycaprolactone scaffolds fabricated via selective laser sintering,” *Biomaterials.* , vol. 26, pp. 4817–4827, 2005

[121] J. Jensen, J.H.D. Rölfing, D.Q. Svend Le, A.A. Kristiansen, J.V. Nygaard, L.B. Hokland, M. Bendtsen, M. Kassem, H. Lysdahl, C.E. Bünger, “Surface-modified functionalized polycaprolactone scaffolds for bone repair: *In vitro* and *in vivo* experiments,” *J. Biomed. Mater. Res. Part A.* , vol.

102, pp. 2993–3003, 2014

[122] C. Zong, D. Xue, W. Yuan, W. Wang, D. Shen, X. Tong, D. Shi, L. Liu, Q. Zheng, C. Gao, J. Wang, "Reconstruction Of Rat Calvarial Defects With Human Mesenchymal Stem Cells and Osteoblast-Like Cells in Poly-Lactic-Co-Glycolic Acid Scaffolds," *Eur. Cells Mater.* , vol. 20, pp. 109–120, 2010

[123] I.-R. SL, C. GM, G. A, M. MJ, Y. AW, Y. MJ, M. AG, "Ectopic Bone Formation by Marrow Stromal Osteoblast Transplantation Using poly(DL-lactic-co-glycolic Acid) Foams Implanted Into the Rat Mesentery," *J. Biomed. Mater. Res.* , vol. 36, 1997

[124] U. Stachewicz, T. Qiao, S.C.F. Rawlinson, F.V. Almeida, W.Q. Li, M. Cattell, A.H. Barber, "3D imaging of cell interactions with electrospun PLGA nanofiber membranes for bone regeneration," *Acta Biomater.* , vol. 27, pp. 88–100, 2015

[125] B.J.R.F. Bolland, J.M. Kanczler, P.J. Ginty, S.M. Howdle, K.M. Shakesheff, D.G. Dunlop, R.O.C. Oreffo, "The application of human bone marrow stromal cells and poly(dl-lactic acid) as a biological bone graft extender in impaction bone grafting," *Biomaterials.* , vol. 29, pp. 3221–3227, 2008

[126] A. Grémare, V. Guduric, R. Bareille, V. Heroguez, S. Latour, N. L'heureux, J.-C. Fricain, S. Catros, D. Le Nihouannen, "Characterization of printed PLA scaffolds for bone tissue engineering," *J. Biomed. Mater. Res. Part A.* , vol. 106, pp. 887–894, 2018

[127] J.P. Fisher, J.W.M. Vehof, D. Dean, J.P.C.M. van der Waerden, T.A. Holland, A.G. Mikos, J.A. Jansen, "Soft and hard tissue response to photocrosslinked poly(propylene fumarate) scaffolds in a rabbit model," *J. Biomed. Mater. Res.* , vol. 59, pp. 547–556, 2002

[128] S.J. Florczyk, M. Leung, Z. Li, J.I. Huang, R.A. Hopper, M. Zhang, "Evaluation of three-dimensional porous chitosan-alginate scaffolds in rat calvarial defects for bone regeneration applications," *J. Biomed. Mater. Res. Part A.* , vol. 101, pp. 2974–2983, 2013

[129] F.G. Lyons, A.A. Al-Munajjed, S.M. Kieran, M.E. Toner, C.M. Murphy, G.P. Duffy, F.J. O'Brien, "The healing of bony defects by cell-free collagen-based scaffolds compared to stem cell-seeded tissue engineered constructs," *Biomaterials.* , vol. 31, pp. 9232–9243, 2010

[130] M.A. Kafi, M.K. Aktar, Y. Phanny, M. Todo, "Adhesion, proliferation and differentiation of human mesenchymal stem cell on chitosan/collagen composite scaffold," *J. Mater. Sci. Mater. Med.* , vol. 30, pp. 1–12, 2019

[131] S. Tong, D.P. Xu, Z.M. Liu, Y. Du, X.K. Wang, "Synthesis of and in vitro and in vivo evaluation of a novel TGF-1-SF-CS three-dimensional scaffold for bone tissue engineering," *Int. J. Mol. Med.* , vol. 38, pp. 367–380, 2016

[132] R.S. Leena, M. Vairamani, N. Selvamurugan, "Alginate/Gelatin scaffolds incorporated with Silibinin-loaded Chitosan nanoparticles for bone formation in vitro," *Colloids Surfaces B Biointerfaces.* , vol. 158, pp. 308–318, 2017

[133] D. Singh, A. Tripathi, S.M. Zo, D. Singh, S.S. Han, "Synthesis of composite gelatin-hyaluronic acid-alginate porous scaffold and evaluation for in vitro stem cell growth and in vivo tissue integration," *Colloids Surfaces B Biointerfaces.* , vol. 116, pp. 502–509, 2014

[134] J.K. Park, J.-H. Shim, K.S. Kang, J. Yeom, H.S. Jung, J.Y. Kim, K.H. Lee, T.-H. Kim, S.-Y. Kim, D.-W. Cho, S.K. Hahn, "Solid Free-Form Fabrication of Tissue-Engineering Scaffolds with a Poly(lactic-co-glycolic acid) Grafted Hyaluronic Acid Conjugate Encapsulating an Intact Bone Morphogenetic Protein-2/Poly(ethylene glycol) Complex," *Adv. Funct. Mater.* , vol. 21, pp. 2906–2912, 2011

[135] A. Sadiasa, T.H. Nguyen, B.-T. Lee, "*In vitro* and *in vivo* evaluation of porous PCL-PLLA 3D polymer scaffolds fabricated via salt leaching method for bone tissue engineering applications," *J.*

Biomater. Sci. Polym. Ed. , vol. 25, pp. 150–167, 2014

[136] S.-R. Son, N.-T.B. Linh, H.-M. Yang, B.-T. Lee, "In vitro and in vivo evaluation of electrospun PCL/PMMA fibrous scaffolds for bone regeneration," *Sci. Technol. Adv. Mater.* , vol. 14, pp. 015009, 2013

[137] T.-H. Nguyen, B.-T. Lee, "*In vitro* and *in vivo* studies of rhBMP2-coated PS/PCL fibrous scaffolds for bone regeneration," *J. Biomed. Mater. Res. Part A.* , vol. 101A, pp. 797–808, 2013

[138] K. Ochi, G. Chen, T. Ushida, S. Gojo, K. Segawa, H. Tai, K. Ueno, H. Ohkawa, T. Mori, A. Yamaguchi, Y. Toyama, J. Hata, A. Umezawa, "Use of isolated mature osteoblasts in abundance acts as desired-shaped bone regeneration in combination with a modified poly-DL-lactic-co-glycolic acid (PLGA)-collagen sponge," *J. Cell. Physiol.* , vol. 194, pp. 45–53, 2003

[139] Y.F. Lui, W.Y. Ip, "Biological evaluation of flexible polyurethane/poly L-lactic acid composite scaffold as a potential filler for bone regeneration," *Materials (Basel).* , vol. 10, 2017

[140] Z. Qian, Ni, Fu, Fan, Guo, Shi, Peng, "Preparation of poly(ethylene glycol)/polylactide hybrid fibrous scaffolds for bone tissue engineering," *Int. J. Nanomedicine.* , vol. 6, pp. 3065, 2011

[141] J. Ju, X. Peng, K. Huang, L. Li, X. Liu, C. Chitrakar, L. Chang, Z. Gu, T. Kuang, "High-performance porous PLLA-based scaffolds for bone tissue engineering: Preparation, characterization, and in vitro and in vivo evaluation," *Polymer (Guildf).* , vol. 180, pp. 121707, 2019

[142] E.L. Hedberg, H.C. Kroese-Deutman, C.K. Shih, R.S. Crowther, D.H. Carney, A.G. Mikos, J.A. Jansen, "Effect of varied release kinetics of the osteogenic thrombin peptide TP508 from biodegradable, polymeric scaffolds on bone formationin vivo," *J. Biomed. Mater. Res. Part A.* , vol. 72A, pp. 343–353, 2005

[143] S.H. Oh, S.G. Kang, E.S. Kim, S.H. Cho, J.H. Lee, "Fabrication and characterization of hydrophilic poly(lactic-co-glycolic acid)/poly(vinyl alcohol) blend cell scaffolds by melt-molding particulate-leaching method," *Biomaterials.* , vol. 24, pp. 4011–4021, 2003

[144] Z. Xia, X. Yu, X. Jiang, H.D. Brody, D.W. Rowe, M. Wei, "Fabrication and characterization of biomimetic collagen-apatite scaffolds with tunable structures for bone tissue engineering," *Acta Biomater.* , vol. 9, pp. 7308–7319, 2013

[145] H. Xie, J. Wang, Y. He, Z. Gu, J. Xu, L. Li, Q. Ye, "Biocompatibility and safety evaluation of a silk fibroin-doped calcium polyphosphate scaffold copolymer: In vitro and in vivo," *RSC Adv.* , vol. 7, pp. 46036–46044, 2017

[146] L. Sun, S.T. Parker, D. Syoji, X. Wang, J.A. Lewis, D.L. Kaplan, "Direct-Write Assembly of 3D Silk/Hydroxyapatite Scaffolds for Bone Co-Cultures," *Adv. Healthc. Mater.* , vol. 1, pp. 729–735, 2012

[147] S. Saravanan, A. Chawla, M. Vairamani, T.P. Sastry, K.S. Subramanian, N. Selvamurugan, "Scaffolds containing chitosan, gelatin and graphene oxide for bone tissue regeneration in vitro and in vivo," *Int. J. Biol. Macromol.* , vol. 104, pp. 1975–1985, 2017

[148] C. Covarrubias, M. Cádiz, M. Maureira, I. Celhay, F. Cuadra, A. von Marttens, "Bionanocomposite scaffolds based on chitosan-gelatin and nanodimensional bioactive glass particles: In vitro properties and in vivo bone regeneration.," *J. Biomater. Appl.* , vol. 32, pp. 1155–1163, 2018

[149] N. Kemençe, N. Bölgen, "Gelatin- and hydroxyapatite-based cryogels for bone tissue engineering: synthesis, characterization, *in vitro* and *in vivo* biocompatibility," *J. Tissue Eng. Regen. Med.* , vol. 11, pp. 20–33, 2017

[150] B.R. Kim, T.B.L. Nguyen, Y.K. Min, B.T. Lee, "In vitro and in vivo studies of BMP-2-loaded PCL-gelatin-BCP electrospun scaffolds," *Tissue Eng. - Part A.* , vol. 20, pp. 3279–3289, 2014

[151] R. Guzmań, S. Nardecchia, M.C. Gutíerrez, M.L. Ferrer, V. Ramos, F. Del Monte, A. Abarrategi,

J.L. López-Lacomba, “Chitosan scaffolds containing calcium phosphate salts and rhBMP-2: In vitro and in vivo testing for bone tissue regeneration,” *PLoS One*. , vol. 9, 2014

[152] S.B. Qasim, S. Husain, Y. Huang, M. Pogorielov, V. Deineka, M. Lyndin, A. Rawlinson, I.U. Rehman, “In-vitro and in-vivo degradation studies of freeze gelated porous chitosan composite scaffolds for tissue engineering applications,” *Polym. Degrad. Stab.* , vol. 136, pp. 31–38, 2017

[153] I. Rodríguez-Méndez, M. Fernández-Gutiérrez, A. Rodríguez-Navarrete, R. Rosales-Ibáñez, L. Benito-Garzón, B. Vázquez-Lasa, J.S. Román, “Bioactive Sr(II)/chitosan/poly(ε-caprolactone) scaffolds for craniofacial tissue regeneration. In vitro and in vivo behavior,” *Polymers (Basel).* , vol. 10, 2018

[154] R. Kumar Saini, L. Prasad Bagri, A.K. Bajpai, “Nano-silver hydroxyapatite based antibacterial 3D scaffolds of gelatin/alginate/poly (vinyl alcohol) for bone tissue engineering applications,” *Colloids Surfaces B Biointerfaces*. , vol. 177, pp. 211–218, 2019

[155] Y. Luo, A. Lode, C. Wu, J. Chang, M. Gelinsky, “Alginate/nanohydroxyapatite scaffolds with designed core/shell structures fabricated by 3D plotting and in situ mineralization for bone tissue engineering,” *ACS Appl. Mater. Interfaces*. , vol. 7, pp. 6541–6549, 2015

[156] B. Chuenjitkuntaworn, W. Inrung, D. Damrongsri, K. Mekaapiruk, P. Supaphol, P. Pavasant, “Polycaprolactone/hydroxyapatite composite scaffolds: Preparation, characterization, and in vitro and in vivo biological responses of human primary bone cells,” *J. Biomed. Mater. Res. - Part A*. , vol. 94, pp. 241–251, 2010

[157] H. Eslami, H. Azimi Lisar, T.S. Jafarzadeh Kashi, M. Tahriri, M. Ansari, T. Rafiei, F. Bastami, A. Shahin-Shamsabadi, F. Mashhadi Abbas, L. Tayebi, “Poly(lactic-co-glycolic acid)(PLGA)/TiO2 nanotube bioactive composite as a novel scaffold for bone tissue engineering: In vitro and in vivo studies,” *Biologicals*. , vol. 53, pp. 51–62, 2018

[158] J. Won Yun, S. Young Heo, M. Ho Lee, H. Beom Lee, “Evaluation of a poly(lactic-acid) scaffold filled with poly(lactide-co-glycolide)/hydroxyapatite nanofibres for reconstruction of a segmental bone defect in a canine model,” *Vet. Med. (Praha)*. , vol. 64, pp. 531–538

[159] S.S. Kim, M. Sun Park, O. Jeon, C. Yong Choi, B.S. Kim, “Poly(lactide-co-glycolide)/hydroxyapatite composite scaffolds for bone tissue engineering,” *Biomaterials*. , vol. 27, pp. 1399–1409, 2006

[160] S. Kim, S.S. Kim, S.H. Lee, S. Eun Ahn, S.J. Gwak, J.H. Song, B.S. Kim, H.M. Chung, “In vivo bone formation from human embryonic stem cell-derived osteogenic cells in poly(d,l-lactic-co-glycolic acid)/hydroxyapatite composite scaffolds,” *Biomaterials*. , vol. 29, pp. 1043–1053, 2008

[161] E. Nejati, V. Firouzdor, M.B. Eslaminejad, F. Bagheri, “Needle-like nano hydroxyapatite/poly(l-lactide acid) composite scaffold for bone tissue engineering application,” *Mater. Sci. Eng. C.* , vol. 29, pp. 942–949, 2009

[162] T.T. Nguyen, T. Hoang, V.M. Can, A.S. Ho, S.H. Nguyen, T.T.T. Nguyen, T.N. Pham, T.P. Nguyen, T.L.H. Nguyen, M.T.D. Thi, “In vitro and in vivo tests of PLA/d-HAp nanocomposite,” *Adv. Nat. Sci. Nanosci. Nanotechnol.* , vol. 8, pp. 045013, 2017

[163] W. Yang, S.K. Both, Y. Zuo, Z.T. Birgani, P. Habibovic, Y. Li, J.A. Jansen, F. Yang, “Biological evaluation of porous aliphatic polyurethane/hydroxyapatite composite scaffolds for bone tissue engineering,” *J. Biomed. Mater. Res. Part A*. , vol. 103, pp. 2251–2259, 2015

[164] K. Kim, D. Dean, A. Lu, A.G. Mikos, J.P. Fisher, “Early osteogenic signal expression of rat bone marrow stromal cells is influenced by both hydroxyapatite nanoparticle content and initial cell seeding density in biodegradable nanocomposite scaffolds,” *Acta Biomater.* , vol. 7, pp. 1249–1264, 2011

[165] M. Dadsetan, T. Guda, M.B. Runge, D. Mijares, R.Z. Legeros, J.P. Legeros, D.T. Silliman, L. Lu,

J.C. Wenke, P.R. Brown Baer, M.J. Yaszemski, “Effect of calcium phosphate coating and rhBMP-2 on bone regeneration in rabbit calvaria using poly(propylene fumarate) scaffolds,” *Acta Biomater.* , vol. 18, pp. 9–20, 2015

[166] S. Uma Maheshwari, V.K. Samuel, N. Nagiah, “Fabrication and evaluation of (PVA/HAp/PCL) bilayer composites as potential scaffolds for bone tissue regeneration application,” *Ceram. Int.* , vol. 40, pp. 8469–8477, 2014

[167] Y. Wang, J. Liu, Q. Li, Y. Wang, C. Wang, “Two natural glucomannan polymers, from Konjac and Bletilla, as bioactive materials for pharmaceutical applications,” *Biotechnol. Lett.* , vol. 37, pp. 1–8, 2015

[168] T. Kondo, T. Shinozaki, H. Oku, S. Takigami, K. Takagishi, “Konjac glucomannan-based hydrogel with hyaluronic acid as a candidate for a novel scaffold for chondrocyte culture,” *J. Tissue Eng. Regen. Med.* , vol. 3, pp. 361–367, 2009

[169] D. Yang, Y. Yuan, L. Wang, X. Wang, R. Mu, J. Pang, J. Xiao, Y. Zheng, “A review on konjac glucomannan gels: Microstructure and application,” *Int. J. Mol. Sci.* , vol. 18, pp. 2250, 2017

[170] F. Alvarez-Manceñido, M. Landin, R. Martínez-Pacheco, “Konjac glucomannan/xanthan gum enzyme sensitive binary mixtures for colonic drug delivery,” *Eur. J. Pharm. Biopharm.* , vol. 69, pp. 573–581, 2008

[171] K. Wang, Z. He, “Alginate-konjac glucomannan-chitosan beads as controlled release matrix,” *Int. J. Pharm.* , vol. 244, pp. 117–126, 2002

[172] L. Fan, C. Cheng, Y. Qiao, F. Li, W. Li, H. Wu, B. Ren, “GNPs-CS/KGM as Hemostatic First Aid Wound Dressing with Antibiotic Effect: In Vitro and In Vivo Study,” *PLoS One.* , vol. 8, pp. e66890, 2013

[173] P. Darmadji, M. Izumimoto, “Effect of chitosan in meat preservation,” *Meat Sci.* , vol. 38, pp. 243–254, 1994

[174] B. Li, J. Li, J. Xia, J.F. Kennedy, X. Yie, T.G. Liu, “Effect of gamma irradiation on the condensed state structure and mechanical properties of konjac glucomannan/chitosan blend films,” *Carbohydr. Polym.* , vol. 83, pp. 44–51, 2011

[175] H. Nie, X. Shen, Z. Zhou, Q. Jiang, Y. Chen, A. Xie, Y. Wang, C.C. Han, “Electrospinning and characterization of konjac glucomannan/chitosan nanofibrous scaffolds favoring the growth of bone mesenchymal stem cells,” *Carbohydr. Polym.* , vol. 85, pp. 681–686, 2011

[176] M.E. Lynge, R. Van Der Westen, A. Postma, B. Städler, “Polydopamine - A nature-inspired polymer coating for biomedical science,” *Nanoscale.* , vol. 3, pp. 4916–4928, 2011

[177] X. Cui, Y. Yin, Z. Ma, Y. Yin, Y. Guan, S. Rong, J. Gao, Y. Niu, M. Li, “Polydopamine used as Hollow Capsule and Core-Shell Structures for Multiple Applications,” *Nano.* , vol. 10, 2015

[178] H. Li, Y. Jia, H. Peng, J. Li, “Recent developments in dopamine-based materials for cancer diagnosis and therapy,” *Adv. Colloid Interface Sci.* , vol. 252, pp. 1–20, 2018

[179] Y. Liu, K. Ai, J. Liu, M. Deng, Y. He, L. Lu, “Dopamine-melanin colloidal nanospheres: An efficient near-infrared photothermal therapeutic agent for in vivo cancer therapy,” *Adv. Mater.* , vol. 25, pp. 1353–1359, 2013

[180] H. Ma, T. Li, Z. Huan, M. Zhang, Z. Yang, J. Wang, J. Chang, C. Wu, “3D printing of high-strength bioscaffolds for the synergistic treatment of bone cancer,” *NPG Asia Mater.* , vol. 10, pp. 31–44, 2018

[181] O. Abdulhameed, A. Al-Ahmari, W. Ameen, S.H. Mian, “Additive manufacturing: Challenges, trends, and applications,” *Adv. Mech. Eng.* , vol. 11, 2019

[182] C. Kelder, A.D. Bakker, J. Klein-Nulend, D. Wismeijer, “The 3D printing of calcium phosphate with

k-carrageenan under conditions permitting the incorporation of biological components—A method," *J. Funct. Biomater.* , vol. 9, pp. 57, 2018

[183] Y. Yang, H. Wang, H. Li, Z. Ou, G. Yang, "3D printed tablets with internal scaffold structure using ethyl cellulose to achieve sustained ibuprofen release," *Eur. J. Pharm. Sci.* , vol. 115, pp. 11–18, 2018

[184] R. Trombetta, J.A. Inzana, E.M. Schwarz, S.L. Kates, H.A. Awad, "3D Printing of Calcium Phosphate Ceramics for Bone Tissue Engineering and Drug Delivery," *Ann. Biomed. Eng.* , vol. 45, pp. 23–44, 2017

[185] S. Bose, S. Vahabzadeh, A. Bandyopadhyay, "Bone tissue engineering using 3D printing," *Mater. Today.* , vol. 16, pp. 496–504, 2013

[186] M.N. Sithole, P. Kumar, L.C. du Toit, T. Marimuthu, Y.E. Choonara, V. Pillay, "A 3D bioprinted *in situ* conjugated- *co* -fabricated scaffold for potential bone tissue engineering applications," *J. Biomed. Mater. Res. Part A.* , vol. 106, pp. 1311–1321, 2018

[187] C.P. Jiang, Y.Y. Chen, "Biofabrication of hybrid bone scaffolds using a dual-nozzle bioplotter and in-vitro study of osteoblast cell," *Int. J. Precis. Eng. Manuf.* , vol. 15, pp. 1947–1953, 2014

[188] L. Shor, S. Güçeri, X. Wen, M. Gandhi, W. Sun, "Fabrication of three-dimensional polycaprolactone/hydroxyapatite tissue scaffolds and osteoblast-scaffold interactions in vitro," *Biomaterials.* , vol. 28, pp. 5291–5297, 2007

[189] C.W. Fedore, L.Y.L. Tse, H.K. Nam, K.L. Barton, N.E. Hatch, "Analysis of polycaprolactone scaffolds fabricated via precision extrusion deposition for control of craniofacial tissue mineralization," *Orthod. Craniofac. Res.* , vol. 20, pp. 12–17, 2017

[190] M. Domingos, F. Chiellini, S. Cometa, E. De Giglio, E. Grillo-Fernandes, P. Bártolo, E. Chiellini, "Evaluation of *in vitro* degradation of PCL scaffolds fabricated via BioExtrusion. Part 1: Influence of the degradation environment," *Virtual Phys. Prototyp.* , vol. 5, pp. 65–73, 2010

[191] S.I. Biscaia, T.F. Viana, H.A. Almeida, P.J. Bártolo, "Production and Characterisation of PCL/ES Scaffolds for Bone Tissue Engineering," in: Mater. Today Proc., Elsevier Ltd, : pp. 208–216, 2015

[192] Y.H. Lin, Y.C. Chiu, Y.F. Shen, Y.H.A. Wu, M.Y. Shie, "Bioactive calcium silicate/poly-ε-caprolactone composite scaffolds 3D printed under mild conditions for bone tissue engineering," *J. Mater. Sci. Mater. Med.* , vol. 29, pp. 1–13, 2018

[193] H. Seyednejad, D. Gawlitta, W.J.A. Dhert, C.F. Van Nostrum, T. Vermonden, W.E. Hennink, "Preparation and characterization of a three-dimensional printed scaffold based on a functionalized polyester for bone tissue engineering applications," *Acta Biomater.* , vol. 7, pp. 1999–2006, 2011

[194] Y. Luo, Y. Li, X. Qin, Q. Wa, "3D printing of concentrated alginate/gelatin scaffolds with homogeneous nano apatite coating for bone tissue engineering," *Mater. Des.* , vol. 146, pp. 12–19, 2018

[195] M. Mattioli-Belmonte, G. Vozzi, Y. Whulanza, M. Seggiani, V. Fantauzzi, G. Orsini, A. Ahluwalia, "Tuning polycaprolactone-carbon nanotube composites for bone tissue engineering scaffolds," *Mater. Sci. Eng. C.* , vol. 32, pp. 152–159, 2012

[196] M. Mattioli-Belmonte, G. Vozzi, K. Kyriakidou, E. Pulieri, G. Lucarini, B. Vinci, A. Pugnaloni, G. Biagini, A. Ahluwalia, "Rapid-prototyped and salt-leached PLGA scaffolds condition cell morpho-functional behavior," *J. Biomed. Mater. Res. Part A.* , vol. 85A, pp. 466–476, 2008

[197] J. Li, L. Zhang, S. Lv, S. Li, N. Wang, Z. Zhang, "Fabrication of individual scaffolds based on a patient-specific alveolar bone defect model," *J. Biotechnol.* , vol. 151, pp. 87–93, 2011

[198] M. Xu, Y. Li, H. Suo, Y. Yan, L. Liu, Q. Wang, Y. Ge, Y. Xu, "Fabricating a pearl/PLGA composite

scaffold by the low-temperature deposition manufacturing technique for bone tissue engineering," *Biofabrication*. , vol. 2, pp. 025002, 2010

[199] L. Liu, Z. Xiong, R. Zhang, L. Jin, Y. Yan, "A Novel Osteochondral Scaffold Fabricated via Multi-nozzle Low-temperature Deposition Manufacturing," *J. Bioact. Compat. Polym.* , vol. 24, pp. 18–30, 2009

[200] N.E. Fedorovich, J.R. De Wijn, A.J. Verbout, J. Alblas, W.J.A. Dhert, "Three-dimensional fiber deposition of cell-laden, viable, patterned constructs for bone tissue printing," *Tissue Eng. - Part A.* , vol. 14, pp. 127–133, 2008

[201] N.E. Fedorovich, H.M. Wijnberg, W.J.A. Dhert, J. Alblas, "Distinct tissue formation by heterogeneous printing of osteo-and endothelial progenitor cells," *Tissue Eng. - Part A.* , vol. 17, pp. 2113–2121, 2011

[202] G.S. Diogo, V.M. Gaspar, I.R. Serra, R. Fradique, I.J. Correia, "Manufacture of β-TCP/alginate scaffolds through a Fab@home model for application in bone tissue engineering," *Biofabrication*. , vol. 6, pp. 025001, 2014

[203] T.T. Demirta\cs, G. Irmak, M. Gümü\csderelio\uglu, "A bioprintable form of chitosan hydrogel for bone tissue engineering," *Biofabrication*. , vol. 9, pp. 35003, 2017

[204] G. Gao, A.F. Schilling, T. Yonezawa, J. Wang, G. Dai, X. Cui, "Bioactive nanoparticles stimulate bone tissue formation in bioprinted three-dimensional scaffold and human mesenchymal stem cells," *Biotechnol. J.* , vol. 9, pp. 1304–1311, 2014

[205] S. Catros, J.-C. Fricain, B. Guillotin, B. Pippenger, R. Bareille, M. Remy, E. Lebraud, B. Desbat, J. Amédée, F. Guillemot, "Laser-assisted bioprinting for creating on-demand patterns of human osteoprogenitor cells and nano-hydroxyapatite," *Biofabrication*. , vol. 3, pp. 025001, 2011

[206] V. Keriquel, H. Oliveira, M. Rémy, S. Ziane, S. Delmond, B. Rousseau, S. Rey, S. Catros, J. Amédée, F. Guillemot, J.C. Fricain, "In situ printing of mesenchymal stromal cells, by laser-assisted bioprinting, for in vivo bone regeneration applications," *Sci. Rep.* , vol. 7, pp. 1–10, 2017

[207] J.A. Barron, P. Wu, H.D. Ladouceur, B.R. Ringeisen, "Biological laser printing: A novel technique for creating heterogeneous 3-dimensional cell patterns," *Biomed. Microdevices*. , vol. 6, pp. 139–147, 2004

[208] C. Mota, D. Puppi, F. Chiellini, E. Chiellini, "Additive manufacturing techniques for the production of tissue engineering constructs," *J. Tissue Eng. Regen. Med.* , vol. 9, pp. 174–190, 2015

[209] "Rapid Prototyping - Stereolithography (SLA)," (Available at: https://www.custompartnet.com/wu/stereolithography. Accessed on: May 4, 2020)

[210] "Fused Deposition Modeling (FDM)," (Available at: https://www.custompartnet.com/wu/fused-deposition-modeling. Accessed on: May 4, 2020)

[211] "Rapid Prototyping - Selective Laser Sintering (SLS)," (Available at: https://www.custompartnet.com/wu/selective-laser-sintering. Accessed on: May 4, 2020)

[212] "Euroceram - Robocasting - Direct Ink Writing," (Available at: https://www.euroceram.org/en/technologies/material-extrusion/robocasting-direct-ink-writing.html. Accessed on: October 31, 2020)

[213] E. Peng, D. Zhang, J. Ding, "Ceramic Robocasting: Recent Achievements, Potential, and Future Developments," *Adv. Mater.* , vol. 30, pp. 1802404, 2018

[214] P. Miranda, E. Saiz, K. Gryn, A.P. Tomsia, "Sintering and robocasting of β-tricalcium phosphate scaffolds for orthopaedic applications," *Acta Biomater.* , vol. 2, pp. 457–466, 2006

[215] P. Miranda, A. Pajares, E. Saiz, A.P. Tomsia, F. Guiberteau, "Mechanical properties of calcium phosphate scaffolds fabricated by robocasting," *J. Biomed. Mater. Res. - Part A.* , vol. 85A, pp.

218–227, 2008

[216] P. Miranda, A. Pajares, E. Saiz, A.P. Tomsia, F. Guiberteau, "Fracture modes under uniaxial compression in hydroxyapatite scaffolds fabricated by robocasting," *J. Biomed. Mater. Res. Part A.* , vol. 83A, pp. 646–655, 2007

[217] C.F. Marques, F.H. Perera, A. Marote, S. Ferreira, S.I. Vieira, S. Olhero, P. Miranda, J.M.F. Ferreira, "Biphasic calcium phosphate scaffolds fabricated by direct write assembly: Mechanical, anti-microbial and osteoblastic properties," *J. Eur. Ceram. Soc.* , vol. 37, pp. 359–368, 2017

[218] G. He, D.A. Hirschfeld, J. Cesarano, J.N. Stuecker, "Robocasting and Cofiiung of Functionally Graded Si3N4-W Materials," in: : pp. 119–125, 2008

[219] S. Ghosh, S.T. Parker, X. Wang, D.L. Kaplan, J.A. Lewis, "Direct-Write Assembly of Microperiodic Silk Fibroin Scaffolds for Tissue Engineering Applications," *Adv. Funct. Mater.* , vol. 18, pp. 1883–1889, 2008

[220] E. García-Tuñon, S. Barg, J. Franco, R. Bell, S. Eslava, E. D'Elia, R.C. Maher, F. Guitian, E. Saiz, "Printing in Three Dimensions with Graphene," *Adv. Mater.* , vol. 27, pp. 1688–1693, 2015

[221] B.A. Tuttle, J.E. Smay, J. Cesarano, J.A. Voigt, T.W. Scofield, W.R. Olson, J.A. Lewis, "Robocast Pb(Zr $_{0.95}$ Ti $_{0.05}$)O $_{3}$ Ceramic Monoliths and Composites," *J. Am. Ceram. Soc.* , vol. 84, pp. 872–874, 2001

[222] F.J. Martínez-Vázquez, M. V. Cabañas, J.L. Paris, D. Lozano, M. Vallet-Regí, "Fabrication of novel Si-doped hydroxyapatite/gelatine scaffolds by rapid prototyping for drug delivery and bone regeneration," *Acta Biomater.* , vol. 15, pp. 200–209, 2015

[223] F.J. Martínez-Vázquez, F.H. Perera, P. Miranda, A. Pajares, F. Guiberteau, "Improving the compressive strength of bioceramic robocast scaffolds by polymer infiltration," *Acta Biomater.* , vol. 6, pp. 4361–4368, 2010

[224] J. Russias, E. Saiz, S. Deville, K. Gryn, G. Liu, R.K. Nalla, A.P. Tomsia, "Fabrication and in vitro characterization of three-dimensional organic/inorganic scaffolds by robocasting," *J. Biomed. Mater. Res. Part A.* , vol. 83A, pp. 434–445, 2007

[225] S. Eqtesadi, A. Motealleh, P. Miranda, A. Lemos, A. Rebelo, J.M.F. Ferreira, "A simple recipe for direct writing complex 45S5 Bioglass® 3D scaffolds," *Mater. Lett.* , vol. 93, pp. 68–71, 2013

[226] S. Eqtesadi, A. Motealleh, A. Pajares, F. Guiberteau, P. Miranda, "Improving mechanical properties of 13-93 bioactive glass robocast scaffold by poly (lactic acid) and poly (ε-caprolactone) melt infiltration," *J. Non. Cryst. Solids.* , vol. 432, pp. 111–119, 2016

[227] J. Franco, P. Hunger, M.E. Launey, A.P. Tomsia, E. Saiz, "Direct write assembly of calcium phosphate scaffolds using a water-based hydrogel," *Acta Biomater.* , vol. 6, pp. 218–228, 2010

[228] Y. Sun, C. Peng, X. Wang, R. Wang, J. Yang, D. Zhang, "Rheological behavior of Al2O3 suspensions containing polyelectrolyte complexes for direct ink writing," *Powder Technol.* , vol. 320, pp. 223–229, 2017

[229] M. Houmard, Q. Fu, M. Genet, E. Saiz, A.P. Tomsia, "On the structural, mechanical, and biodegradation properties of HA/β-TCP robocast scaffolds," *J. Biomed. Mater. Res. Part B Appl. Biomater.* , vol. 101, pp. 1233–1242, 2013

[230] E. Feilden, E.G.T. Blanca, F. Giuliani, E. Saiz, L. Vandeperre, "Robocasting of structural ceramic parts with hydrogel inks," *J. Eur. Ceram. Soc.* , vol. 36, pp. 2525–2533, 2016

[231] A.R.C. Duarte, J.F. Mano, R.L. Reis, "Preparation of chitosan scaffolds loaded with dexamethasone for tissue engineering applications using supercritical fluid technology," *Eur. Polym. J.* , vol. 45, pp. 141–148, 2009

[232] V. Mouriño, J.P. Cattalini, J.A. Roether, P. Dubey, I. Roy, A.R. Boccaccini, "Composite polymer-

bioceramic scaffolds with drug delivery capability for bone tissue engineering," *Expert Opin. Drug Deliv.* , vol. 10, pp. 1353–1365, 2013

[233] V. Mouriño, A.R. Boccaccini, "Bone tissue engineering therapeutics: Controlled drug delivery in three-dimensional scaffolds," *J. R. Soc. Interface.* , vol. 7, pp. 209–227, 2010

[234] O. Böstman, H. Pihlajamäki, "Clinical biocompatibility of biodegradable orthopaedic implants for internal fixation: A review," *Biomaterials.* , vol. 21, pp. 2615–2621, 2000

[235] W.J.E.M. Habraken, J.G.C. Wolke, J.A. Jansen, "Ceramic composites as matrices and scaffolds for drug delivery in tissue engineering," *Adv. Drug Deliv. Rev.* , vol. 59, pp. 234–248, 2007

[236] M. Cicuéndez, J.C. Doadrio, A. Hernández, M.T. Portolés, I. Izquierdo-Barba, M. Vallet-Regí, "Multifunctional pH sensitive 3D scaffolds for treatment and prevention of bone infection," *Acta Biomater.* , vol. 65, pp. 450–461, 2018

[237] M. Ferreira, O. Rzhepishevska, L. Grenho, D. Malheiros, L. Gonçalves, A.J. Almeida, L. Jordão, I.A. Ribeiro, M. Ramstedt, P. Gomes, A. Bettencourt, "Levofloxacin-loaded bone cement delivery system: Highly effective against intracellular bacteria and Staphylococcus aureus biofilms," *Int. J. Pharm.* , vol. 532, pp. 241–248, 2017

[238] I. Cantón, R. Mckean, M. Charnley, K.A. Blackwood, C. Fiorica, A.J. Ryan, S. MacNeil, "Development of an Ibuprofen-releasing biodegradable PLA/PGA electrospun scaffold for tissue regeneration," *Biotechnol. Bioeng.* , vol. 105, pp. 396–408, 2010

[239] H. Kim, H.W. Kim, H. Suh, "Sustained release of ascorbate-2-phosphate and dexamethasone from porous PLGA scaffolds for bone tissue engineering using mesenchymal stem cells," *Biomaterials.* , vol. 24, pp. 4671–4679, 2003

[240] H.W. Kim, J.C. Knowles, H.E. Kim, "Hydroxyapatite/poly(ε-caprolactone) composite coatings on hydroxyapatite porous bone scaffold for drug delivery," *Biomaterials.* , vol. 25, pp. 1279–1287, 2004

[241] J.S. Son, M. Appleford, J.L. Ong, J.C. Wenke, J.M. Kim, S.H. Choi, D.S. Oh, "Porous hydroxyapatite scaffold with three-dimensional localized drug delivery system using biodegradable microspheres," *J. Control. Release.* , vol. 153, pp. 133–140, 2011

[242] A. López-Noriega, D. Arcos, M. Vallet-Regí, "Functionalizing Mesoporous Bioglasses for Long-Term Anti-Osteoporotic Drug Delivery," *Chem. - A Eur. J.* , vol. 16, pp. 10879–10886, 2010

[243] W. Chaisri, A.H. Ghassemi, W.E. Hennink, S. Okonogi, "Enhanced gentamicin loading and release of PLGA and PLHMGA microspheres by varying the formulation parameters," *Colloids Surfaces B Biointerfaces.* , vol. 84, pp. 508–514, 2011

[244] F. Ungaro, M. Biondi, I. d'Angelo, L. Indolfi, F. Quaglia, P.A. Netti, M.I. La Rotonda, "Microsphere-integrated collagen scaffolds for tissue engineering: Effect of microsphere formulation and scaffold properties on protein release kinetics," *J. Control. Release.* , vol. 113, pp. 128–136, 2006

[245] L. De Laporte, A. Des Rieux, H.M. Tuinstra, M.L. Zelivyanskaya, N.M. De Clerck, A.A. Postnov, V. Préat, L.D. Shea, "Vascular endothelial growth factor and fibroblast growth factor 2 delivery from spinal cord bridges to enhance angiogenesis following injury," *J. Biomed. Mater. Res. - Part A.* , vol. 98 A, pp. 372–382, 2011

[246] N. Itoh, T. Santa, M. Kato, "Rapid evaluation of the quantity of drugs encapsulated within nanoparticles by high-performance liquid chromatography in a monolithic silica column," *Anal. Bioanal. Chem.* , vol. 407, pp. 6429–6434, 2015

[247] J. Lozano-Sánchez, I. Borrás-Linares, A. Sass-Kiss, A. Segura-Carretero, "Chromatographic Technique: High-Performance Liquid Chromatography (HPLC)," in: Mod. Tech. Food Authentication, Elsevier, : pp. 459–526, 2018

[248] “How Does High Performance Liquid Chromatography Work? : Waters,” (Available at: https://www.waters.com/waters/en_US/How-Does-High-Performance-Liquid-Chromatography-Work%3F/nav.htm?cid=10049055&locale=en_US. Accessed on: May 27, 2020)

[249] P.J. Worsfold, “Spectrophotometry | overview,” in: Encycl. Anal. Sci., Elsevier, : pp. 244–248, 2019

[250] T. Tuhkanen, A. Ignatev, “Humic and fulvic compounds,” in: Encycl. Anal. Sci., Elsevier, : pp. 411–417, 2019

[251] P.M. V Raja, A.R. Barron, “8.5: Using UV-Vis for the detection and characterization of silicon quantum dots - Chemistry LibreTexts,” (Available at: https://chem.libretexts.org/Bookshelves/Analytical_Chemistry/Book%3A_Physical_Methods_in_Chemistry_and_Nano_Science_(Barron)/08%3A_Structure_at_the_Nano_Scale/8.05%3A_Using_UV-Vis_for_the_detection_and_characterization_of_silicon_quantum_dots. Accessed on: May 27, 2020)

[252] R.T. Tupinamba´branquinho, V. Carla, F. Mosqueira, E.K. Kano, J. De Souza, D. Dias, R. Dorim, D. De^nia, A. Sau´de, S.-G. Guimara˜es, M. De Lana, “HPLC-DAD and UV-Spectrophotometry for the Determination of Lychnopholide in Nanocapsule Dosage Form: Validation and Application to Release Kinetic Study,”

[253] S.M. Dhole, N.D. Amnerkar, P.B. Khedekar, “Comparison of UV spectrophotometry and high performance liquid chromatography methods for the determination of repaglinide in tablets,” *Pharm. Methods.* , vol. 3, pp. 68–72, 2012

[254] J. Patel, A. Patel, “Artificial Neural Networking in Controlled Drug Delivery,” in: Artif. Neural Netw. Drug Des. Deliv. Dispos., Elsevier Inc., : pp. 195–218, 2016

[255] U. Edlund, A.C. Albertsson, “Degradable polymer microspheres for controlled drug delivery,” in: Adv. Polym. Sci., Springer, Berlin, Heidelberg, : pp. 67–112, 2002

[256] C. Engineer, J. Parikh, A. Raval, “Review on Hydrolytic Degradation Behavior of Biodegradable Polymers from Controlled Drug Delivery System,” 2011

[257] M. Prabaharan, “Characterization of tissue scaffolds drug release profiles,” in: Characterisation Des. Tissue Scaffolds, Elsevier Inc., : pp. 149–168, 2016

[258] S.D.’ Souza, C.M. Keck, “A Review of In Vitro Drug Release Test Methods for Nano-Sized Dosage Forms,” 2014

[259] S. Amatya, E.J. Park, J.H. Park, J.S. Kim, E. Seol, H. Lee, H. Choi, Y.H. Shin, D.H. Na, “Drug release testing methods of polymeric particulate drug formulations,” *J. Pharm. Investig.* , vol. 43, pp. 259–266, 2013

[260] G. Kumar, S. Sharma, N. Shafiq, G.K. Khuller, S. Malhotra, “Optimization, in vitro-in vivo evaluation, and short-term tolerability of novel levofloxacin-loaded PLGA nanoparticle formulation,” *J. Pharm. Sci.* , vol. 101, pp. 2165–2176, 2012

[261] V.V.S.R. Karri, G. Kuppusamy, S.V. Talluri, S.S. Mannemala, R. Kollipara, A.D. Wadhwani, S. Mulukutla, K.R.S. Raju, R. Malayandi, “Curcumin loaded chitosan nanoparticles impregnated into collagen-alginate scaffolds for diabetic wound healing,” *Int. J. Biol. Macromol.* , vol. 93, pp. 1519–1529, 2016

[262] D.F. de Andrade, C. Zuglianello, A.R. Pohlmann, S.S. Guterres, R.C.R. Beck, “Assessing the In Vitro Drug Release from Lipid-Core Nanocapsules: a New Strategy Combining Dialysis Sac and a Continuous-Flow System,” *AAPS PharmSciTech.* , vol. 16, pp. 1409–1417, 2015

[263] T.E. Yalcin, S. Ilbasmis-Tamer, B. Ibisoglu, A. Özdemir, M. Ark, S. Takka, “Gemcitabine hydrochloride-loaded liposomes and nanoparticles: comparison of encapsulation efficiency, drug

release, particle size, and cytotoxicity," *Pharm. Dev. Technol.* , vol. 23, pp. 76–86, 2018

[264] S. Evrim Kepekci Tekkeli, M. Volkan Kiziltas, "Current HPLC Methods for Assay of Nano Drug Delivery Systems," *Curr. Top. Med. Chem.* , vol. 17, pp. 1588–1594, 2017

[265] S. Azizian, A. Hadjizadeh, H. Niknejad, "Chitosan-gelatin porous scaffold incorporated with Chitosan nanoparticles for growth factor delivery in tissue engineering," *Carbohydr. Polym.* , vol. 202, pp. 315–322, 2018

[266] P. Gentile, D. Bellucci, A. Sola, C. Mattu, V. Cannillo, G. Ciardelli, "Composite scaffolds for controlled drug release: Role of the polyurethane nanoparticles on the physical properties and cell behaviour," *J. Mech. Behav. Biomed. Mater.* , vol. 44, pp. 53–60, 2015

[267] M. Kouhi, M. Morshed, J. Varshosaz, M.H. Fathi, "Poly (ε-caprolactone) incorporated bioactive glass nanoparticles and simvastatin nanocomposite nanofibers: Preparation, characterization and in vitro drug release for bone regeneration applications," *Chem. Eng. J.* , vol. 228, pp. 1057–1065, 2013

[268] M. Rivas, M. Pelechà, L. Franco, P. Turon, C. Alemán, L.J. Del Valle, J. Puiggalí, "Incorporation of chloramphenicol loaded hydroxyapatite nanoparticles into polylactide," *Int. J. Mol. Sci.* , vol. 20, 2019

[269] Q. Zhang, M. Qin, X. Zhou, W. Nie, W. Wang, L. Li, C. He, "Porous nanofibrous scaffold incorporated with S1P loaded mesoporous silica nanoparticles and BMP-2 encapsulated PLGA microspheres for enhancing angiogenesis and osteogenesis," *J. Mater. Chem. B.* , vol. 6, pp. 6731–6743, 2018

[270] S. Bagherifard, "Mediating bone regeneration by means of drug eluting implants: From passive to smart strategies," *Mater. Sci. Eng. C.* , vol. 71, pp. 1241–1252, 2017

[271] Y. Yan, H. Chen, H. Zhang, C. Guo, K. Yang, K. Chen, R. Cheng, N. Qian, N. Sandler, Y.S. Zhang, H. Shen, J. Qi, W. Cui, L. Deng, "Vascularized 3D printed scaffolds for promoting bone regeneration," *Biomaterials.* , vol. 190–191, pp. 97–110, 2019

[272] V. Martin, I.A. Ribeiro, M.M. Alves, L. Gonçalves, R.A. Claudio, L. Grenho, M.H. Fernandes, P. Gomes, C.F. Santos, A.F. Bettencourt, "Engineering a multifunctional 3D-printed PLA-collagen-minocycline-nanoHydroxyapatite scaffold with combined antimicrobial and osteogenic effects for bone regeneration," *Mater. Sci. Eng. C.* , vol. 101, pp. 15–26, 2019

[273] Q. Yao, Y. Liu, B. Selvaratnam, R.T. Koodali, H. Sun, "Mesoporous silicate nanoparticles/3D nanofibrous scaffold-mediated dual-drug delivery for bone tissue engineering," *J. Control. Release.* , vol. 279, pp. 69–78, 2018

[274] S. Jahangir, S. Hosseini, F. Mostafaei, F.A. Sayahpour, M. Baghaban Eslaminejad, "3D-porous ß-tricalcium phosphate–alginate–gelatin scaffold with DMOG delivery promotes angiogenesis and bone formation in rat calvarial defects," *J. Mater. Sci. Mater. Med.* , vol. 30, pp. 1–14, 2019

[275] C.F. Marques, S.M. Olhero, P.M.C. Torres, J.C.C. Abrantes, S. Fateixa, H.I.S. Nogueira, I.A.C. Ribeiro, A. Bettencourt, A. Sousa, P.L. Granja, J.M.F. Ferreira, "Novel sintering-free scaffolds obtained by additive manufacturing for concurrent bone regeneration and drug delivery: Proof of concept," *Mater. Sci. Eng. C.* , vol. 94, pp. 426–436, 2019

[276] J. Lee, M.M. Farag, E.K. Park, J. Lim, H.S. Yun, "A simultaneous process of 3D magnesium phosphate scaffold fabrication and bioactive substance loading for hard tissue regeneration," *Mater. Sci. Eng. C.* , vol. 36, pp. 252–260, 2014

[277] Q. Yue, M. Wang, Z. Sun, C. Wang, C. Wang, Y. Deng, D. Zhao, "A versatile ethanol-mediated polymerization of dopamine for efficient surface modification and the construction of functional core-shell nanostructures," *J. Mater. Chem. B.* , vol. 1, pp. 6085–6093, 2013

[278] R.M. da S. Presa, “Development of a novel 3D-scaffold to promote bone regeneration,” MSc Thesis of Universidade do Porto, 2019

[279] T. Kokubo, H. Takadama, “How useful is SBF in predicting in vivo bone bioactivity?,” *Biomaterials*. , vol. 27, pp. 2907–2915, 2006

[280] J.P. Carrel, A. Wiskott, M. Moussa, P. Rieder, S. Scherrer, S. Durual, “A 3D printed TCP/HA structure as a new osteoconductive scaffold for vertical bone augmentation,” *Clin. Oral Implants Res.* , vol. 27, pp. 55–62, 2016

[281] A. Kakar, B.H.S. Rao, S. Hegde, N. Deshpande, A. Lindner, H. Nagursky, A. Patney, H. Mahajan, “Ridge preservation using an in situ hardening biphasic calcium phosphate (ß-TCP/HA) bone graft substitute—a clinical, radiological, and histological study,” *Int. J. Implant Dent.* , vol. 3, pp. 1–10, 2017

[282] J.P. Carrel, A. Wiskott, S. Scherrer, S. Durual, “Large Bone Vertical Augmentation Using a Three-Dimensional Printed TCP/HA Bone Graft: A Pilot Study in Dog Mandible,” *Clin. Implant Dent. Relat. Res.* , vol. 18, pp. 1183–1192, 2016

[283] E.W.H. Bodde, J.G.C. Wolke, R.S.Z. Kowalski, J.A. Jansen, “Bone regeneration of porous ß-tricalcium phosphate (Conduit™ TCP) and of biphasic calcium phosphate ceramic (Biosel®) in trabecular defects in sheep,” *J. Biomed. Mater. Res. Part A.* , vol. 82A, pp. 711–722, 2007

[284] C. Shuai, P. Li, J. Liu, S. Peng, “Optimization of TCP/HAP ratio for better properties of calcium phosphate scaffold via selective laser sintering,” *Mater. Charact.* , vol. 77, pp. 23–31, 2013

[285] R.P. Chhabra, “Non-Newtonian Fluids: An Introduction”

[286] A. M’Barki, L. Bocquet, A. Stevenson, “Linking Rheology and Printability for Dense and Strong Ceramics by Direct Ink Writing,” *Sci. Rep.* , vol. 7, pp. 1–10, 2017

[287] A.C.F. Marques, “Design and processing of porous scaffolds based on calcium phosphates by robocasting for bone tissue engineering,” PhD Thesis of Universidade de Aveiro, 2019

[288] F. Wang, E. Guo, E. Song, P. Zhao, J. Liu, “Structure and properties of bone-like-nanohydroxyapatite/gelatin/polyvinyl alcohol composites,” *Adv. Biosci. Biotechnol.* , vol. 01, pp. 185–189, 2010

[289] A.L. Boskey, “Bone composition: relationship to bone fragility and antiosteoporotic drug effects,” *Bonekey Rep.* , vol. 2, 2013

[290] M. Bartoš, T. Suchý, Z. Tonar, R. Foltán, M.H. Kalbáčová, “Micro-CT in tissue engineering scaffolds designed for bone regeneration: Principles and application,” *Ceram. - Silikaty.* , vol. 62, pp. 194–199, 2018

[291] G. Hannink, J.J.C. Arts, “Bioresorbability, porosity and mechanical strength of bone substitutes: What is optimal for bone regeneration?,” *Injury.* , vol. 42, pp. S22–S25, 2011

[292] E.F. Morgan, G.U. Unnikrisnan, A.I. Hussein, “Bone Mechanical Properties in Healthy and Diseased States,” *Annu. Rev. Biomed. Eng.* , vol. 20, pp. 119–143, 2018

[293] L.C. Gerhardt, A.R. Boccaccini, “Bioactive glass and glass-ceramic scaffolds for bone tissue engineering,” *Materials (Basel).* , vol. 3, pp. 3867–3910, 2010

[294] I. Sabree, J.E. Gough, B. Derby, “Mechanical properties of porous ceramic scaffolds: Influence of internal dimensions,” *Ceram. Int.* , vol. 41, pp. 8425–8432, 2015

[295] Q.L. Loh, C. Choong, “Three-dimensional scaffolds for tissue engineering applications: Role of porosity and pore size,” *Tissue Eng. - Part B Rev.* , vol. 19, pp. 485–502, 2013

[296] B. Huang, G. Caetano, C. Vyas, J. Blaker, C. Diver, P. Bártolo, “Polymer-Ceramic Composite Scaffolds: The Effect of Hydroxyapatite and ß-tri-Calcium Phosphate,” *Materials (Basel).* , vol. 11, pp. 129, 2018

[297] S. Prasadh, R.C.W. Wong, “Unraveling the mechanical strength of biomaterials used as a bone scaffold in oral and maxillofacial defects,” *Oral Sci. Int.* , vol. 15, pp. 48–55, 2018

[298] J. Zhao, W. Han, H. Chen, M. Tu, S. Huan, G. Miao, R. Zeng, H. Wu, Z. Cha, C. Zhou, “Fabrication and in vivo osteogenesis of biomimetic poly(propylene carbonate) scaffold with nanofibrous chitosan network in macropores for bone tissue engineering,” *J. Mater. Sci. Mater. Med.* , vol. 23, pp. 517–525, 2012

[299] C.L. Camiré, S. Jegou Saint-Jean, C. Mochales, P. Nevsten, J.-S. Wang, L. Lidgren, I. McCarthy, M.-P. Ginebra, “Material characterization andin vivo behavior of silicon substituted α-tricalcium phosphate cement,” *J. Biomed. Mater. Res. Part B Appl. Biomater.* , vol. 76B, pp. 424–431, 2006

[300] Y.-J. Seol, K.-H. Kim, I.A. Kim, S.-H. Rhee, “Osteoconductive and degradable electrospun nonwoven poly(ε-caprolactone)/CaO-SiO $_2$ gel composite fabric,” *J. Biomed. Mater. Res. Part A.* , vol. 9999A, pp. NA-NA, 2010

[301] L.X. Wang, A.R. Lee, Y. Yuan, X.M. Wang, T.J. Lu, “Preparation and FTIR, Raman and SEM characterizations of konjac glucomannan-KCl electrogels,” *Food Chem.* , vol. 331, pp. 127289, 2020

[302] H. Huang, G. Wang, J. Chen, W. Zhou, “Characterization of Sulfate Groups and Assessment of Anti-Coagulant Activity of Glucomannan Sulfate Prepared from Konjac Glucomannan,” *Trop. J. Pharm. Res.* , vol. 14, pp. 1217–1224, 2015

[303] N. Gierlinger, L. Sapei, O. Paris, “Insights into the chemical composition of Equisetum hyemale by high resolution Raman imaging,” *Planta.* , vol. 227, pp. 969–980, 2008

[304] E. Kreedapathy Girija, E. Kolanthai, P. Parthiban, R. Vani, A.E.K. Girija, A.K. Elayaraja, A.S. Prakash, P. Ae, R. Kesavamoorthy, A.S. Narayana Kalkura, “Hydrothermal synthesis of porous triphasic hydroxyapatite/(α and ß) tricalcium phosphate Hydrothermal synthesis of porous triphasic hydroxyapatite/ (a and b) tricalcium phosphate,” *Artic. J. Mater. Sci. Mater. Med.*, 2008

[305] J.A. Stammeier, B. Purgstaller, D. Hippler, V. Mavromatis, M. Dietzel, “In-situ Raman spectroscopy of amorphous calcium phosphate to crystalline hydroxyapatite transformation,” *MethodsX.* , vol. 5, pp. 1241–1250, 2018

[306] U. Anjaneyulu, D.K. Pattanayak, U. Vijayalakshmi, “Snail Shell Derived Natural Hydroxyapatite: Effects on NIH-3T3 Cells for Orthopedic Applications,” *Mater. Manuf. Process.* , vol. 31, pp. 206–216, 2016

[307] A.J. Steeves, A. Atwal, S.C. Schock, F. Variola, “Evaluation of the direct effects of poly(dopamine) on the: In vitro response of human osteoblastic cells,” *J. Mater. Chem. B.* , vol. 4, pp. 3145–3156, 2016

[308] H. Coskun, A. Aljabour, L. Uiberlacker, M. Strobel, S. Hild, C. Cobet, D. Farka, P. Stadler, N.S. Sariciftci, “Chemical vapor deposition - based synthesis of conductive polydopamine thin-films,” 2017

[309] M. Araújo, M. Miola, E. Bertone, G. Baldi, J. Perez, E. Verné, “On the mechanism of apatite-induced precipitation on 45S5 glass pellets coated with a natural-derived polymer,” *Appl. Surf. Sci.* , vol. 353, pp. 137–149, 2015

[310] H. Pan, X.Y. Liu, R. Tang, H.Y. Xu, “Mystery of the transformation from amorphous calcium phosphate to hydroxyapatite,” *Chem. Commun.* , vol. 46, pp. 7415–7417, 2010

[311] T. Kokubo, S. Yamaguchi, “Chemical surface modification of a titanium scaffold,” in: Met. Foam Bone Process. Modif. Charact. Prop., Elsevier Inc., : pp. 161–179, 2017

[312] N. Hild, O.D. Schneider, D. Mohn, N.A. Luechinger, F.M. Koehler, S. Hofmann, J.R. Vetsch, B.W. Thimm, R. Müller, W.J. Stark, “Two-layer membranes of calcium phosphate/collagen/PLGA

nanofibres: In vitro biomineralisation and osteogenic differentiation of human mesenchymal stem cells," *Nanoscale*. , vol. 3, pp. 401–409, 2011

[313] F. Viti, M. Landini, A. Mezzelani, L. Petecchia, L. Milanesi, S. Scaglione, "Osteogenic differentiation of MSC through calcium signaling activation: Transcriptomics and functional analysis," *PLoS One*. , vol. 11, pp. 148173, 2016

[314] B. Gharibi, G. Cama, M. Capurro, I. Thompson, S. Deb, L. Di Silvio, F.J. Hughes, "Gene expression responses to mechanical stimulation of mesenchymal stem cells seeded on calcium phosphate cement," in: Tissue Eng. - Part A, Mary Ann Liebert Inc., : pp. 2426–2438, 2013

[315] M. Amirikia, S.M.A. Shariatzadeh, S.G.A. Jorsaraei, M. Soleimani Mehranjani, "Impact of pre-incubation time of silk fibroin scaffolds in culture medium on cell proliferation and attachment," *Tissue Cell*. , vol. 49, pp. 657–663, 2017

[316] D.W. Weisgerber, S.R. Caliari, B.A.C. Harley, "Mineralized collagen scaffolds induce hMSC osteogenesis and matrix remodeling," *Biomater. Sci.* , vol. 3, pp. 533–542, 2015

[317] S.N. Rath, L.A. Strobel, A. Arkudas, J.P. Beier, A.K. Maier, P. Greil, R.E. Horch, U. Kneser, "Osteoinduction and survival of osteoblasts and bone-marrow stromal cells in 3D biphasic calcium phosphate scaffolds under static and dynamic culture conditions," *J. Cell. Mol. Med.* , vol. 16, pp. 2350–2361, 2012

[318] M. López-López, A. Fernández-Delgado, M.L. Moyá, D. Blanco-Arévalo, C. Carrera, R.R. de la Haba, A. Ventosa, E. Bernal, P. López-Cornejo, "Optimized preparation of levofloxacin loaded polymeric nanoparticles," *Pharmaceutics*. , vol. 11, 2019

[319] M. Sharma, "Transdermal and Intravenous Nano Drug Delivery Systems," in: Appl. Target. Nano Drugs Deliv. Syst., Elsevier, : pp. 499–550, 2019

[320] R. Singh, J.W. Lillard, "Nanoparticle-based targeted drug delivery," *Exp. Mol. Pathol.* , vol. 86, pp. 215–223, 2009

[321] T. Mudalige, H. Qu, D. Van Haute, S.M. Ansar, A. Paredes, T. Ingle, "Characterization of Nanomaterials: Tools and Challenges," in: Nanomater. Food Appl., Elsevier, : pp. 313–353, 2018

[322] M. Danaei, M. Dehghankhold, S. Ataei, F. Hasanzadeh Davarani, R. Javanmard, A. Dokhani, S. Khorasani, M.R. Mozafari, "Impact of particle size and polydispersity index on the clinical applications of lipidic nanocarrier systems," *Pharmaceutics*. , vol. 10, pp. 57, 2018

[323] S. Honary, F. Zahir, "Effect of Zeta Potential on the Properties of Nano-Drug Delivery Systems-A Review (Part 2)," *Trop. J. Pharm. Res.* , vol. 12, pp. 265–273, 2013

[324] "HPLC Analysis of Antibiotics (Fluoroquinolones from Tablets) on Discovery® HS C18 | Sigma-Aldrich," (Available at: https://www.sigmaaldrich.com/technical-documents/articles/analytical-applications/hplc/hplc-analysis-of-antibiotics-fluoroquinolones-from-tablets-g001425.html. Accessed on: August 11, 2020)

[325] H.M. Redhead, S.S. Davis, L. Illum, "Drug delivery in poly(lactide-co-glycolide) nanoparticles surface modified with poloxamer 407 and poloxamine 908: In vitro characterisation and in vivo evaluation," *J. Control. Release*. , vol. 70, pp. 353–363, 2001

[326] F. Sousa, A. Cruz, I.M. Pinto, B. Sarmento, "Nanoparticles provide long-term stability of bevacizumab preserving its antiangiogenic activity," *Acta Biomater*. , vol. 78, pp. 285–295, 2018

[327] W. Ding, S.A. Chechetka, M. Masuda, T. Shimizu, M. Aoyagi, H. Minamikawa, E. Miyako, "Lipid Nanotube Tailored Fabrication of Uniquely Shaped Polydopamine Nanofibers as Photothermal Converters," *Chem. - A Eur. J.* , vol. 22, pp. 4345–4350, 2016

[328] M. Vaselbehagh, H. Karkhanechi, S. Mulyati, R. Takagi, H. Matsuyama, "Improved antifouling of anion-exchange membrane by polydopamine coating in electrodialysis process," *Desalination*. ,

vol. 332, pp. 126–133, 2014

[329] Y. Liu, C. Xu, Y. Gu, X. Shen, Y. Zhang, B. Li, L. Chen, “Polydopamine-modified poly(L-lactic acid) nanofiber scaffolds immobilized with an osteogenic growth peptide for bone tissue regeneration,” *RSC Adv.* , vol. 9, pp. 11722–11736, 2019

[330] Z. Xu, N. Wang, P. Liu, Y. Sun, Y. Wang, F. Fei, S. Zhang, J. Zheng, B. Han, “Poly(dopamine) coating on 3D-printed poly-lactic-co-glycolic acid/β-tricalcium phosphate scaffolds for bone tissue engineering,” *Molecules*. , vol. 24, 2019